Novel insights into the corrosion mechanism of decorative multilayer nickel-chromium coatings on ABS: towards a correlation between CASS and electrochemical tests

Larraitz Ganborena Imaz

2020

Supervised by Dr. Jesús Manuel Vega and Dra. Eva García Lecina

Ph.D Thesis

Novel insights into the corrosion mechanism of decorative multilayer nickel-chromium coatings on ABS: towards a correlation between CASS and electrochemical tests

Larraitz Ganborena Imaz

2020

cidetec surface engineering

eman ta zabal zazu

UPV EHU

Acknowledgements

First, I would like to thank Cidetec for offering me the opportunity to carry out this thesis. At the same time, I would also like to acknowledge Atotech Deutschland GmbH for providing samples, assistance in the discussion of the results and having introduced me in the field of decorative nickel-chromium plating and characterisation during my visit to their facilities.

Next, I wish to show my gratitude to my supervisors for their guidance through the entire course of this thesis. I would like to express my thanks to Dr. Jesús Manuel Vega Vega for his valuable suggestions during the planning, development of this research work and writing, his time and dedication and for showing me that there is always a different perspective, thank you. I wish to acknowledge Dra. Eva García Lecina for the technical discussions and advices, her supervision and support throughout this thesis.

I would like to express my special thanks to Dra. Yaiza Gonzalez García for introducing, helping me with better understanding of the SECM and being so supportive. SECM has been a key technique in my research and has reported very interesting and relevant results to my investigation.

Special thanks also to my tutor Dra. Miren Ostra Beldarrain that so quickly and efficiently has solved my infinite questions related to administrative procedures. She has also introduced and guided me in the subject of Chemometrics and her help has been fundamental in the study of the correlation between accelerated and electrochemical assays.

I would also like to thank my colleagues from ACCT, Jonathan, Larraitz, Patricia, Javier, María and Alba, their help. The talks with Jonathan about electrochemistry and corrosion, the references... Larraitz's help with the tests, especially in the final stage of this thesis. Javier, Maria and Patricia's help in metallography and Alba's support.

Beyond ACCT, I would like to extend my thanks to the rest of the people of Cidetec Surface Engineering and especially to Asier for his support, to Dra. Naroa Imaz Molina for her help in issues related to electrochemistry, corrosion and chemometry, and to Yolanda, for her friendship, support and nice coffee time together.

I wish to express my special thanks to Iker and Ione for their friendship, motivation, help and understanding in my most difficult times. Thank you very much!

And finally, I would like to express my gratitude to Ama, Juanjo and Aita (I cannot forget you).

And to the amazing family I have, Udane, Eñaut and Sergio, thank you for you continuous support. Mila esker!

Contents

Resumen **9**

Summary **15**

Chapter 1 General Introduction **19**

1.1. Decorative nickel-chromium coatings **21**

1.1.1. Decorative nickel-chromium: coatings development 22

1.1.2. Decorative nickel-chromium: corrosion mechanism 27

1.2. Corrosion evaluation **29**

1.2.1. Accelerated corrosion tests. CASS test 29

1.2.1.1. CASS test background 31

1.2.1.2. Current impact of Copper in the environment 33

1.2.2. Electrochemical techniques 34

1.2.2.1. Conventional electrochemical techniques 35

1.2.2.2. Localised electrochemical techniques 40

1.3. Chemiometrics **43**

1.3.1. Pattern recognition methods 44

1.3.2. Prediction methods 44

1.3.3. Chemiometrics in corrosion 45

1.4. Objectives **45**

1.5. References **47**

Chapter 2 An SKP and EIS study of microporous nickel-chromium coatings in copper containing electrolyte **53**

2.1. Introduction **55**

2.2. Experimental **57**

2.2.1. Materials 57

2.2.2. Conventional electrochemical tests in bulk solution 57
2.2.3. Localised tests: SKP droplet and surface scan measurements 58
2.2.4. Electrolyte analysis 59
2.2.5. Surface analysis 59
2.2.6. Morphological characterisation 59
2.3. Results and discussion 60
2.3.1. Conventional electrochemical tests in bulk solution 60
2.3.1.1. Open Circuit Potential (OCP) 60
2.3.1.2. Morphological characterisation 61
2.3.1.3. Electrochemical Impedance Spectroscopy (EIS) 62
2.3.2. Scanning technique. SKP tests 67
2.3.2.1. Electrolyte composition 69
2.3.2.2. Identification of the white precipitate 70
2.3.2.3. Phenomena inside the Cu+Cl droplet 72
2.3.2.4. Surface area scan 74
2.3.2.5. Morphological characterisation 75
2.4. Conclusions 77
2.5. References 77

Chapter 3 The impact of corrosion on microporous nickel-chromium coatings as a function of the electrolyte 83
3.1. Introduction 85
3.2. Experimental 87
3.2.1. Materials 87
3.2.2. Electrochemical evaluation 87
3.2.3. Electrolyte transformation test 88
3.2.4. Characterisation 89
3.3. Results and Discussion 89
3.3.1. OCP under Cl and Cu+Cl electrolytes 89
3.3.2. Surface modification 90
3.3.3. Cross-section characterisation by FE-SEM 90
3.3.3.1. Shape of the active sites 91
3.3.3.2. Type and width of active sites 92
3.3.3.3. Height of active sites 94

3.3.4. Polarisation curves of microporous nickel-chromium multilayer samples... 94
3.3.4.1. Complete samples ... 94
3.3.4.2. Incomplete samples ... 96
3.3.4.2.1. Polarisation curves in Cl electrolyte ... 97
3.3.5. Electrolyte transformation test ... 100
3.4. Conclusions ... 103
3.5. References ... 103

Chapter 4 SECM study of microporous nickel-chromium coatings: monitoring Cu^{2+} and oxygen reduction reactions ... 107
4.1. Introduction ... 109
4.2. Experimental ... 111
4.2.1. Materials ... 111
4.2.2. OCP measurements ... 111
4.2.3. Characterisation ... 111
4.2.4. SECM ... 112
4.2.4.2. Approaching curves ... 113
4.2.4.3. Area scans ... 113
4.2.4.4. Point measurements ... 114
4.3. Result and Discussion ... 114
4.3.2. Surface characterisation ... 114
4.3.2.1. FE-SEM analysis ... 114
4.3.2.2. GD-OES Analysis ... 117
4.3.3. SECM monitoring of as received ... 118
4.3.3.1. Determination of UME´s potentials in Cu+Cl electrolyte ... 118
4.3.3.2. Approaching curves ... 119
4.3.3.3. Area scans of as-received samples ... 121
4.3.4. SECM monitoring of exposed samples ... 122
4.3.4.1. Determination of UME´s potential in Cl electrolyte ... 123
4.3.4.2. Determination of sample´s polarisation potential in Cl electrolyte ... 123
4.3.4.3. Area scans ... 124
4.3.5. Effects of copper deposition in the corrosion mechanism ... 125
4.4. Conclusions ... 129

4.5. Bibliography 129

Chapter 5 Towards a correlation between Copper Acetic Acid-Salt Spray test and electrochemical results for decorative multilayer nickel-chromium coatings ... 135

5.1. Introduction 137

5.2. Experimental 140

5.2.1. Materials 140

5.2.2. Electrochemical tests 141

5.2.3. Accelerated corrosion tests 142

5.2.4. Characterisation 142

5.2.5. PCA and PLS-DA analysis 142

5.3. Results and discussion 143

5.3.1. Electrochemical tests 143

5.3.2. CASS test 147

5.3.3. Exploratory data analysis. Principal component analysis (PCA) 148

5.3.3.1. CASS electrolyte 149

5.3.3.2. NaCl electrolyte 150

5.3.3.3. CASS and NaCl electrolytes together 151

5.3.4. Cross-section characterisation by FE-SEM 152

5.3.5. Identification of the most discrimating variables 153

5.3.6. Classification methods. Prediction by PLS-DA 155

5.3.6.1. PLS-DA theory 155

5.3.6.2. PLS-DA methodology 155

5.3.6.3. PLS-DA results 156

5.4. Conclusions 158

5.5 Bibliography 159

Chapter 6 Annex I-Chapter 3 163

6.1. Corrosion mechanism as a function of the electrolyte 165

6.1.1. Cl electrolyte 165

6.1.1.1. Deaerated polarisation curves 166

6.1.1.2. Confirmation of the effect of nickel layers potential difference decrease in corrosion. Study of pH effect in chloride electrolyte 167

6.1.2. Cu+Cl electrolyte 170

6.2. References 172

Conclusions 175

List of contributions 177

Resumen

Esta tesis se centra en la investigación de la corrosión de recubrimientos decorativos multicapa de níquel-cromo sobre ABS bajo las condiciones de ensayos acelerados. El principal propósito de la tesis es obtener un mayor conocimiento del mecanismo de corrosión en condiciones CASS y explorar si existe una correlación entre los ensayos CASS y las técnicas electroquímicas, de forma que se posible la predicción del comportamiento de los recubrimientos decorativos multicapa de níquel-cromo en el ensayo CASS por medio de ensayos electroquímicos.

La tesis consta de seis capítulos. El primer capítulo es una introducción general al tema de la investigación y sus antecedentes. Los siguientes cuatro capítulos presentan los resultados de la tesis y están basados en artículos publicados o a enviar a revistas científicas internacionales. El último capítulo es un anexo al Capítulo 3. Por último, la tesis termina con las conclusiones, la lista de contribuciones a congresos y las publicaciones derivadas del trabajo.

El primer capítulo describe brevemente los recubrimientos decorativos de cromo, los métodos de evaluación de la corrosión y los métodos quimiométricos. Los recubrimientos de cromo decorativo consisten en una disposición multicapa de varios depósitos de níquel recubiertos por una última capa de cromo expuesta al exterior. Estos recubrimientos se caracterizan por su aspecto elegante y altamente reflectante y su alta resistencia a la corrosión, entre otras características. Los recubrimientos de cromo decorativo se usan como acabado en una gran variedad de aplicaciones, desde artículos de uso en interiores (p.ej. mobiliario), hasta aplicaciones que requieren una alta resistencia a la corrosión como los componentes exteriores de automoción.

En el caso de las aplicaciones de automoción, los recubrimientos de cromo decorativo son expuestos a condiciones ambientales muy diversas y agresivas tales como gradientes de temperatura, sales descongelantes de carreteras, humedad, lluvia, nieve y contaminación. Por ello, además de preservar la apariencia estética con el tiempo, estos recubrimientos deben mostrar una alta resistencia a la corrosión en ambientes diversos y condiciones extremas, y por lo tanto la evaluación de la resistencia a la corrosión se convierte en una cuestión relevante.

La evaluación de la corrosión puede realizarse mediante ensayos de corrosión acelerada o mediante técnicas electroquímicas. Los ensayos de corrosión acelerada

son muy utilizados en la industria, siendo el ensayo de niebla salina cupro-acética (ensayo CASS) el más empleado para la caracterización de los recubrimientos de cromo decorativo. Una de las principales particularidades de este ensayo acelerado es que incluye el ión cúprico en la composición del electrolito. El ión cúprico es un contaminante relacionado con los ambientes de tráfico rodado, sin embargo, su efecto en la corrosión de los recubrimientos de cromo decorativo no ha sido investigado en profundidad y el ensayo CASS es utilizado indiscriminadamente sin comprender correctamente la agresividad de la exposición del ensayo. A pesar de las muchas ventajas que los ensayos de corrosión acelerada presentan, existen algunos inconvenientes tales como la subjetividad de la evaluación, el tiempo necesario para completar el ensayo y la falta de información de los motivos por los que un recubrimiento pasa o falla el ensayo.

Muchos estudios de corrosión son abordados mediante técnicas electroquímicas dado el carácter electroquímico de los procesos de corrosión. Estas técnicas permiten determinar parámetros termodinámicos y cinéticos característicos de los procesos de corrosión, y por lo tanto, obtener datos cuantitativos. Además, el tiempo necesario para realizar los ensayos electroquímicos es normalmente inferior al tiempo requerido para los ensayos acelerados. Las citadas características de los ensayos electroquímicos dan solución a los principales problemas de los ensayos acelerados. Por lo tanto, resulta interesante explorar si existe una correlación entre los resultados obtenidos en los ensayos CASS y ensayos electroquímicos dado que podría suponer una importante mejora en la evaluación de la corrosión de los recubrimientos decorativos de níquel-cromo.

Las técnicas electroquímicas pueden dividirse en dos categorías: técnicas electroquímicas convencionales y técnicas electroquímicas localizadas. La principal diferencia entre ambas se encuentra en la distancia a la superficie con la que se hace la medida y la escala en tamaño. En los métodos convencionales la respuesta medida es promediada al área estudiada, mientras que en los métodos localizados, gracias a su mayor resolución, es posible estudiar localmente los procesos que pueden estar ocurriendo en una determinada zona dentro del área total. Dada la complementariedad de ambas métodos, convencionales y localizados, la combinación de sus resultados brinda un mejor conocimiento de los procesos de corrosión estudiados.

Por lo tanto, la combinación de técnicas electroquímicas convencionales y localizadas puede ser un enfoque interesante de cara a profundizar en el conocimiento de la agresividad del ensayo CASS en recubrimientos de cromo decorativo, sobre todo

teniendo en cuenta que el estudio de la corrosión de estos recubrimientos no ha sido abordado aún mediante técnicas localizadas.

Por otro lado, con respecto al estudio de la correlación entre ensayos electroquímicos y ensayos de corrosión acelerados, cabe esperar la obtención de una gran cantidad de variables dado el gran número de ensayos electroquímicos disponibles para el estudio del comportamiento de los recubrimientos de níquel-cromo decorativo. Este hecho dificultaría la interpretación de los resultados y la búsqueda de una correlación por medio de un análisis univariable.

En este sentido, los métodos quimiométricos pueden resultar ser una herramienta muy útil. La quimiometría permite la observación de más de una variable al mismo tiempo mediante el análisis multivariable, simplificando de esta forma la búsqueda de interrelaciones cuando se maneja una gran cantidad de parámetros.

La parte final del primer capítulo incluye los objetivos de la tesis que son: (1) comprender el mecanismo de corrosión bajo condiciones de ensayo CASS de los recubrimientos de níquel-cromo decorativo y (2) explorar si existe una correlación entre ensayos electroquímicos y ensayos en cámara CASS, de forma que permita la predicción de los resultados de los recubrimientos en el ensayo CASS por medio de ensayos electroquímicos.

El capítulo concluye con las hipótesis de las tesis: (1) El mecanismo de corrosión de los recubrimientos estudiados en inmersión (mismo electrolito que en ensayo CASS) es similar al mecanismo de corrosión que tiene lugar en el ensayo CASS y (2) existe una correlación entre el daño estético en ensayo CASS de los recubrimientos decorativos estudiados y la respuesta electroquímica de los recubrimientos.

En el segundo capítulo de la tesis se investiga el efecto perjudicial de los cationes Cu^{2+} en los recubrimientos de microporosos de níquel-cromo decorativo. Se trata de un estudio exploratorio por medio de las técnicas convencionales de potencial de circuito abierto (también conocido como OCP) y espectroscopia de impedancia electroquímica (también conocida como EIS) y la técnica localizada de sonda kelvin de barrido (también conocida como SKP). Para ello se emplearon 2 electrolitos, el electrolito del ensayo CASS y ese mismo electrolito sin iones Cu^{2+}. Los ensayos convencionales se llevaron a cabo en celda de corrosión mientras que los ensayos mediante SKP se llevaron a cabo siguiendo dos metodologías: 1) gotas de electrolito sobre las muestras y medida simultánea de la evolución del potencial y altura de la gota y 2) mapas de potenciales

de las superficies (secas) que previamente habían sido expuestas a las gotas. Así mismo, se llevaron a cabo ensayos de caracterización de la morfología del ataque de la corrosión, de la composición de la superficie y del cambio de la composición del electrolito con el tiempo.

Los resultados muestran el efecto perjudicial de los cationes Cu^{2+} en el aspecto de la superficie después del ataque y en la resistencia a la corrosión. La precipitación del compuesto CuCl en el interior de la gota confirma la reducción de Cu^{2+} a Cu^{+}, la estabilización de Cu^{+} en el electrolito mediante la formación de complejos cloruros y su papel clave en el proceso de corrosión. El trabajo presentado en este capítulo fue publicado: Larraitz Ganborena, Jesús Manuel Vega, Berkem Özkaya, Hans-Jürgen Grande, Eva García-Lecina, “Electrochimica Acta”, 2019, 318, 683-694.

El tercer capítulo de la tesis muestra el impacto del catión Cu^{2+} en la corrosión de las diferentes capas de níquel de los recubrimientos microporosos de níquel-cromo. En este capítulo se han empleado técnicas convencionales tales como OCP, curvas de polarización y EIS. Se han estudiado diferentes condiciones mediante el empleo de diferentes electrolitos: CASS, CASS sin Cu^{2+} y CASS con el doble de concentración de Cu^{2+}, y de diferente aireación de los electrolitos. Tras la exposición a los electrolitos, las muestras fueron caracterizadas mediante microscopía óptica y microscopía electrónica de barrido de emisión de campo (conocida también como FE-SEM), lo que permitió valorar la degradación de las muestras. Los resultados han mostrado que al añadir Cu^{2+} a un electrolito de cloruros, además de un aumento de la velocidad de corrosión, tiene lugar un cambio de mecanismo de corrosión que afecta al tipo de capa de níquel que es atacado por la corrosión. Las curvas de polarización mostraron que la clave estaba en las diferentes reacciones de reducción y los potenciales establecidos entre las distintas capas de níquel durante el proceso de corrosión. El trabajo presentado en este capítulo será enviado a la revista “Corrosion Science”.

El cuarto capítulo de esta tesis demuestra que la reducción de los iones Cu^{2+} protege la capa de níquel microporoso de la corrosión durante la exposición del recubrimiento al electrolito CASS. El proceso de corrosión de los recubrimientos microporosos de níquel-cromo es estudiado a nivel localizado mediante el empleo del microscopio electroquímico de barrido (también conocido como SECM). La combinación de diferentes modos de SECM ha confirmado la reducción escalonada de Cu^{2+} a Cu^{0} durante la corrosión de los recubrimientos. La caracterización de muestras mediante la técnica de espectroscopia de emisión óptica por descarga luminiscente (también conocida como GD-OES) y FE-SEM han permitido detectar la presencia de partículas

de cobre en la capa de níquel microporoso expuesta a través de los microgrietas de la capa de cromo. Además, el SECM ha permitido identificar los depósitos de cobre monitorizando su actividad catalítica reduciendo el oxígeno disuelto en el electrolito. El conjunto de estos resultados indica que la protección de la capa de níquel microporoso durante el proceso de corrosión en electrolito CASS pude ser debido a su comportamiento catódico y al aumento local del pH consecuencia de la actividad catalítica de las partículas de cobre depositadas sobre dicho níquel. El trabajo presentado en este capítulo será enviado a la revista “Electrochimica Acta”.

El quinto capítulo que conforma esta tesis explora, mediante el empleo de métodos quimiométricos, la correlación entre los resultados en ensayos CASS y ensayos electroquímicos para los recubrimientos decorativos de níquel-cromo. Para ello se ha estudiado el comportamiento de cuatro recubrimientos diferentes de níquel-cromo (uno obtenido mediante baños de cromo hexavalente y tres sistemas, dos de ellos defectuosos debido a modificaciones de la capa de cromo, obtenidos a partir de baños de cromo trivalente). Las técnicas electroquímicas empleadas han sido: OCP, EIS y curvas de polarización, y los ensayos electroquímicos se han llevado a cabo con electrolito CASS y electrolito CASS sin Cu^{2+}. El análisis mediante componentes principales (también conocido como PCA) de los diferentes grupos de datos electroquímicos obtenidos ha mostrado que las muestras estudiadas se pueden agrupar en tres grupos que están perfectamente separados: uno perteneciente a las muestras obtenidas mediante baños de cromo hexavalente, otro a piezas de baños trivalente y un último grupo con piezas trivalente con la capa de cromo modificada (capa no porosa y con doble espesor, respectivamente). Los datos de OCP en electrolito CASS son, de entre las distintas variables electroquímicas estudiadas, los que incluían las variables más discriminantes a la hora de describir las muestras. El método de análisis discriminante de mínimos cuadrados parciales (Conocido también como PLS-DA) ha permitido construir un modelo de predicción del comportamiento en ensayo CASS a partir de datos electroquímicos obtenidos en electrolito CASS y después de una etapa de selección de variables electroquímicas. Los resultados presentados muestran una correlación entre los resultados en ensayo CASS y los ensayos electroquímicos y que la aplicación de las herramientas quimiométricas parece ser un enfoque muy prometedor en la búsqueda de un modelo de predicción para el comportamiento frente a la corrosión de los recubrimientos de níquel-cromo decorativo. El trabajo presentado en este capítulo será enviado a la revista “Corrosion Science”.

Y para concluir, el último capítulo incluido en la tesis es un anexo que contiene resultados adicionales que corroboran las conclusiones presentadas en el capítulo 3.

Summary

The corrosion mechanism of decorative chromium coatings has been investigated in detail under aggressive conditions with and without cupric ions in the environment (either immersion or cabinet exposure). The main purpose of the thesis is to achieve a better understanding of the corrosion mechanism in order to explore whether a correlation between CASS test and electrochemical techniques exists. It could allow the prediction of CASS test performance by means of electrochemical tests.

This thesis is divided into six chapters. The first chapter is a general introduction based on the background and the different techniques to be used. The analysis and discussion of the results are addressed from chapter 2 to 5 which are based on articles published and to be submitted in international scientific journals. For consistency's sake, these chapters are structured like a research article (except the abstract section). Chapter 6 is an annex to chapter 3. Finally, the thesis ends with the chapter of conclusions and a list of conference presentations and publications.

Chapter 1 briefly describes the development of decorative chromium coatings during the last decades. These coatings consist of a multilayer arrangement of nickel deposits and a top layer of chromium confers an elegant and high reflective appearance among other features. It provide them a huge variety of applications from indoor (e.g. furniture) to outdoor (e.g. automotive exterior components). In the later, coatings are exposed to miscellaneous ambient conditions such as temperature gradients, de-icing road salts, humidity, rain, snow and pollution, where degradation and corrosion play an important role.

Therefore, not only the aesthetic appearance with time becomes one of the most important issues of the coating, but also corrosion resistance. In fact, corrosion evaluation is usually performed by accelerated corrosion tests or by electrochemical techniques. Accelerated corrosion tests are widely used in industry such us Copper Accelerated Acetic Acid Salt Spray test (CASS test). This peculiar test includes cupric ions into the electrolyte composition (which is a pollutant related to automotive environments) although there are uncertainties about its role and impact. Moreover, its main drawbacks are the subjectivity during their evaluation for passing or failing the test.

Then, in order to obtain complementary information to the CASS test and considering the electrochemical character of corrosion processes, there are a broad variety of electrochemical techniques that could be used to explore the corrosion of these coatings.

In general, it is possible to obtain information about the thermodynamic and kinetic features of the corrosion process, and hence, quantitative data. In addition, the time required for electrochemical tests is usually shorter than the one for accelerated tests. Therefore, not only electrochemical tests provide additional information, but also are able to overcome the drawbacks of accelerated ones. As a consequence, it seems interesting to explore whether exists a correlation between the results obtained by CASS test and the ones by electrochemical tests. Definitely, it could result in an improvement of the corrosion evaluation of the decorative nickel-chromium samples.

Electrochemical methods can be divided in two categories: conventional electrochemical techniques and localised ones. The main difference are based on how close the measurement is made from the surface and its scale in size. Conventional methods provide an averaged response from the studied area, whereas in localised methods, due to the higher resolution of these techniques, local redox processes that are taking place on the surface can be measured. The combination of both, conventional and localised techniques, leads to a better understanding of the corrosion processes due to the complementarity of the information that is obtained.

Then, in order to get in-depth knowledge of CASS aggressiveness in multilayer nickel-chromium coatings, conventional and localised electrochemical techniques has been used as an innovative approach, taking into account that localised techniques have not been explored yet for these systems.

On the other hand, it has been explored whether a correlation between electrochemical tests and accelerated test exists. Thanks to the variety of electrochemical tests used to study the corrosion of multilayer nickel-chromium coatings, a large amount of variables and parameters were obtained. Unfortunately, this fact would make difficult to seek for a correlation by univariate analysis and to handle all the results. In that sense, chemiometric methods could be a very useful tool that enable to observe more than one variable at the same time by multivariate analysis, that extremely simplify the search for interrelationships when dealing with a high number of parameters.

The final part of the first chapter includes the objectives of the thesis: (1) understanding the corrosion mechanism under CASS test conditions and (2) exploring whether exits a correlation between electrochemical test and CASS chamber test that could allow the prediction of CASS test performance by electrochemical tests. Finally, the chapter ends with the hypothesis of the thesis.

In the second chapter, the harmful effect of Cu^{2+} cations in decorative nickel-chromium coatings was investigated. The conventional electrochemical techniques Open Circuit Potential (OCP) and Electrochemical Impedance Spectroscopy (EIS) and the localised technique Scanning Kelvin Probe (SKP) were used in the study. Two electrolytes were employed, CASS test electrolyte and CASS test electrolyte without cupric ions. OCP and EIS measurements were performed in bulk solution, whilst Scanning Kelvin Probe (SKP) measurement were carried out using two methodologies: i) electrolyte droplets monitoring (measuring simultaneously potential and droplet height with time), and ii) potential maps of dried surfaces that previously were exposed to droplets. The morphology of the attack, composition on the surface and electrolyte composition with time were characterised. Results showed the different morphological impact on the surface and the harmful effect in the corrosion resistance of Cu^{2+} cations. Apparently, the Cu^{+} generated by Cu^{2+} reduction in the cathodic reaction of the corrosion process was stabilised in bulk solution by the formation of chloride complexes, as was confirmed by the precipitation of a white CuCl compound during droplet evaporation, pointing out the key role of Cu^{+} in the corrosion process. The work presented in this chapter was published: Larraitz Ganborena, Jesús Manuel Vega, Berkem Özkaya, Hans-Jürgen Grande, Eva García-Lecina, Electrochimica Acta, 2019, 318, 683-694.

The third chapter illustrates the effect of Cu^{2+} ions in the corrosion behaviour of microporous nickel-chromium multilayer coatings. It was investigated by means of electrochemical techniques such as OCP, potentiodynamic polarisation curves and EIS. Data was obtained under exposure to chloride electrolytes, varying cupric ions concentration and aeration conditions. Field Emission Scanning Electronic Microscopy (FE-SEM) was used to obtain cross-section images of the degradation front. Results have shown that Cu^{2+} is governing the reduction reaction independently of the presence of oxygen. Moreover, the corrosion mechanism was modified in absence of Cu^{2+} ions affecting several nickel layers during corrosion. The work presented in this chapter will be submitted to Corrosion Science.

The fourth chapter of the thesis demonstrates that microporous nickel layer does not undergo corrosion during exposure to CASS electrolyte. The corrosion of microporous nickel-chromium multilayer coatings was studied at localised scale by Scanning Electrochemical Microscopy (SECM) under such electrolyte. The combination of different modes of the SECM confirmed the Cu^{2+} stepwise reduction to Cu^{0}. In fact, additional characterisation by Glow Discharge-Optical Emission Spectroscopy (GD-OES) and FE-SEM showed the deposition of Cu^{0} particles along microcracks belonging to the chromium layer, although they were located over the surface of the microporous nickel

layer. Interestingly, the combination of two different modes (competition one and transient Surface Generation/Tip Collection mode) facilitated the identification of such copper deposits by monitoring their catalytic activity for ORR. All these results pointed out that the protection of microporous nickel layer during the corrosion process might be due to: (i) The formation of a protective layer of cuprous-chloride complexes ($CuCl$, $CuCl_2^-$) due to the reduction reactions of cupric ions on the surface, (ii) the increase of the pH at local scale caused by the catalytic activity of copper particles, and (iii) the presence of microcathodes confer a cathodic behaviour to the microporous nickel layer. The work presented in this chapter will be submitted to Electrochimica Acta.

The last chapter of this thesis explores the correlation between results in CASS test and electrochemical test for multilayer nickel-chormium multilayer coatings. The behaviour of four different nickel-chromium coatings (a system based on chromium (VI) bath and three systems, two of them defective due to the modification of the chromium layer, based on chromium (III) baths) were studied by the exposure to CASS test and by means of conventional electrochemical techniques such as OCP, EIS and potentiodynamic polarisation curves. Two different electrolytes were used based on CASS test electrolyte with and without cupric ions. Principal component analysis (PCA) of the electrochemical data set showed the clustering of the data into three different groups. It was possible to split samples from hexavalent plating bath, trivalent plating bath and the two systems plated from trivalent bath but with modified chromium layer (defective ones). OCP data recorded in CASS electrolyte was found to include the most discriminating variables in the description of the samples. Finally, a predictive model was built applying Partial Least Squares Discriminant Analysis (PLS-DA) to the electrochemical data set obtained in CASS electrolyte after an screening step for variable selection. Results showed that a correlation between electrochemical data and the corrosion behavior exist. It confirmed that the application of chemometric tools seem to be a very promising approach seeking for a prediction model in terms of corrosion behavior for multilayer nickel-chromium coatings. The work presented in this chapter will be submitted to Corrosion Science.

The last chapter of this thesis is an annex containing additional results that sustain the conclusions of Chapter 3.

1

General Introduction

1.1. Decorative nickel-chromium coatings

Chromium finish is widely demanded for decorative purposes due to its elegant bright and highly reflective appearance and the advantageous physical and chemical properties that provides to the coated surface. The main characteristics of chromium as a metal coating are high corrosion, wear, tarnish and scratch resistance [1,2]. Decorative chromium has many different applications: from indoor used items such as domestic appliances, plumbing tabs and furniture, to the high corrosion resistance requiring automotive exterior components (see Figure 1.1).

Figure 1.1. - Typical applications of decorative chromium coatings [3].

Nickel-chromium coatings consist on a thin chromium layer plated over an electroplated nickel deposit. These underneath nickel electrodeposits are normally preceded by a copper layer and they are usually composed by more than one nickel layer. Nickel-chromium coatings can be plated over a great variety of substrates such as plastics, aluminium, steel and copper alloys. In decorative applications, plastic substrates are widely use due to their lower cost, flexibility in parts design and reduced weight compared to metal substrates. Acrylonitrile Butadiene Styrene (ABS) is the most used plastic substrate because just a chemical etching process step is enough for the later plating of an adherent metal deposit on it [4]. Chromium layer usually has a thickness lower than 0.5 µm whereas the overall nickel deposit ranges from 5 to 50 µm, depending on the application of the decorative coating [1,2].

Traditionally, chromium has been plated from electrolytes composed by hexavalent chromium salts. However, hexavalent chromium has been classified as a carcinogenic and its use is limited and controlled by the European Chemicals Agency (ECHA) [5]. Therefore, great efforts have been made by the industry in order to search for viable alternatives to hexavalent chromium which meets the established performance standards of the chromium decorative coatings [6]. Among these alternatives, chromium

plating baths composed by trivalent chromium ions is found to be the most promising one. Even if trivalent chromium baths were known and described in patents since late 1920s [7], it was not until about 1975 that trivalent chromium processes started to be more seriously developed, even substituting some decorative hexavalent chromium baths installations [1]. Nowadays, thanks to these intensive efforts, trivalent chromium baths are widely used for producing decorative coatings with a bluish white appearance and performance characteristics comparable to the coatings obtained by hexavalent chromium plating baths [1,8].

1.1.1. Decorative nickel-chromium: coatings development

At the beginning of the XX century, despite of nickel coatings were used for decorative purposes, its main role was the corrosion protection of metallic substrates rather than its visual appearance. In fact, aesthetics requirements were not so demanding at that time, a slight degree of dulling or blemishes on the surface were permitted if corrosion requirement was fulfilled. Unfortunately, it implied much more maintenance (e.g. cleaning and buffing) for keeping a lustrous appearance due to its initial dull finish when plated and as consequence of tarnishing by the exposure to atmosphere.

Meanwhile, chromium plating processes were under development and it was in 1924 when the first commercial electrodeposition of chromium processes came out. These first chromium deposits were thick and dull and also needed to be polished to become a shiny coating. As a consequence, it was accepted that chromium plating could not replace nickel electrodeposits for decorative purposes. The electrodeposition of a thin chromium layer over nickel was found to have a beneficial effect in the appearance of the plated piece. The top chromium layer plated over the polished and mirror-like nickel deposit ensured the decorative finish of the coating. Additionally, the nickel-chromium pairing also showed an improvement in the corrosion resistance and protection of the metallic substrate. However, there was still a need for better systems in terms of performance and cost [9,10]. Figure 1.2 shows the corrosion progress in nickel-chromium coatings. A galvanic cell is established between nickel, chromium layer and environmental electrolyte (salt solution) as a consequence of the exposure of interior nickel by chromium layer defects. Due to the differences in the electrochemical potential in between chromium and nickel, chromium layer becomes the cathode (-) whereas nickel acts as the anode (+). As a result of this galvanic coupling, nickel layer corrodes. Once corrosion has reached the basis metal (of lower nobility than nickel deposits), it spreads there and the piece integrity is at risk as consequence of the substrate degradation.

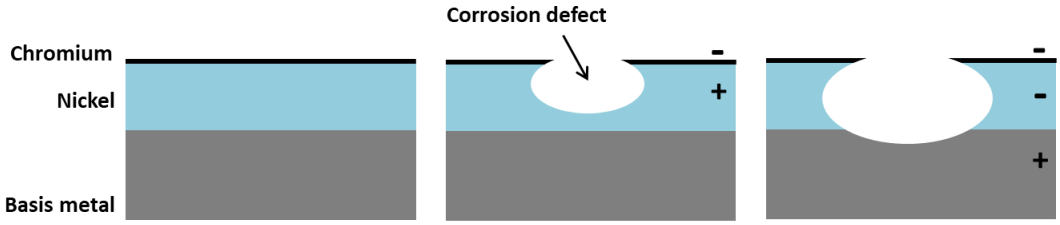

Figure 1.2.- Corrosion mechanism of nickel-chromium coatings.

The evolution of this type of coatings was described below, where Table 1. 1 shows the main achievements. One of the issues to overcome was the need of polishing the nickel deposit for achieving a brilliant substrate for chromium plating. A process for plating nickel that led to a bright finish was encountered by the addition of organic compounds that accomplished for brilliant and levelled sulphur-containing nickel coatings. However, it was observed that the bright nickel-chromium coating was not as good in corrosion as the Watts nickel-chromium combination it intended to substitute. The responsible for the lower performance of the coatings was ascribed to the presence of sulphur in the bright nickel plating, which seemed to increase the activity of nickel [11]. As a consequence, the efforts in the improvement of the nickel-chromium coatings were focused in the search for a sulphur-free bright nickel.

The next key achievement in the improvement of decorative nickel-chromium coatings was the development of semibright nickel coatings. Semibright nickel is a sulphur free coating that exhibited a corrosion resistance similar to polished Watts nickel. Despite the need of polishing to make the deposit bright before chromium plating, it was very employed in the plating of automobiles bumpers from 1945 to 1950 due to its improved corrosion resistance. In a further development in order to suppress semibright nickel layer polishing step and its associated cost, bright nickel layer was plated over semibright nickel layer [12], giving rise to a deposit called “duplex nickel”. Results showed that the corrosion performance of duplex nickel-chromium coating on automotive applications was better than the chromium plated semibright nickel coatings. From an electrochemical point of view, the improved corrosion performance observed was a consequence of the different activities (potentials) of the nickel layers [13]. Bright nickel, with lower nobility as consequence of sulphur incorporation on its composition, behaved anodically and preferentially corroded when galvanically coupled with semibright nickel and in the overall nickel-chromium deposit, acting as a sacrificial anode. As a result, the corrosion spread laterally in the bright nickel layer, without reaching the metallic substrate underneath semibright nickel, ensuring a longer life to the plated piece, as detailed in Figure 1.3.

Table 1. 1.- Summary of the principal achievements in nickel-chromium decorative coatings development.

Period	Challenge	Result	Corrosion mechanisms
1924	Improvement of decorative nickel coatings appearance	Nickel-chromium coatings	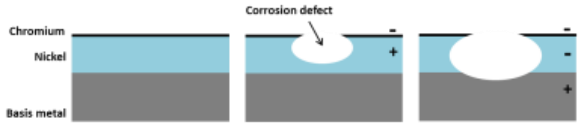
1936-1940	Bright nickel substrate	Bright nickel	
1953	Sulphur free bright nickel	Semibright nickel	
1953	Suppress semibright nickel polishing	Duplex nickel	
1960-1965	Microdiscontinuos chromium	Reduction of current per corrosion cell	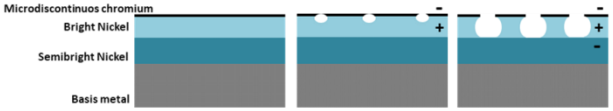
1963-1968	Microporous chromium	Triple nickel: hidden corrosion is achieved	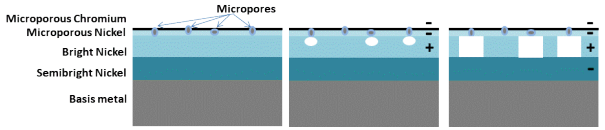

Figure 1.3.- Corrosion mechanism of duplex nickel-chromium coatings.

At the late 1950s, a new finding this time related to the chromium plated layer characteristics resulted in an improvement in the corrosion protection of the multilayer coatings. It was known that corrosion in the nickel layer started at pores or defects in the chromium layer that, due to the lower potential of the nickel layer with regards to noble top chromium layer, corroded preferentially. Therefore, it was supposed that crack-free or defect-free chromium layers could improve the corrosion protection avoiding the set-up of nickel-chromium corrosion cells. Several processes for crack-free chromium plating were developed by the 1960s but they were abandoned because these coatings quickly developed large cracks during service negatively affecting the appearance and corrosion resistance. At that time, it was observed that microdiscontinuities in the chromium layer were advantageous for the overall corrosion protection. The low amount of pores or defects obtained in conventionally plated chromium layer caused that the established nickel-chromium corrosion cells were characterised by having a small anodic site surrounded by a large cathodic area. As a consequence, corrosion at those few sites was fast. On the other hand, if cathodic area (chromium layer) was decreased while anodic area was increased (nickel), the amount of current per corrosion cell was significantly less and corrosion at each site was diminished [14]. This beneficial effect of decreasing the surrounding cathodic area at each corrosion site was achieved by microdiscontinuos chromium deposits and is detailed in Figure 1.4. Different approaches were developed for plating microdiscontinuos chromium layers, resulting in either the formation of micropores [15] or microcracks [16]. Among them, the most popular process is the plating of microporous chromium layers by electrodepositing the top chromium layer over a thin nickel layer that incorporates no conducting microparticles (known as microporous nickel). These particles avoid the deposition of a continuous chromium layer and create micropores that provide access to the underneath nickel deposit.

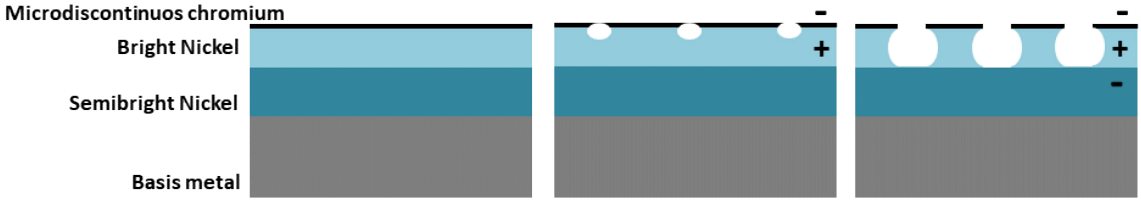

Figure 1.4.- Corrosion mechanism of duplex nickel and microdiscontinuous chromium coatings.

Another extra role was identified for microporous nickel layer. Duplex nickel showed the effect that nickel layers with different electrochemical potential could have in the overall corrosion protection of the coatings. Therefore, it was assumed that the electrochemical potential of the microporous nickel layer could also play an important role in the performance of the nickel-chromium coatings. Plating a microporous nickel layer with a higher electrochemical potential than the underneath bright nickel layer, favoured the penetration of the corrosion front through the micropores to the non-noble bright nickel layer, which corroded preferentially as detailed in Figure 1.5.

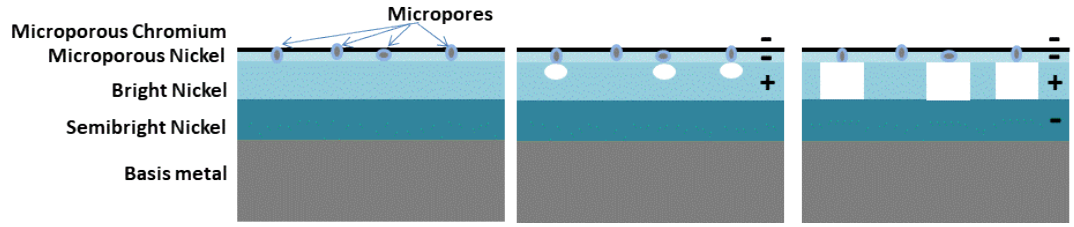

Figure 1.5.- Corrosion mechanism of triple nickel layer and microporous chromium coatings.

The main advantage of this electrochemical potential configuration leading to the bright nickel layer corrosion is that corrosion defects are hidden while the surface looks free of blemish, greatly improving the aesthetic performance of the coatings. At this stage, it can be considered an optimum performance for these coatings: delaying corrosion penetration to the bases metal and improving the aesthetic appearance. Despite bright nickel layer corrosion, chromium undermining (visible superficial defect) is delayed by the mechanically support provided by the non-corroded microporous nickel layer until bigger corrosion defects size are developed, leading to a better corrosion performance even after extensive exposure to severely corrosive environments. The effect of the microporous nickel layer hiding corrosion defects is clearly observed in Figure 1.6 cross-section images from [17], where duplex nickel plus highly porous chromium layer corrosion (Figure 1.6 (a)) is compared to the corrosion underwent by a triple nickel-

chromium coating (Figure 1.6 (b)). Whereas in the first coating corrosion defects are open, and therefore visible from the exterior, in the triple nickel-chromium coating, corrosion defects are not observable from the exterior, they are underneath microporous nickel and chromium layer.

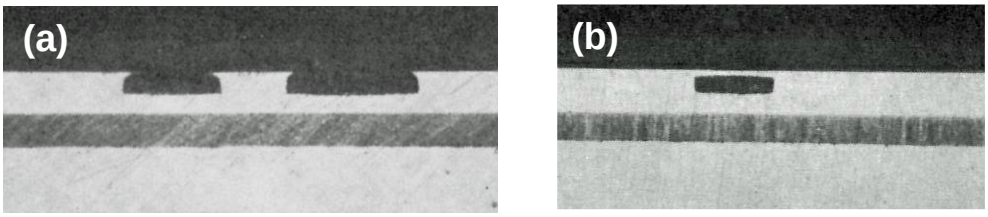

Figure 1.6.- (a) Corrosion defects differences between duplex nickel and highly porous chromium coating, and (b) triple nickel layer and highly porous chromium coating [17].

In the last decades, decorative nickel-chromium coatings became a demanded finish in the automotive industry characterised for being a very challenging application due to the aggressiveness of the outdoor exposure (de-icing road salts, pollutant, temperature gradients, etc.). As a consequence, corrosion and aesthetic requirements for these coatings greatly increased, pushing to the improvement of the coatings through the development and refining of processes and specifications.

Nowadays, decorative nickel-chromium coatings based in the triple layer and microporous chromium configuration are used for very severe corrosion services. One example of the most used decorative components in automotive industry are ABS substrates (previously plated with copper) coated by a triple nickel layer and top microporous chromium layer (similar to Figure 1.5). The triple nickel layer is arranged with semibright nickel layer at the bottom and with the highest electrochemical potential, coated by the non-noble bright nickel layer, and on top, the microporous nickel layer, with an electrochemical potential higher than bright nickel layer one´s.

1.1.2. Decorative nickel-chromium: corrosion mechanism

The aforementioned last developments in microdiscontinuos and multilayer nickel-chromium coatings lead to the targeted and hidden bright nickel corrosion (Figure 1.5 and Figure 1.6 (b)). The key characteristics of the corrosion protection of these coatings are: the good passivation properties of chromium that favour the formation of passive chromium oxide on the top of the chromium layer, the cathodic protection of chromium by the multilayer arrangement of nickels, the decreased amount of current per corrosion

cell due to chromium microdiscontinuities and the potential differences between nickel layers.

However, a different corrosion phenomenon has been recently identified. Visual defects have been observed after short winter exposure. The reasons for such a different corrosion mechanism are related with the new trends in the de-icing of roads. The use of de-icing road salt mixtures comprising calcium chloride and magnesium chloride along with the traditional sodium chloride is extending over different countries. The chloride concentration in calcium and magnesium salts is twice the concentration of chloride in sodium chloride. In addition, these salts are strongly hygroscopic and the temperature and humidity range for corrosion events is increased.

Several corrosion mechanisms have been proposed for this corrosion phenomenon. One of them ascribed the premature visual defects observed in nickel-chromium coatings to chromium layer attack under a mixed chemical and electrochemical corrosion reactions [18]. The chemical attack of chromium was found to be very sensitive to the electrolyte pH: low pHs favours the dissolution of chromium layers.

Other authors described a mechanism that included the oxygen concentration effect [19]. They stated that the absence of oxygen in the pores in saturated $CaCl_2$ electrolyte changed the corrosion mechanism from nickel dissolution to chromium corrosion depending on proton concentration. As a consequence of the hydrolysis of the solvated nickel ions within the pores in the absence of oxygen, pH will decrease and cause the autocatalytic dissolution of the passive chromium film. Chromium will become the anode because its potential is more negative than nickel´s one and proton reduction reaction will become the cathodic reaction at the nickel. An autocatalytic passivation of chromium will take place if the pH increases sufficiently, turning back nickel into the anode and chromium into the cathode.

A more recent work described that two corrosion mechanisms could also occur simultaneously or separately under exposure to high concentrated calcium chloride electrolytes in addition to the well-known bright nickel layer corrosion mechanism [20]: the corrosion of the chromium layer and the corrosion of microporous nickel layer. Both mechanisms cause visual defects on the coating surface in a very short period of time.
The corrosion of chromium layer was described to be based on the destruction of the chromium oxide layer as consequence of the composition or pH of the electrolyte, which caused the shift from nickel anode to chromium anode. In addition, they showed that the corrosion of the chromium layer in their system took place from the surface of the coating instead of from the bottom of the chromium layer as in the corrosion described previously

[19]. Whereas to microporous nickel corrosion, the use of specific de-icing electrolytes comprising calcium chloride and potassium ferrocyanide could lead to the anodic behaviour of microporous nickel layer in the absence of oxygen. As a result, chromium layer undermined due to the lack of mechanical support, leading to visual defects on the surface of the coating.

The explanation given for the simultaneous heterogeneous corrosion attack was based on the formation of different galvanic coupling depending on the size and orientation of the inert particles incorporated in microporous nickel layer (chromium/microporous nickel or chromium/microporous nickel/bright nickel) and the use of different de-icing road salts mixtures, oxygen concentration and acidity.

As a summary, the particular arrangement of nickel-chromium coatings, based on a microporous chromium layer and multiple nickel layers with different electrochemical potentials, seems to be very sensitive to high chloride concentration ions and changes in corrosive parameters such as oxygen concentration and pH.

1.2. Corrosion evaluation

As previously mentioned, one particular challenging example of the nickel-chromium decorative applications is found in the exterior components of the automotive industry. These components are exposed to wide environmental conditions, such as high temperature, low temperature, humidity, weather features (e.g. snow, rain), pollution and exposure to aggressive agents (e.g. deicing road salts). This exposure to miscellaneous conditions leads to a high corrosion resistance requirement in diverse and extreme environments. As a consequence, corrosion evaluation becomes an important issue in decorative nickel-chromium coatings.

Real exposure tests are the most certain way to assess corrosion resistance in relevant environment, however they are costly and time consuming [21]. Therefore, there is a need for alternatives to field tests that give relatively quick and reliable information about the corrosion behavior, similar to the one resulting under real service exposure. This issue is actually achieved by the use of accelerated corrosion tests and/or electrochemical techniques.

1.2.1. Accelerated corrosion tests. CASS test

Accelerated corrosion tests are widely used in the industry for addressing and comparing the corrosion performance of metallic coatings. These tests intend to simulate the

environmental conditions under service, but they are much more aggressive, promoting the damage/failure earlier. They are usually based on the exposure of the samples inside of a chamber to a fog of 5 wt % sodium chloride (NaCl) in weight solution at a controlled temperature (usually in the range of 35-49ºC) and, therefore, are also known as salt spray tests. Figure 1.7 shows a scheme of a typical chamber used in accelerated corrosion test [22] and the placement of the samples inside for the exposure to the solution fog.

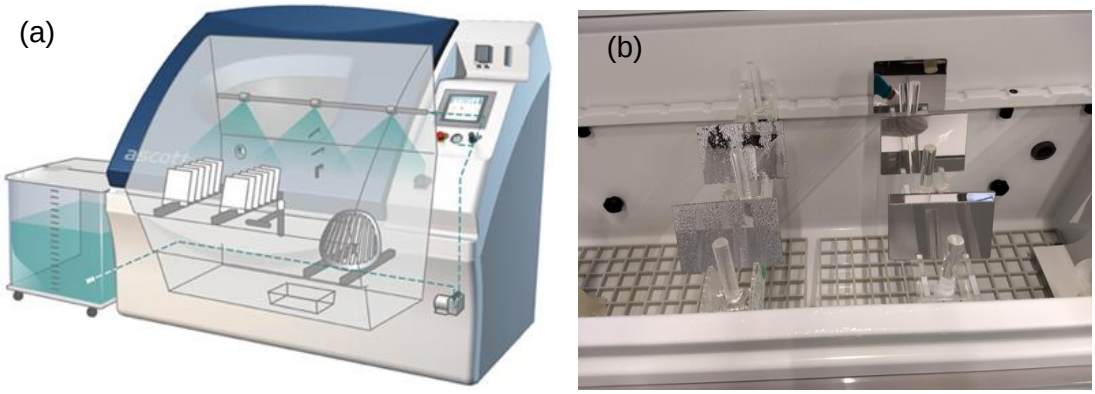

Figure 1.7.- Scheme of a typical chamber used in (a) accelerated corrosion test [22] and, (b) example of the samples placement in the interior of the cabinet.

In order to simulate different corrosive environments, the composition of the electrolyte can be modified by the incorporation of other additives [23]. The use of accelerated corrosion tests is quite common in the industry (e.g. following the standard ASTM B117), which enables quick comparisons between different coatings behavior and it is possible to test samples or components of big dimensions that hardly could be characterised by other tests.

The evaluation of the corrosion performance of the coatings in accelerated corrosion tests is done by means of periodic visual inspection of the surface appearance [24], no quantitative or objective information is obtained from the test. Based on the visual appearance, samples pass the test only if they are not showing defects on the surface (Figure 1.8 (a)). Once a sample has visible corrosion defects (Figure 1.8 (b)), that sample has failed the test, being the time of this last inspection the time to failure assigned to the sample.

However, accelerated corrosion tests have some drawbacks such as the reproducibility between specimens and cabinets, the large testing time periods (as consequence of the continuous improvement of the coatings performance), the subjectivity during evaluation

of the results (it depends on the person in charge of the evaluation) and that no information is achieved about the reasons for passing or failing the test.

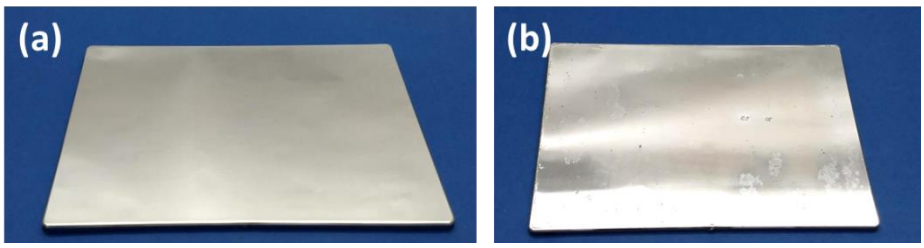

Figure 1.8.- Example of the aspect of microporous nickel-chromium coated samples that (a) passed and (b) failed the accelerated corrosion test.

Copper Accelerated Acetic Acid Salt Spray (CASS) test is an accelerated corrosion test and its standard was published as ASTM B368 in 1961 [25]. This test is one of the most widely used methods for evaluating the corrosion performance of decorative copper/nickel/chromium or nickel/chromium coatings on substrates such as steel, zinc alloys, aluminum alloys, and plastics designed for severe outdoor exposure. Moreover, results obtained from CASS test are used for evaluation of the corrosion resistance as well as quality control, specification acceptance and research and development tasks. CASS test has been a fundamental tool in the development of the nickel multilayer arrangement and microporous chromium deposits that led to an improved corrosion resistance of the nickel-chromium decorative coatings [26].

The main characteristics of CASS test are the composition of the solution and the temperature of the test (49ºC). The composition of the 5 wt. % NaCl in weight solution is modified by the addition of 0.25 g of copper chloride dihydrate ($CuCl_2 \cdot 2H_2O$) and glacial acetic acid until pH = 3.1-3.3 [25]. These particularities of the CASS test promote the simulation of the specific corrosion of external automotive components in an accelerated way [23].

Nowadays, CASS test is used indiscriminately and by default. Despite it is well known its higher aggressiveness, there is a lack of understanding about its impact in the corrosion mechanism.

1.2.1.1. CASS test background

Neutral salt spray test (NSS) is one of the most used worldwide and simplest accelerated corrosion tests. It consists on spraying a fog of a 5 wt. % neutral NaCl solution to samples

in the interior of a chamber. It was developed in 1914 [27] but it was not until 1939 that the American Society for Testing and Materials (ASTM) published it as a standard, ASTM B117. NSS was used for several metallic coatings; however, many times results did not correlate with real service exposure: coatings failed very early in service when they were expected to have a good corrosion performance according to NSS results.

In an attempt to improve the NSS accelerated corrosion test, acetic acid was incorporated to the formulation of the solution [28]. Interestingly, this modification led to the development of corrosion in decorative nickel-chromium similar to the one developed in vehicles drove in locations with severe corrosion (i.e. Detroit). One of the main drawbacks of this test was that it required 200h to produce corrosion, making the test very time consuming and unworkable as a quality control test [26]. This modification of NSS later became an ASTM standard: ASTM B287 Acetic Acid Salt Spray (AASS) test.

The growing dissatisfaction existing with the NSS and AASS tests by the early 1950s caused the Research Committee of the American Electroplaters´ Society to sponsor “Project 15”. The aim of the project was the development of a new accelerating corrosion test for decorative platings. The major automobile companies, suppliers of plated parts and plating chemicals were involved in the project.

The first phase of the project consisted of the design, fabrication and service exposure of plated components on the place of the front number plate of automobiles in Detroit in 1953-1954 winter. The selection of Detroit location was because it had been identified as a place where decorative coatings corroded the fast in the USA, especially in winter as consequence of the used of deicing road salts. In the second phase of the project, all the data known or supposed to have an effect in the corrosion of the decorative coatings in Detroit was gathered and analysed with the aim of identify the most corrosive factors. The third and last phase of the project was intended to perform exploratory accelerated corrosion tests with the aim of selecting the most promising ones for an in-depth investigation [29].

As a result, chloride, sulphate and nitrate anions along with twenty metallic elements were found in mud and rainwater collected in the streets. One interesting observation was that the corrosion rate was faster when dirtiness and mud was accumulated over the metallic coatings. The identification of the copper and iron salts as the most corrosive contaminants came after the systematic study done by the application to the coatings of a slurry of kaolin containing the previously identified contaminants. This finding led to the development of Corrodkote Procedure, ASTM B380, which included a kaolin slurry with

copper nitrate, ferric chloride, sodium chloride and ammonium chloride. The slurry formulation was adjusted to produce in 20 hours of test the corrosion developed in cars on one year of exposure in Detroit [26].

On the other hand, the impact of copper and iron as the most corrosive contaminants for decorative nickel-chromium corrosion in Corrodkote test motivated its extrapolation to salt spray tests. As a conclusion, it was observed that the incorporation of copper to AASS test decreased the time from 20 hours of Corrodkote test to 16h in order to achieve a similar corrosion degree. It was the beginning of CASS test [26].

1.2.1.2. Current impact of Copper in the environment

Copper was found to be one of the most corrosion accelerating chemicals among the pollutant agents present in the road transport environment in Project 15. A recent study prepared for the European Commission stated that around the 90% of the total copper emitted in EU27 in 2010 to the atmosphere came from road transport (2,9kTon of 3,3kTon) [30]. Road transport emissions can be classified in two types: (1) exhaust emissions and (2) non-exhaust emissions. Whereas the origin of exhaust emissions is in the combustion of fuel and motor oils, non-exhaust emissions come from brake wear. It is probably that by the time of Project 15 copper contaminants in the road transport environment were mainly consequence of exhaust emissions due to the presence of heavy metals in the fuels. Nowadays, exhaust emissions are not the main source of the released copper. Heavy metals reduction policies targeted on Pb, Cd and Hg emissions reduced also copper emission because the different heavy metals present in the fuels had the same source. However, at the present, brake wear has become a very important source for copper as a consequence of the substitution of asbestos brake lining for new ones containing copper [31].

Despite the sources of copper emissions have changed since Project 15 in automotive environment, copper is still a contaminant undoubtedly present and has to be seriously considered in the corrosion resistance of decorative nickel-chromium coatings. Therefore, due to the continuous exposure of automotive decorative components to copper and chloride environments, together with the intensive use of CASS test in industry, a better understanding of the corrosion mechanism under CASS conditions is essential for further improvement of the decorative exterior parts corrosion performance and its quality control testing.

1.2.2. Electrochemical techniques

Traditionally, decorative nickel-chromium systems have been extensively evaluated by corrosion accelerated test such as Russian-mud (ASTM B995: Standard Test Method for Chloride Resistance Test for Chromium Electroplated Parts) and CASS tests. However, electrochemical techniques have not been exploited so much in the study of the corrosion behavior of nickel-chromium coatings. Since nickel duplex systems, electrochemical studies have been devoted to explore the performance of the coatings under chloride ions [13,14]. Recently, their use has been extended in order to explore different aggressive conditions (e.g. calcium chloride for Russian-mud under a film containing hygroscopic chlorides and solid material (mud)) [19,20]. In contrast, although the effect of cupric ions is crucial in the corrosion behavior of nickel-chromium coatings, it has not been investigated in detail.

Nowadays, many electrochemical techniques are used in the study of the corrosion phenomena of metals and coatings [32]: i.e. anodic and cathodic reactions that result in the oxidation and degradation of a metallic coating [33]. These techniques allow determining thermodynamic and kinetic parameters, which are characteristic of the process, and hence, obtaining quantitative data. Electrochemical techniques have been successfully used in the study of the corrosion performance of materials, corrosion inhibitors and corrosion mechanism and in monitoring corrosion processes. If compared to accelerated tests, electrochemical techniques provide quantitative data in a short time with respect to the qualitative visual evaluation and the longer test time required in CASS test and could provide valuable information about the effect of cupric ions.

Electrochemical methods can be divided in two categories: conventional electrochemical techniques and localised electrochemical techniques. In conventional techniques, typical working electrodes areas are in the mm^2 to cm^2 range and the overall response of the sample surface is measured, averaging the contribution of the whole surface. Localised techniques allow gaining in-depth comprehension of the corrosion processes by the use of electrodes in the range of 5-500 microns diameter. These electrodes can be laterally and vertically scanned with high resolution over the surface of the sample, focusing on the local corrosion processes. The information obtained by both, conventional and localised techniques, if complemented, leads to a better understanding of the corrosion processes.

Hence, the complementary use of conventional and localised electrochemical techniques is a promising approach in the study of the role of copper and chloride ions

(i.e. composition of the CASS electrolyte) in decorative nickel-chromium samples, in particular taking into account that such a study has not been made yet by means of localised techniques.

1.2.2.1. Conventional electrochemical techniques

The tests performed by conventional electrochemical techniques are usually carried out by the basic configuration of three electrodes, as shown in Figure 1.9. The electrochemical cell comprises the working electrode (WE, the system to study), the reference electrode (RE), the counter electrode (CE) and the electrolyte. The reference electrode has a stable and well-known electrode potential and it is used to measure the potential. The counter electrode is used to complete the electrical circuit with the working electrode and is made with inert materials (e.g. platinum or graphite). The three electrode are connected to a potentiostat that will regulate and measure the potential between the working electrode and the reference electrode and the current between the counter and the working electrode.

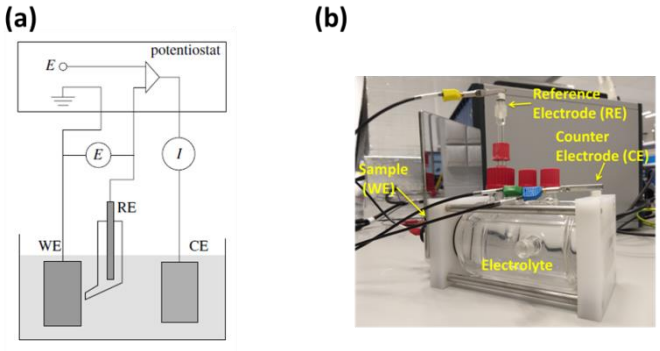

Figure 1.9.- (a) Three electrode set-up connected to the potentiostat [34], and (b) and electrochemical cell.

The below summary describes some of the most used conventional electrochemical techniques: Open Circuit Potential (OCP), Linear Polarisation Resistance (LPR), potentio-dynamic polarisation and Electrochemical Impedance Spectroscopy (EIS).

1.2.2.1.1. Open Circuit Potential (OCP)

Open circuit potential (OCP) measures the potential of the working electrode (sample) with respect to a reference electrode when no potential or current is applied to the system. The potential measured by OCP is the potential of the sample at which the anodic and cathodic reaction rates are in equilibrium in a particular corrosive

environment. It shows the thermodynamic trend of the sample to be affected by the surrounding electrolyte and take part in the corrosion process.

OCP allows the evaluation and study of changes in the corrosion process with exposure time. The use of stable reference electrodes assures that changes registered in OCP are consequence of modifications in the working electrode and electrolyte interface. However, the information obtained by OCP tests has to be completed by additional techniques in order to reach to the conclusions behind the changes in OCP measurements.

1.2.2.1.2. Linear Polarisation Resistance (LPR)

Polarisation techniques are methods in which, in contrast to OCP technique, the potential of the working electrode is imposed (vs the reference electrode) while the resulting current is measured as a function of the potential or time.

Linear Polarisation Resistance (LPR) technique is used for calculating the polarisation resistance (R_p), parameter widely used for the calculation of corrosion rates and the determination of time effect on the corrosion process. This technique is based on the mixed potential theory [35], which explains that the cathodic and anodic reactions in a corrosion process in the metal-electrolyte interface take place at a mixed or corrosion potential, so that the sum of all cathodic reaction rates equals the sum of all anodic reaction rates.

Experimentally, R_p is obtained from the usually linear relationship between the potential and current density in a potential range close to the corrosion potential. (±5-10mV).

1.2.2.1.3. Potentiodynamic polarisation

Potentiodynamic polarisation is often used for measuring the corrosion rate of metals, which is calculated from the corrosion current density ($\boldsymbol{i}$), defined as the sum of cathodic ($\boldsymbol{i_c}$) and anodic current densities ($\boldsymbol{i_a}$), equation (1).

$$\boldsymbol{i} = \boldsymbol{i_c} + \boldsymbol{i_a} \qquad (1)$$

However, the corrosion current or the corrosion potential (E_{corr}) cannot be measured when the sample is at OCP because the electrons produced in the anodic reactions are

consumed in the cathode and no net current is flowing from the system. Therefore, at E_{corr}, $\boldsymbol{i_c}$ and $\boldsymbol{i_a}$ have an equal absolute value and the corrosion current density ($\boldsymbol{i}_{corr}$) is the value of the current density at that potential, which coincides the value of $\boldsymbol{i_c}$ and $\boldsymbol{i_a}$.

Figure 1.10 shows the partial current densities and total current density ($\boldsymbol{i}$) of mixed electrode near the corrosion potential (E_{corr}).

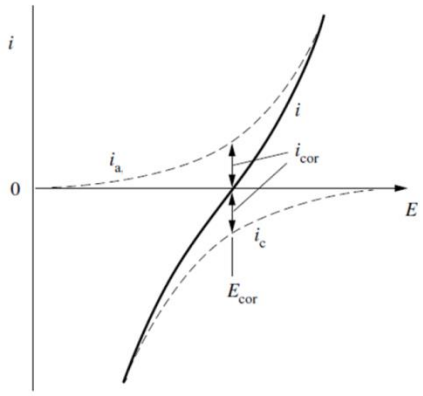

Figure 1.10.- Partial current densities ($\boldsymbol{i_a}$, $\boldsymbol{i_c}$), total current density ($\boldsymbol{i}$) and corrosion current density ($\boldsymbol{i}_{corr}$) of mixed electrode near the corrosion potential (E_{corr}).

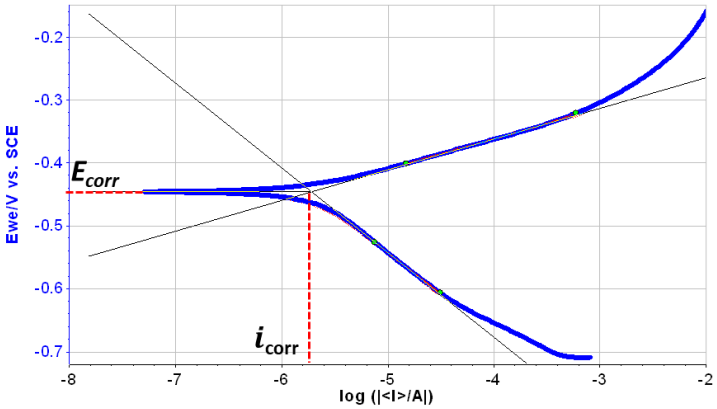

Figure 1.11.- Polarisation curve showing anodic and cathodic linear regions, corrosion current density ($\boldsymbol{i}_{corr}$) and corrosion potential (E_{corr}).

In order to shift the OCP from the equilibrium, potentiodynamic polarisation tests consist in measuring the current density as a function of the applied potential. Consequently, current density versus potential curves (polarisation curves) are obtained (Figure 1.11). These curves represent the relationship between the change from equilibrium

(polarisation) and the value of the current density resulting from such a displacement from the steady state.

The experimental procedure consists on polarising the potential, anodically (progress in the positive potential direction) or cathodically (progress in the negative potential direction), at a constant scan rate (mV/s). The scan rate can largely influence the final information obtain from the test. It is generally accepted that high scan rates do not allow the system to stabilise at each potential, therefore, distorting results such as passivation or pitting potential. A scan rate of 0.1667 mV/s was selected following the ASTM standard [36].

These tests allow obtaining information about the corrosion rate, the anodic characteristic of the material (e.g. pitting corrosion or passivation), and cathodic characteristics (e.g. metal reduction) as well as the different aspects of the corrosion process of the system, such as information about the kinetic phenomena governing the corrosion process: charge transfer or mass transfer control.

In the case of corrosion processes essentially under activation control, an exponential relationship between the current and the potential is obtained by Butler-Volmer equation. The equations for the anodic and cathodic processes are the following:

$$\boldsymbol{i_a} = \boldsymbol{i_{corr}} \cdot \mathbf{exp}(\eta/\beta_\alpha) \qquad (2)$$

$$\boldsymbol{i_c} = \boldsymbol{i_{corr}} \cdot \mathbf{exp}(-\eta/\beta_c) \qquad (3)$$

being β_a and β_c the anodic and cathodic Tafel coefficients, respectively, and η the polarisation overpotential, which is the difference between the potential of the polarised sample and the corrosion potential. The Butler-Volmer equation (4) for a mixed potential is obtained by including the equations (2) and (3) in equation (1):

$$\boldsymbol{i} = \boldsymbol{i_{corr}} \cdot [\exp(\eta/\beta_\alpha) - \exp(-\eta/\beta_c)] \qquad (4)$$

When the polarisation overpotential is high, one of the exponential terms of equation (4), depending on the polarisation sign, can be neglected and Butler-Volmer equation can be rewritten. When $\eta/\beta_\alpha >> 1$,the anodic Tafel region is the domain of the potential:

$$\boldsymbol{i} \approx \boldsymbol{i_a} = \boldsymbol{i_{corr}} \cdot \exp(\eta/\beta_\alpha) \qquad (5)$$

That taking logarithms yield:

$$\eta = -\beta_a \ln \boldsymbol{i_{corr}} + \beta_a \ln \boldsymbol{i} \qquad (6)$$

By converting the later expression to base-10 logarithm with a_a and b_a as anodic Tafel constants:

$$\eta = -2.303\beta_a \log \boldsymbol{i_{corr}} + 2.303\beta_a \log \boldsymbol{i} = a_a + b_a \log \boldsymbol{i} \qquad (7)$$

In a similar way, the cathodic Tafel region is the domain of the potential when $\eta/\beta_c \ll 1$, leading to the final equation, a_c and b_c as cathodic Tafel constants:

$$\eta = 2.303\beta_c \log \boldsymbol{i_{corr}} - 2.303\beta_c \log \boldsymbol{i} = a_c + b_c \log \boldsymbol{i} \qquad (8)$$

In order to obtain i_{corr} graphically from polarisation curves, the anodic and cathodic linear regions have to be extrapolated back to the point anodic and cathodic currents are equivalent, being the potential at which it falls E_{corr}, see Figure 1.11 [37]. On the other hand, i_{corr} can be mathematically obtained by the Stern-Geary equation: anodic and cathodic tafel slopes from the linear regions of the polarisation curves and the R_p from LPR tests [38]:

$$\boldsymbol{i_{corr}} = \frac{\boldsymbol{\beta_a \beta_c}}{\boldsymbol{2.3 R_p (\beta_a + \beta_c)}} \qquad (9)$$

If the corrosion process is mass controlled, the Stern-Geary equation can be simplified.

1.2.2.1.4. Electrochemical Impedance Spectroscopy (EIS)

Electrochemical Impedance Spectroscopy (EIS) began to be used in the 1970s and is based on the analysis of the response of the sample to sinusoidal potential perturbations. A potential perturbation with known amplitude (usually 10 mV) is applied to the sample over a wide range of frequencies and where the current response of the sample is measured. In this context, the impedance can be defined as the quotient of the applied potential divided by the current measured from the sample. The analysis of the system response to EIS tests leads to valuable information about details of corrosion rate, the reactions taking place, the interface and structure of the sample [39,40].

The impedance is a complex number and EIS results are usually represented as the real component (Z') vs. imaginary (Z") component (Nyquist plots, Figure 1.12 (a)) and impedance modulus |Z| vs. frequency, or impedance phase angle vs. frequency (Bode plots). EIS results can be adjusted to a model equivalent circuit, Figure 1.12 (b), which

is built of basic electrical elements such as resistor and capacitors that are related to the physical and electrochemical properties of the system under study [41].

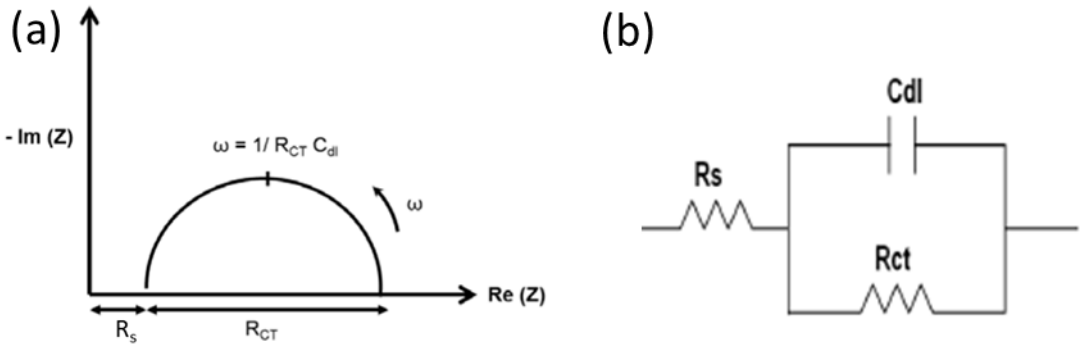

Figure 1.12.- Nyquist plot and equivalent circuit of a metal/electrolyte interphase.

From the different parameters obtained by EIS test, charge transfer resistance (R_{CT}), has special relevance in corrosion because brings information about the corrosion kinetics.

1.2.2.2. Localised electrochemical techniques

Among the different localised electrochemical techniques developed during the last decades, Scanning Kelvin Probe (SKP) and Scanning Electrochemical Microscopy (SECM) are described below due to their interest in the study of decorative nickel-chromium systems.

1.2.2.2.1. Scanning Kelvin probe (SKP)

Scanning Kelvin probe (SKP) measures the work function difference or surface potential between the sample and the probe (Figure 1.13 (a)). It benefits from the direct correlation between work function and surface condition due to the modifications that adsorbed species, oxide layers, defects, contamination have in work function values [32]. Potential representations are obtained by means of point measurements or area scans in different conditions such as in humid air exposure or in the corrosion process established under electrolyte droplets, being the potential in this case the corrosion potential. The use of electrolyte droplets allows to study corrosion processes simulating atmospheric conditions [42] in a more realistic way than in the traditional set up where the sample is immersed in bulk electrolyte. SKP potential maps (Figure 1.13 (b)) allow the identification

of cathodic and anodic areas over a sample, such as in the classic Evans drop experiment [43], due to the differences in the potentials values.

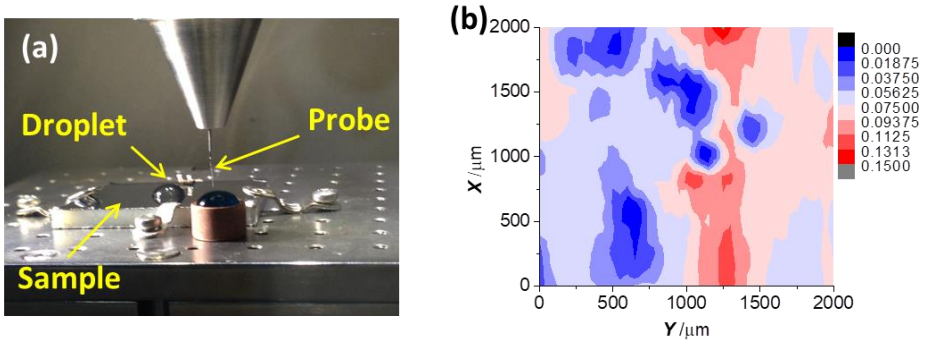

Figure 1.13.- (a) SKP electrolyte droplet test set up, and (b) example of surface potential distribution map of microporous nickel-chromium sample after CASS electrolyte exposure.

The basis of SKP technique is a vibrating capacitor constituted by the probe and the sample. The probe, placed close to the sample surface (or drop surface), is electrically connected to the sample. Due to their energy differences, one surface charges positively and the other surface charges negatively, forming a capacitor. The probe is vibrated and a potential is applied to it in order to reduce the capacitance to zero. This applied potential allows measuring the work function difference between the probe and the sample surface. The measurements are made with movement flexibility in the x, y and z directions, resulting in point measurements, line or area scans and height or topographic measurements. The resolution of the technique is affected by the probe diameter, which are usually 150µm-200 µm and provide a resolution close to 100 µm [44].

1.2.2.2.2. Scanning electrochemical microscopy (SECM)

Scanning Electrochemical Microscopy (SECM), developed in 1989 by Allen J. Bard [45], uses a probe connected to a potentiostat that collects electrochemical information (e.g. current) while hold in an electrolyte at close proximity to the sample to study. This technique can be operated in three different modes: amperometric, potentiometric and AC, allowing the collection of different electrochemical parameters data. SECM allows the study of localised corrosion with high spatial resolution thanks to the probe diameter in the range of nm to 25 µm, hence the name ultra-micro-electrode (UME), and the X and Y scanning directions. SECM has been used in corrosion field in the study of pitting initiation and propagation, surface reactions, inhibitors effectiveness, corrosion activity of metallic coatings and electron transfer kinetics, among others. In addition, the sample

can be connected to a second potentiostat, allowing the sample polarisation for the study of processes not taking placing at the OCP.

Running the SECM in the amperometric mode allows current data acquisition in several working modes: feedback, generation/collection and redox competition. While feedback mode requires the presence of electron mediator in the solution (a redox specie that it is not taking part in the corrosion reaction), in generation/collection and competition modes no extra redox mediator is needed. In the amperometric experiments, the UME is polarised at a potential that permits sensing the redox specie of interest via the electro-reduction or electro-oxidation of such redox specie.

Feedback mode allows the identification of active/passive regions over the sample surface [46]. On the other hand, in generation/collection and competition mode, the UME measures changes in the electrochemical species present in the electrolyte as consequence of the sample corrosion process, such as O_2 [47] by cathodic reactions or the release of metal cations in the anodic sites. The obtained microscopy data about the distribution of the chemical species allows measuring local differences in electrochemical activity and locating anodic and/or cathodic sites. Figure 1.14 (a) and (b), show an example of SECM set up and an area scan run in competition mode that leads to the identification of cathodic sites during the corrosion process. O_2 was reduced at the UME, the locations where a lower current is measured correspond to cathode sites where O_2 was consumed.

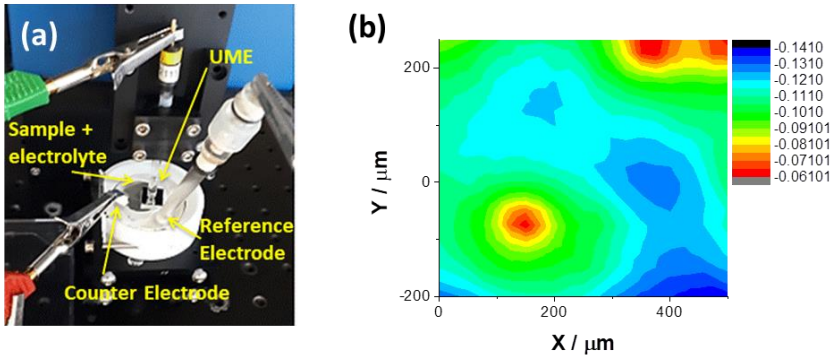

Figure 1.14.- (a) SECM test set up, and (b) O_2 consumption surface area scan of microporous nickel-chromium sample after CASS electrolyte exposure measured in NaCl electrolyte.

1.3. Chemiometrics

As stated above, accelerated corrosion tests present several disadvantages, being the main ones the time required for achieving results (the better the coating performance, the longer the time required), the subjective nature of the evaluation results obtained and the lack of information about the reasons why a coating passed or failed the test. Interestingly, the electrochemical characterisation of the corrosion behaviour of the decorative nickel-chromium coatings could overcome these issues due to the characteristics of these tests: quantitative data is obtained in a shorter time and the obtained data could lead to the interpretation of the corrosion mechanisms behind the performance of the coatings.

Therefore, it seems interesting to explore whether exists a correlation between the results obtained by CASS test and electrochemical tests that could result in the improvement of the corrosion evaluation/control and/or replacement of the CASS test by electrochemical ones. However, due to the several available electrochemical tests that could be used in the study of decorative nickel-chromium coatings behaviour, a large amount of variables would be obtained, making difficult the interpretation of the results and the search of a correlation by univariate analysis.

In this sense, chemiometric methods can be a very useful tool in the study whether a correlation between electrochemical test results and CASS test exist in the corrosion behaviour of decorative nickel-chromium coatings. The multivariate analysis performed by chemiometric methods allows the observation of more than one variable at a time, resulting in a simplification of the search for intercorrelations when working with a number of parameters.

The IUPAC defines chemometric as ‘‘the science of relating measurements made on a chemical system or process to the state of the system via application of mathematical or statistical methods” [48]. The increased specialisation of the scientific instrumentation and the inclusion of powerful computational tools in scientific research have benefited the development of these mathematical and statistical methods. Among the different chemiometric tools, pattern recognition and prediction methods have been identified as the most useful ones in the study of a correlation between CASS test and electrochemical tests.

1.3.1. Pattern recognition methods

The main objective of pattern recognition is to draw the maximum information available from the experimental data by the classification of the samples into categories or groups. The classes can be defined (supervised classification) or learned from the data (unsupervised classification).

Principal Component Analysis (PCA) is an unsupervised tool for pattern recognition extensively employed in exploratory data analysis. PCA returns an overall view of the system under study by the identification of similitudes/differences among samples, the presence of clusters and patterns and the significant variables contributing the most to the clustering [49,50]. It reduces the number of the variables by establishing relations among the parameters, transforming original variables into new variables, the principal components (PCs). PCs are plotted in a new coordinate system that represents the directions of greatest variance in the dataset.

As a consequence, a data exploratory analysis by PCA of the electrochemical data could be very useful for the identification of which electrochemical parameters are able to account for the maximum data variance and allow a better clustering and greater differentiation among the different groups of samples.

1.3.2. Prediction methods

In some instances, pattern recognition methods are not enough for addressing a specific issue because these methods do not allow making predictions on new samples measurements. In this context, Partial Least Squares (PLS) regression is a technique used in order to obtain predictions of the behaviour of new samples. PLS finds the fundamental relations between two matrices: X (predictors) and Y (response) by, first, reducing the original data to a smaller set of uncorrelated components and later performing least square regression to those components [51,52].

However, when the dependent variables represent classes, qualitative values or non-continuous values, it is not possible to run a PLS regression for prediction and classification methods have to be applied. Partial Least Squares Discriminant Analysis (PLS-DA) is based on the classical PLS regression [51] used for building predictive models. However, the dependent variables in PLS-DA represent qualitative values or classes instead of quantitative values and a discriminant analysis is applied to the samples for the classification [53,54]. In PLS-DA the relationship between X matrix and

the classification Y matrix is established in a way that the separation between sample groups is increased for achieving a maximum separation among the classes.

1.3.3. Chemiometrics in corrosion

There are several examples of the applications of chemometrics tools for prediction in corrosion studies. Artificial Neural Networks have been used in the search for a correlation between EIS and NSS, with the aim of predicting the performance of alloy substrates coated by conversion coatings in the salt spray test [55]. The prediction of different features of the corrosion behaviour have been addressed by PLS, such as the corrosion current density on reinforced concrete corrosion from data obtained by different electrochemical tests [56] and the inhibition of the corrosion on steel surfaces from the metallic composition and molecular properties of the inhibitors [57].

PCA is another chemometric tool successfully used in corrosion research. Some interesting examples are the relationship found between microclimate factors and the corrosion products on bronze monuments that allowed gathering the weathering type [58] and the evaluation and diagnosis of the corrosion process in carbon steel [59].

1.4. Objectives

In view of the stated throughout these pages, the aim of this thesis is to investigate the corrosion mechanisms/behavior of decorative chromium coatings under the conditions of accelerated test. For this purpose, samples of decorative multilayer nickel-chromium coatings plated with commercial baths on ABS supplied by Atotech GmbH were studied. The main objectives are listed below:

- **Understanding the corrosion mechanisms of chromium coatings under CASS test conditions**

The influence of copper ions in the corrosion resistance of decorative nickel-chromium has not been previously studied in detail, despite CASS test has been used indiscriminately without a deep understanding of the aggressiveness of the environment. Therefore, there is a need to understand the corrosion mechanism of the chromium coatings in CASS conditions in order to improve their corrosion behavior.

The methodology used for addressing this objective has been based in the use of conventional and localised electrochemical techniques with the aim of combining the information achieved by both in order to get a better understanding of the corrosion

process. Additional characterisation techniques, such as Field Emission Scanning Electron Microscopy (FE-SEM) and X-ray Photoelectron Spectroscopy (XPS) techniques have also been used for a better understanding of the corrosion mechanisms.

- **Explore whether exits a correlation between electrochemical test and CASS chamber test that could allow the prediction of CASS test performance by electrochemical tests**

Due to the disadvantages of accelerated corrosion tests such as subjectivity of the evaluation, large duration of the test, reproducibility between chambers and lack of information of the reasons for failing/passing the test, electrochemical tests seem to be the most promising corrosion evaluation tool to use for overcoming accelerated test issues. Therefore, a correlation between electrochemical tests and CASS test is explored, where the use of electrochemical tests data can be used for building a model that could predict CASS test performance.

The methodology used for addressing this objective has been based on the use of conventional electrochemical techniques, CASS tests and chemiometric tools.

The hypotheses of the thesis are stated below:

- The corrosion mechanism in bulk electrolyte immersion (same composition in both tests) is similar to the one underwent in CASS test.
- There is a correlation between the aesthetic damage in the decorative coating in CASS conditions and the electrochemical response of the decorative coatings.

1.5. References

[1] D.L. Snyder, Decorative chromium plating basics, Met. Finish. 110 (2012) 14–21. https://doi.org/10.1016/S0026-0576(13)70110-7.

[2] M. Tsang, Ami (Enthone GmbH), Wing, Linda (Enthone), Dahlhaus, Calculating Corrosion. Advancement in the control and prediction of CASS test performance, (2005). http://www.pfonline.com/articles/calculating-corrosion.

[3] Decorative chromium coatings applications, (n.d.). https://www.atotech.com/.

[4] S. Olivera, H.B. Muralidhara, K. Venkatesh, K. Gopalakrishna, C.S. Vivek, Plating on acrylonitrile–butadiene–styrene (ABS) plastic: a review, J. Mater. Sci. 51 (2016) 3657–3674. https://doi.org/10.1007/s10853-015-9668-7.

[5] European Parliament and Council, Directive 2000/53/EC on end-of-life vehicles, Off. J. Eur. Union. L (2000) 34–42. https://doi.org/10.1016/j.jclepro.2010.02.014.

[6] M. Brandes, I. Chung, L. Wing, Technical Article Hatched in Europe , REACH Regulations Impact U . S . Auto Manufacturers, 2015.

[7] G. Dubpernell, History of Chromium Plating, Plat. Surf. Finish. 71 (1984) 84–91.

[8] A. Gardner, Meeting high performance decorative chromium plating specifications using trivalent chrome plating systems, in: SAE Tech. Pap., SAE International, 2008. https://doi.org/10.4271/2008-01-1459.

[9] B.B. Knapp, Research and Decorative Coatings, Plat. Surf. 65 (1978) 24–30.

[10] J.K. Dennis, T.E. Such, Nickel and Chromium Plating, Butterworth and Co. Limited, 1993.

[11] G.A. Di Bari, J. V. Petrocelli, The Effect of Composition and Structure on the Electrochemical Reactivity of Nickel, J. Electrochem. Soc. 112 (1965) 99. https://doi.org/10.1149/1.2423478.

[12] J.F. Vogt, R.J. Herbert, U.S. patent, 2,635,075, 1953.

[13] G.N. Flint, S.H. Melbourne, The corrosion of decorative nickel+chromium coatings: A metallographic and potential study, Trans. IMF. 38 (1961) 35–44.

[14] S.R. Maloof, The Electrochemical Behavior of Decorative Nickel-Chromium

Coatings in 3% NaCl under Porentiostaric Conditions, J. Electrochem. Soc. 116 (1969) 1293. https://doi.org/10.1149/1.2412304.

[15] T.W. Tomaszewski, R.J. Clauss, H. Brown, No Title, Proc. Am. Electroplat. Soc. 50 (1963).

[16] W.. Lovell, E.H. Shotwell, J. Boyd, No Title, Proc. Am. Electroplat. Soc. 47 (1960).

[17] H. Brown, Addition Agents , Anions and Inclusions in Bright Nickel Plating The William Blum Lectures, Plating. 55 (1968) 1047–1055.

[18] T. Pearson, S. Handy, L. Forst, Elektochemische Untersuchungen zum Korrosionsmechanismus dekorativer Chromoberflächen durch Calciumchlorid, Galvanotechnik. 8 (2009) 1730–1739.

[19] L. Pohlmann, G. Bauer, P. Hartmann, P. Wachter, C. Donner, Oscillatory passive active transition during the corrosion in nickel chromium layer systems, J. Solid State Electrochem. 17 (2013) 489–496. https://doi.org/10.1007/s10008-012-1949-3.

[20] C. Langer, W. Wendland, K. Honold, L. Schmidt, J.S. Gutmann, M. Dornbusch, Corrosion analysis of decorative microporous chromium plating systems in concentrated aqueous electrolytes, Eng. Fail. Anal. 91 (2018) 255–274. https://doi.org/10.1016/j.engfailanal.2018.04.031.

[21] N. Lebozec, D. Thierry, Influence of climatic factors in cyclic accelerated corrosion test towards the development of a reliable and repeatable accelerated corrosion test for the automotive industry, Mater. Corros. 61 (2010) 845–851. https://doi.org/10.1002/maco.200905497.

[22] Salt Spray Chamber, (n.d.). http://www.ascott-analytical.co.uk.

[23] S.W. Dean, Corrosion Testing of Materials with Metallic and Inorganic Coatings, in: W.B. Harding, G.A.B. Di (Eds.), Test. Met. Inorg. Coatings, ASTM International, West Conshohocken, PA, 1987: pp. 177–192. https://doi.org/10.1520/STP20037S.

[24] ISO 10289:1999 Methods for corrosion testing of metallic and other inorganic coatings on metallic substrates — Rating of test specimens and manufactured articles subjected to corrosion tests, ISO Stand. (2016) 1–22.

[25] Standard Test Method for Copper-Accelerated Acetic Acid-Salt Spray (Fog) Testing (CASS Test), Annu. B. ASTM Stand. B368 (2011) 1–5. https://doi.org/10.1520/B0368-09.2.

[26] D. Carl, Corrosion in the automobile industry, in: Man. Ind. Corros. Stand. Control, 1973: pp. 81–88.

[27] J.A. Capp, No Title, Proceedings, Am. Soc. Tessting Mater. 14 (1914) 474.

[28] C.F. Nixon, No Title, Am. Electroplat. Soc. Mon. Rev. 32 (1945) 1105.

[29] W.L. Pinner, Progress Report on Development of a New Accelerated Corrosion Test, Plating. december (1953).

[30] AMEC Environment and Infrastucture UK Limited, Bio Intelligence Service, Milieu, IEEP, REC, Contribution of industry to pollutant emissions to air and water, 2014. https://doi.org/10.2779/25422.

[31] H.A.C. Denier van der Gon, J.H.J. Hulskotte, A.J.H. Visschedijk, M. Schaap, A revised estimate of copper emissions from road transport in UNECE-Europe and its impact on predicted copper concentrations, Atmos. Environ. 41 (2007) 8697–8710. https://doi.org/10.1016/j.atmosenv.2007.07.033.

[32] J. Leiva-García, L. Sánchez-Tovar, R. Escrivà-Cerdán, C. García-Antón, Role of Modern Localised Electrochemical Techniques to Evaluate the Corrosion on Heterogeneous Surfaces, in: Mod. Electrochem. MEthods Nano, Surf. Corros. Sci., n.d.

[33] W.R. Whitney, THE CORROSION OF IRON., J. Am. Chem. Soc. 25 (1903) 394–406. https://doi.org/10.1021/ja02006a008.

[34] D. Landolt, Corrosion and Surface Chemistry of Metals, EPFL Press, New York, 2007. https://doi.org/10.1201/9781439807880.

[35] C. Wagner, W. Traud, Über die Deutung von Korrosionsvorgängen durch Überlagerung von elektrochemischen Teilvorgängen und über die Potentialbildung an Mischelektroden, Zeitschrift Für Elektrochem. 44 (1938) 391–454.

[36] ASTM G5-14, Standard Reference Test Method for Making Potentiodynamic Anodic Polarization, Annu. B. ASTM Stand. (2014) 1–9. https://doi.org/10.1520/G0005-14.2.

[37] D.G. Enos, The Potentiodynamic Polarization Scan, 2014.

[38] M. Stern, A.L. Geary, Electrochemical Polarization, J. Electrochem. Soc. 104 (1957) 559. https://doi.org/10.1149/1.2428653.

[39] Z.Q. Bai, C.F. Chen, M.X. Lu, J.B. Li, Analysis of EIS characteristics of CO2 corrosion of well tube steels with corrosion scales, Appl. Surf. Sci. 252 (2006) 7578–7584. https://doi.org/https://doi.org/10.1016/j.apsusc.2005.09.011.

[40] C. Liu, A. Leyland, S. Lyon, A. Matthews, An a.c. impedance study on PVD CrN-coated mild steel with different surface roughnesses, Surf. Coatings Technol. 76–77 (1995) 623–631. https://doi.org/https://doi.org/10.1016/0257-8972(95)02544-8.

[41] F. Mansfeld, Electrochemical impedance spectroscopy (EIS) as a new tool for investigating methods of corrosion protection, Electrochim. Acta. 35 (1990) 1533–1544. https://doi.org/https://doi.org/10.1016/0013-4686(90)80007-B.

[42] M.S. Thomson, G.S. Frankel, Atmospheric Pitting Corrosion Studies of AA7075-T6 under Electrolyte Droplets: Part I. Effects of Droplet Size, Concentration, Composition, and Sample Aging, J. Electrochem. Soc. 164 (2017) C653–C663. https://doi.org/10.1149/2.1051712jes.

[43] C. Chen, F. Mansfeld, Potential distribution in the evans drop experiment, Corros. Sci. 39 (1997) 409–413. https://doi.org/10.1016/S0010-938X(97)83355-0.

[44] N. Jadhav, V.J. Gelling, Review—The Use of Localized Electrochemical Techniques for Corrosion Studies, J. Electrochem. Soc. 166 (2019) C3461–C3476. https://doi.org/10.1149/2.0541911jes.

[45] A.J. Bard, F.R.F. Fan, J. Kwak, O. Lev, Scanning electrochemical microscopy. Introduction and principles, Anal. Chem. 61 (1989) 132–138. https://doi.org/10.1021/ac00177a011.

[46] S.S. Jamali, S.E. Moulton, D.E. Tallman, M. Forsyth, J. Weber, G.G. Wallace, Applications of scanning electrochemical microscopy (SECM) for local characterization of AZ31 surface during corrosion in a buffered media, Corros. Sci. 86 (2014) 93–100. https://doi.org/10.1016/j.corsci.2014.04.035.

[47] L.C. Abodi, Y. Gonzalez-Garcia, O. Dolgikh, C. Dan, D. Deconinck, J.M.C. Mol,

H. Terryn, J. Deconinck, Simulated and measured response of oxygen SECM-measurements in presence of a corrosion process, Electrochim. Acta. 146 (2014) 556–563. https://doi.org/10.1016/j.electacta.2014.09.010.

[48] G. Luciano, P. Traverso, P. Letardi, Applications of chemometric tools in corrosion studies, Corros. Sci. 52 (2010) 2750–2757. https://doi.org/10.1016/j.corsci.2010.05.016.

[49] B.K. Lavine, Chemometrics, Anal. Chem. 72 (2000) 91–98. https://doi.org/10.1021/a1000016x.

[50] A. Biancolillo, F. Marini, Chemometric methods for spectroscopy-based pharmaceutical analysis, Front. Chem. 6 (2018) 1–14. https://doi.org/10.3389/fchem.2018.00576.

[51] S. Wold, M. Sjöström, L. Eriksson, PLS-regression: A basic tool of chemometrics, Chemom. Intell. Lab. Syst. 58 (2001) 109–130. https://doi.org/10.1016/S0169-7439(01)00155-1.

[52] P. Geladi, B.R. Kowalski, Partial Least-Squares regression: A tutorial, Anal. Chim. Acta. 185 (1986) 1–17. https://doi.org/10.1016/0003-2670(86)80028-9.

[53] D. Ballabio, V. Consonni, Classification tools in chemistry. Part 1: Linear models. PLS-DA, Anal. Methods. 5 (2013) 3790–3798. https://doi.org/10.1039/c3ay40582f.

[54] M. Bevilacqua, R. Nescatelli, R. Bucci, A. D. Magri, A. L. Magri, F. Marini, Chemometric Classification Techniques as a Tool for Solving Problems in Analytical Chemistry, J. AOAC Int. 97 (2014) 19–28. https://doi.org/10.5740/jaoacint.SGEBevilacqua.

[55] G. Kumar, R.G. Buchheit, Use of artificial neural network models to predict coated component life from short-term electrochemical impedance spectroscopy measurements, Corrosion. 64 (2008) 241–254. https://doi.org/10.5006/1.3278469.

[56] P. Monzón, J.E. Ramón, J.M. Gandía-Romero, M. Valcuende, J. Soto, D. Palací-López, PLS multivariate analysis applied to corrosion studies on reinforced concrete, J. Chemom. 33 (2019) 1–12. https://doi.org/10.1002/cem.3096.

[57] A.L. de de Queiroz Baddini, S.P. Cardoso, E. Hollauer, J.A. da C.P. Gomes,

Statistical analysis of a corrosion inhibitor family on three steel surfaces (duplex, super-13 and carbon) in hydrochloric acid solutions, Electrochim. Acta. 53 (2007) 434–446. https://doi.org/10.1016/j.electacta.2007.06.050.

[58] K. Polikreti, V. Argyropoulos, D. Charalambous, A. Vossou, V. Perdikatsis, C. Apostolaki, Tracing correlations of corrosion products and microclimate data on outdoor bronze monuments by Principal Component Analysis, Corros. Sci. 51 (2009) 2416–2422. https://doi.org/10.1016/j.corsci.2009.06.039.

[59] J.M. Gandía, P. Monzón, R. Bataller, I. Campos, J. Manuel Lloris, J. Soto, Principal component analysis applied to study of carbon steel electrochemical corrosion, Corros. Eng. Sci. Technol. 50 (2015) 320–329. https://doi.org/10.1179/1743278214Y.0000000231.

2

An SKP and EIS study of microporous nickel-chromium coatings in copper containing electrolyte

The work presented in this chapter was previously published: Larraitz Ganborena, Jesús Manuel Vega, Berkem Özkaya, Hans-Jürgen Grande, Eva García-Lecina; Electrochimica Act., 2019, 318 (2019) 683-694

2.1. Introduction

Microporous nickel-chromium multilayer coatings are widely used for decorative purposes due to their outstanding corrosion resistance and aesthetic finish even in automotive applications where a high corrosion resistance is required. The development of these plating coatings during the lasts decades has led to the following multilayer configuration on a polymeric substrate like Acrylonitrile Butadiene Styrene (ABS): a top microporous chromium layer plated over an arrangement of at least three nickel layers with different thickness and potential (from top to bottom: microporous nickel, bright nickel and semibright nickel) and a copper-layer at the bottom in contact with the substrate. In order to preserve the aesthetic appearance intact during its lifetime, a top microporous layer is used to decrease the cathodic area (chromium) and to increase the anodic one (nickel). As a consequence, an homogeneous current distribution can occurs along the surface during the corrosion process of the nickel and minimize the aesthetic degradation of the system. In addition, the multilayer structure has been designed to guide the corrosion front to a specific less noble nickel layer (mainly bright nickel layer) underneath microporous chromium. Meanwhile, semibright nickel layer assures the inner substrate integrity [1].

In order to evaluate the corrosion performance of this coating system, Copper-Accelerated Acetic Acid-Salt Spray test (CASS test, ASTM B368) [2] is the most common test used in the industry. It consists in atomizing an acidic cupric chloride and sodium chloride mixture in the interior of a salt spray chamber at 49ºC. Such solution leads to a more severe accelerated corrosion than chlorides itself, providing results more comparable to the corrosion observed in real service life [3]. However, CASS test is often used indiscriminately and by default without properly understanding the role of the aggressive environment.

Conventional electrochemical techniques, such as OCP, potentiodynamic polarization curves have been extensively used to study the corrosion behaviour of microporous nickel-chromium systems. OCP oscillations led to the identification of a change in corrosion mechanism from active nickel corrosion to active chromium corrosion, caused by absence of oxygen in the pores [4]. Potentiodynamics polarization curves under different aggressive agents (chloride, calcium, cupric and ferric cations) showed a similar corrosion mechanism in different multilayer nickel-chromium systems, where the corrosion front went through the micro-discontinuities toward the underlying bright nickel

layer where the anodic reaction (nickel oxidation) takes place [5]. In contrast, Electrochemical Impedance Spectroscopy (EIS) has not been employed so often to study the complete multilayer system. Experiments have mainly focused to explore the properties and the chemical stability of chromium top oxide layer with the pH in de-icing solutions [6].

A more novel technique like scanning Kelvin probe (SKP) is being used to measure the corrosion potential (after calibration) on metals using several scenarios: potential maps of bare and/or contaminated surfaces, delamination front of coating/metal interfaces, corrosion process under droplets, etc. [7,8]. Results allow the identification of cathodic and anodic areas over a sample such as in the classic Evans drop experiment [9]. This technique allows to study corrosion processes simulating atmospheric conditions rather than using a bulk electrolyte and therefore is extensively used in the study of atmospheric corrosion of metallic substrates by chloride electrolyte droplets [10–12], and the effect of corrosion inhibitors [13].

The combination of SKP and EIS has been mainly used to explore the degradation of coating/metal interface [12, 13] and corrosion of bare metal [16,17]. EIS provided information of chloride adsorption during the pitting process whereas the potential differences along the surface was detected by SKP [16]. Hence, the combination of EIS and SKP seems to be a promising approach for studying the degradation of nickel-chromium multilayer systems paying attention to their microporosity. Particularly, SKP droplet tests could reveal features, at localised scale, of the corrosion process sensitive to concentration/solubility of species (e.g. oxygen diffusion inside the droplet), which would be exacerbated during the dynamic droplet stabilization (i.e. evaporation of the droplet) but hindered in bulk solution tests. Moreover, as far as the authors of this paper are concerned, there are no studies published using aggressive agents like Cu^{2+} in droplet tests by SKP.

The objective of this work is to exploit the combination of conventional electrochemical techniques (OCP and EIS) and SKP to study the corrosion of microporous nickel-chromium systems. Two electrolytes with different aggressiveness (one simulating the electrolyte composition of the accelerated corrosion test known as CASS and other without cupric cations in their composition, respectively) have been used. Different test methodologies and additional characterisation by ICP-OES, XPS, OM and FE-SEM was carried out.

2.2. Experimental

2.2.1. Materials

Microporous nickel-chromium multilayer specimens of 10 cm x 15 cm were plated from trivalent chromium bath on ABS as substrate. The multilayer system is formed by the following five metallic layers, from top to bottom: microporous chrome (Cr), microporous nickel (MPS Ni), bright nickel (B Ni), semibright nickel (SB Ni) and copper. Figure 2. 1 shows the multilayer scheme and the typical thicknesses for each layer. The coatings were plated on both sides of the ABS panels, ensuring electric contact from the tested side to the back side of the sample. Prior to testing, samples were cleaned with acetone, rinsed with deionized water and dried by compressed air gun.

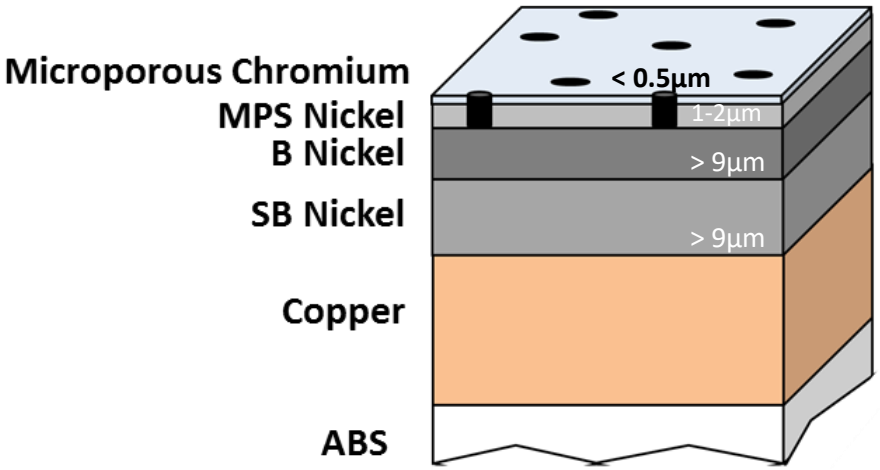

Figure 2. 1.- Cross-section image of microporous nickel-chromium multilayer system.

The electrolytes were 0.9M NaCl (Cl electrolyte) and 0.9M NaCl+1.5mM $CuCl_2$, (Cu+Cl electrolyte) which were prepared from analytical grade reagent and 18.5 MΩcm deionized water. Solutions pH was adjusted in both electrolytes to 3.1 by addition of glacial acetic acid.

2.2.2. Conventional electrochemical tests in bulk solution

Open circuit potential (OCP) and electrochemical impedance spectroscopy (EIS) were performed in a flat jacketed three electrode cell using a VSP-300 Biologic potentiostat and were repeated at least three times for reproducibility. A working electrode surface area of 1cm^2 was exposed to a volume of 250 mL of quiescent electrolyte, Ag/AgCl (3M KCl) as reference electrode and a platinum mesh as counter electrode. The reference

electrode was coupled to a platinum wire in series with a 10 nF capacitor to minimize experimental artifacts usually observed at high frequency domain (HF) for this electrode. Tests were run at 49ºC during 22 h. OCP was continuously measured except for the time that it was interrupted to do the EIS measurement, once per hour. EIS were done applying ± 10mV sinusoidal wave perturbation versus OCP, being the frequency range from 100kHz to 10mHZ, with 10 points per decade.

2.2.3. Localised tests: SKP droplet and surface scan measurements

The Kelvin probe experiments were carried out on a Wicinski-Wicinski GbR device with a Ni-Cr probe tip and were repeated a minimum of three times for reproducibility. The relative humidity in the chamber was kept at 85%. Before each experiment, the SKP tip was calibrated with a saturated $Cu/CuSO_4$ (320mV Vs. Standard Hydrogen Electrode (SHE)). Two types of measurement were performed:

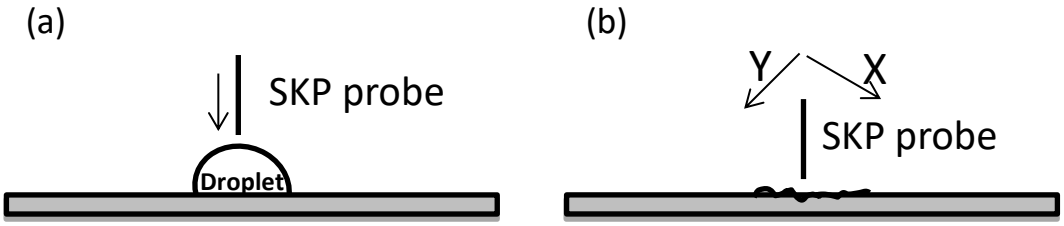

Figure 2. 2.- SKP tests scheme, droplet test (a) and surface area scan (b) after droplet removal.

(A) The SKP droplet tests (Figure 2. 2 (a)) were done as follows: droplets of 50 µL instead of the more usual volumes in the range of 4-6 µL were deposited over the samples in order to explore larger areas susceptible for corrosion [12]. The probe tip was placed above the center of the droplet, where its height was maximum, using a digital microscope and the vibration frequency was set at 938Hz. At that point, potential and height measurement was started and recorded for 20h. The digital microscope taking images of the droplet every 5 minutes allowed the time-lapse following of the droplet evolution.

(B) Once the test (A) was finished, the remaining droplet was removed and the sample was cleaned with deionized water. Surface area scans with a scanning area of 2 mm x 2 mm were done within the region where the droplet test was done (Figure 2. 2 (b)). During the area scans a step size of 50 µm was set.

Finally, the comparison of the two types of experiments (section 2.3.1 and 2.3.2) provides complementary information: electrochemical tests allowed setting steady state conditions (i.e. electrolyte concentration) and a higher temperature (49ºC), whereas droplet test was subjected to environmental conditions (i.e. humidity) that could influence the change of the electrolyte aggressiveness (e.g. concentration of the solution) when a drop is used. Moreover, SKP maps are able to reveal the presence of anodes and cathodes at localised level rather than an overall performance of the exposed area shown by electrochemical tests.

2.2.4. Electrolyte analysis

Electrolyte concentrations of Cu and Ni were determined by ICP-OES using the equipment ICPE-9000 from Shimadzu. For these measurements, 1mL aliquots were taken from the corrosion cell at different times. In the case of SKP droplet test, a volume of 1 mL was placed over the surface in order to get enough volume for the compositional analysis.

2.2.5. Surface analysis

The chemical composition of the products formed on the nickel-chromium surfaces exposed to Cu+Cl droplet test was analysed by XPS. Spectra were registered in a SPECS Sage HR 100 spectrometer with a non-monochromatic X-ray source (Aluminum Kα line of 1486.6 eV energy and 300 W), placed perpendicular to the analyser axis and calibrated using the $3d_{5/2}$ line of Ag with a full width at half maximum (FWHM) of 1.1 eV. The resolution was 30 and 15 eV of Pass Energy and 0.5 and 0.15 eV/step for the survey and high resolution spectra, respectively. All analyses were made in an ultra-high vacuum (UHV) chamber at a pressure around $8 \cdot 10^{-8}$ mbar. In the fittings Gaussian-Lorentzian functions were used (after a Shirley background correction) where the FWHM of all the peaks were constrained while the peak positions and areas were set free.

2.2.6. Morphological characterisation

A Leica DM4000M optical microscope was used for the superficial microstructure characterisation. Field emission scanning electron microscope (FE-SEM) Gemini Ultraplus from Zeiss was employed with 8.0 kV accelerating voltage.

2.3. Results and discussion

2.3.1. Conventional electrochemical tests in bulk solution

2.3.1.1. Open Circuit Potential (OCP)

OCP measurements were conducted in Cl and Cu+Cl electrolytes for a period of 22 h, as shown in Figure 2. 3.

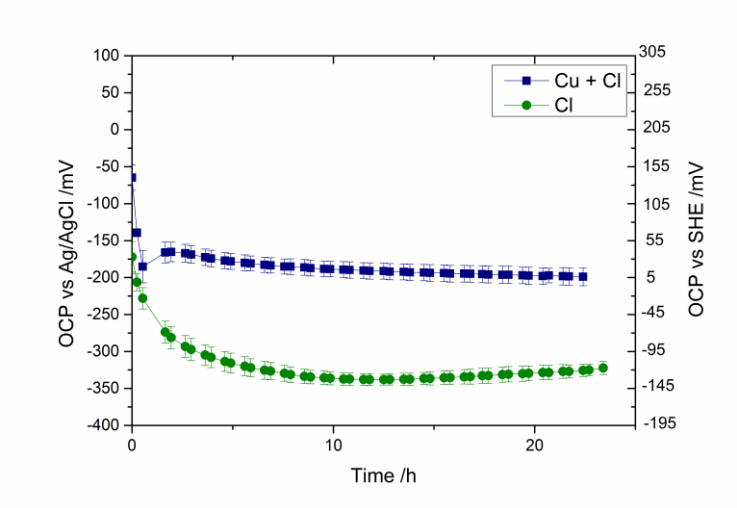

Figure 2. 3- OCP data versus time for microporous nickel-chromium samples in Cl and Cu+Cl electrolytes.

A sudden decrease of the OCP can be observed in both electrolytes at the beginning of the exposure before stabilization. In the case of the electrolyte with cupric cations, a steady state value is obtained after 2 h. On the other hand, during exposure to Cl electrolyte, it takes a longer time to reach a stabilized potential value. A potential difference close to 120 mV was found between Cl and Cu+Cl electrolyte OCP data by the end of the test. This indicates that the presence of cupric cations in the composition of the electrolyte shifts the potential to more noble values due to their oxidizing effect [18–20]. Therefore, considering that nickel dissolution is the anodic reaction, it is expected to have different cathodic reactions depending on the electrolyte, where the reduction of cupric cations ($Cu^{2+} + e^{-} \leftrightarrow Cu^{+}$) is clearly governing in Cu+Cl electrolyte.

2.3.1.1.1. Electrolyte composition

The composition was only determined for Cu+Cl electrolyte to monitor the copper and nickel concentration at different testing time (0, 5 and 22h). Results did not show any measurable variation of the copper concentration during the test in bulk electrolyte, indicating that the oxidizing effect due to the reduction of cupric cations should be

maintained along the measurement. With respect to nickel, it is already detected (1.5 ppm) by five hours as consequence of corrosion process, reaching by the end of the test a concentration around 10.1 ppm.

2.3.1.2. Morphological characterisation

Nickel-chromium samples have been characterised by optical microscopy and FE-SEM before and after 22h of exposure in both electrolytes (Figure 2. 4). Surfaces have developed different attack as consequence of the exposure to the electrolyte. In general, micropores/defects have evolved growing in diameter after the exposure to the electrolyte in a different way: i) an homogeneous distribution of numerous and similar defects in size along the surface for Cl electrolyte (Figure 2. 4 (b)), ii) an heterogeneous distribution of lower amount of defects but bigger in size for Cu+Cl electrolyte (Figure 2. 4 (c)). Aesthetically, such a difference indicates higher damage on the surface when cupric cations are present in the electrolyte, which should be confirmed by a lower corrosion resistance.

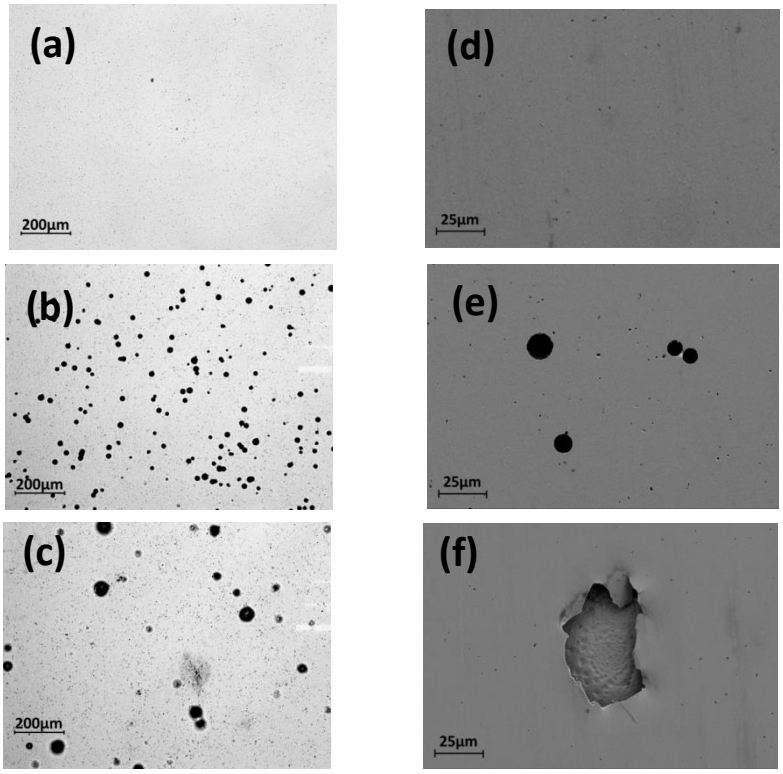

Figure 2. 4.- Images for microporous nickel-chromium sample by OM exposed to electrochemical tests: (a) before exposure, (b) exposed to Cl electrolyte, (c) exposed to Cu+Cl electrolyte; and by FE-SEM: (d) before exposure, (e) exposed to Cl electrolyte, (f) exposed to Cu+Cl electrolyte.

Related to FE-SEM images, Figure 2. 4 (d, e & f) are showing the variation of morphology before and after the corrosion attack. So far, EDX analysis was unable to detect the presence of copper or nickel on the surface, indicating that the chromium layer is free of these ions.

2.3.1.3. Electrochemical Impedance Spectroscopy (EIS)

Impedance of microporous nickel-chromium samples is presented in both Nyquist (Figure 2. 5) and Bode (**Figure 2. 6** & Figure 2. 7) formats at different times of exposure (1, 9 and 22h). In the Nyquist plane, the diagrams show a semicircle in the range of high frequency-medium frequency (HF-MF) as well as a small loop that starts to appear at low frequency (LF). An initial analysis of the EIS results has been done to have an idea of the difference between both electrolytes, independently if a constant phase element (CPE) is required or not as it has been discussed below. Graphically, the diameter of such semicircle can provide information of the resistance of the process taking place, whilst the capacitance can be obtained using the following expression:

$$Z_{max} = {}^{1}/_{j\omega C} \qquad \text{Equation 1}$$

where j = √-1; ω is the angular frequency (ω = 2 π f_{max}) at which the imaginary part of the impedance ($-Z_{max}$) is maximal and f_{max} is alternate current frequency at maximum (see Figure 2. 5).

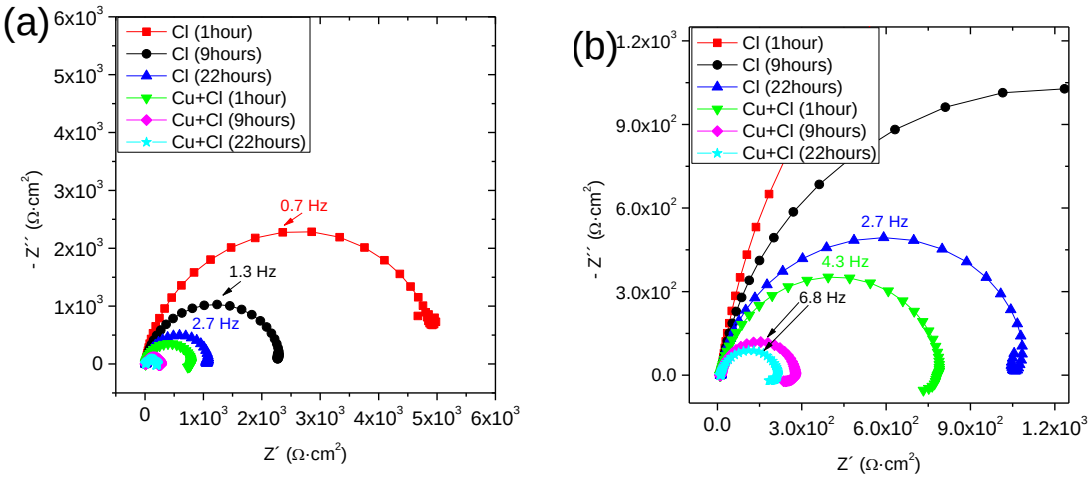

Figure 2. 5.- Nyquist plots recorded at OCP for the microporous nickel-chromium samples in both electrolytes: (a) Nyquist and (b) zoom at high frequency of the graph (a).

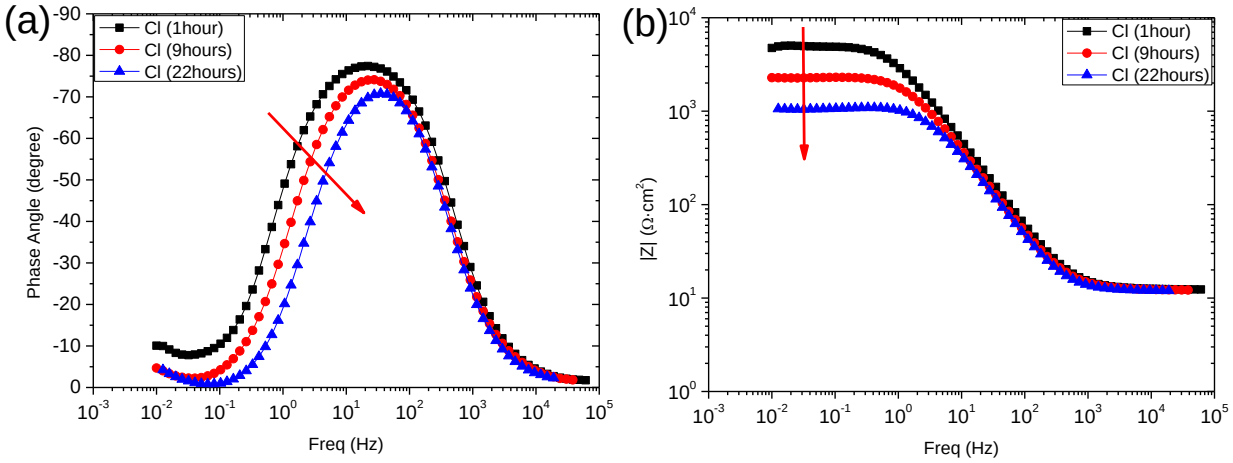

Figure 2. 6.- Bode plots recorded at OCP for the microporous nickel-chromium samples in Cl electrolyte: (a) Phase angle and (b) Impedance modulus.

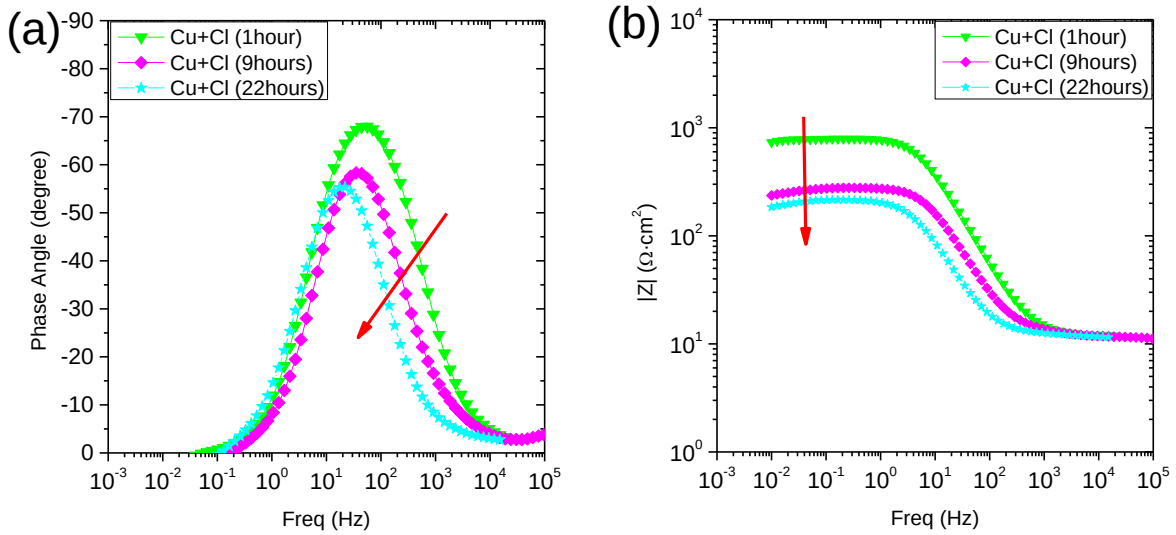

Figure 2. 7.- Bode plots recorded at OCP for the microporous nickel-chromium samples in Cu+Cl electrolyte: (a) Phase angle and (b) Impedance modulus.

According to the capacitance values that have been obtained (Table 2. 1 shows an average value of the different measurements) for the HF-MF time constant, it can be associated to the double layer (C_{dl}) and to the electron transfer effects corresponding to the corrosion process of Ni [5]: charge transfer resistance (R_{ct}).

On the other hand, the relaxation process at LF is not well defined in most of the measurements (such time constant it is roughly present in a decade of frequency). This inductive behaviour may be associated to the adsorption of species like Cl^-_{ads} and H^+_{ads} on the electrode surface [21–24] or to the re-dissolution of the passive surface at low frequencies [25]. However, the LF part is not going to be considered for the analysis of

the results because the idea is just to focus the main discussion at HF-MF where a new time constant appears when copper is present in the electrolyte as can be observed during the graphical analysis below.

Table 2. 1.- Average of capacitance and resistance values obtained graphically.

Electrolyte	Time (h)	C_{dl} ($F \cdot cm^{-2}$)	R_{ct} (Ωcm^2)
Cl	1	$8.9 \cdot 10^{-5} \pm 1.4 \cdot 10^{-5}$	$5.4 \cdot 10^{3} \pm 9.1 \cdot 10^{2}$
	9	$1.2 \cdot 10^{-4} \pm 2.8 \cdot 10^{-6}$	$2.1 \cdot 10^{3} \pm 2.8 \cdot 10^{2}$
	22	$1.2 \cdot 10^{-4} \pm 5.3 \cdot 10^{-6}$	$1.1 \cdot 10^{3} \pm 5 \cdot 10^{1}$
Cu+Cl	1	$9.0 \cdot 10^{-5} \pm 8.5 \cdot 10^{-6}$	$9.0 \cdot 10^{2} \pm 1.8 \cdot 10^{2}$
	9	$1.8 \cdot 10^{-4} \pm 6.6 \cdot 10^{-5}$	$4.0 \cdot 10^{2} \pm 3.3 \cdot 10^{1}$
	22	$3.5 \cdot 10^{-4} \pm 1.6 \cdot 10^{-4}$	$2.4 \cdot 10^{2} \pm 1.3 \cdot 10^{0}$

Further analysis shows that R_{ct} is decreasing continuously with the exposure time, indicating an increase of the corrosion rate during exposure to the aggressive environment, independently of the electrolyte, typical of a reactive system. Such decrease in the corrosion resistance can be easily observed in the Bode format indicated by the progressive decay of the impedance modulus |Z| in the plateau at low frequency (arrows in Figure 2. 6 (b) and Figure 2. 7 (b)). Although a similar trend is observed for both electrolytes, the corrosion is much higher in the case of Cu+Cl electrolyte compared to Cl electrolyte most probably due to the oxidizing effect of cupric cations [18].

In addition, the variation of the phase angle from Bode plot with time provides a different trend depending on the electrolyte. Figure 2. 6 (a) shows a maximum angle value that is shifting to higher frequency with time (indicated by the arrow) and with higher absolute values. In contrast, Figure 2. 7 (a) indicates an opposite trend, where the maximum of the phase angle is shifting to lower frequency values and with lower absolute values. This discrepancy clearly indicates that the influence of the cupric cations in the corrosion process (increasing the dissolution of nickel) is evident and quite strong, shifting this maximum to lower frequencies instead to higher frequencies that is expected during the corrosion process with and without inhibitors in the electrolyte [26].

Finally, the variation of the impedance diagrams from 1h to 9h and 22h of exposure does not look monotonous in Figure 2. 7 (a) compared to Cl electrolyte (Figure 2. 6 (a)). An

additional process (time constant) at HF (10^2-10^4 Hz) seems to appear although it is not quite clear. Therefore, further analysis using corrected Bode plots has been done to detect if there is an additional time constant or not.

2.3.1.3.1. Graphical analysis of the EIS results using corrected Bode plots

To find out if there is an additional time constant at HF and to determine the physical process that is behind it, several approaches can be used. Usually, equivalent circuits (EC) are a powerful tool to obtain the different parameters (resistance, capacitance, diffusion, etc.) and to distinguish which phenomena can be linked to them. However, the selection of the proper EC is not trivial for complex system like microporous ones and the goodness of the fitting could be good even though an EC without physical sense is chosen. As an example, the conventional Randles-type equivalent circuit, which treats the electrode as a homogeneous system, does not count the ionic resistance in the electrode [27]. Therefore, more complicated EC are needed taking into account porous electrodes, radial diffusion and combined effects could be used [28].

Recently, a different approach based on graphical analysis to analyse impedance diagrams using corrected Bode plots is being used [29], although caution should be used when interpreting electrolyte-resistance-corrected Bode plots to avoid the appearance of an additional high-frequency relaxation process [30]. Particularly, Bode plots are confounded by the influence of the electrolyte resistance. Therefore, alternative graphical representation of data is needed to provide complementary information for reactive systems: e.g. ohmic-resistance-corrected Bode plots, logarithmic plots of the imaginary component of the impedance among others [30].

The resistance-corrected Bode plots are presented in Figure 2. 8 for both electrolytes after 22h of exposure. The slope of the corrected modulus and the corrected phase-angle plots yields valuable information concerning the existence of CPE behaviour that is obscured in the traditional Bode representation. As seen in Figure 2. 8 (a), both systems are exhibiting a CPE behaviour because the phase angle reaches a HF asymptote such that

$$\Phi_{adj}(\infty) = -90\alpha \qquad \text{Equation 2}$$

whilst purely capacitive systems should had reached a value of -90º. On the other hand, the corrected modulus is dominated by the contribution of the imaginary part of the

impedance at HF. Such correction allows obtaining the parameter –α (Figure 2. 8 (b)) from the slope on a logarithmic plot at high frequencies.

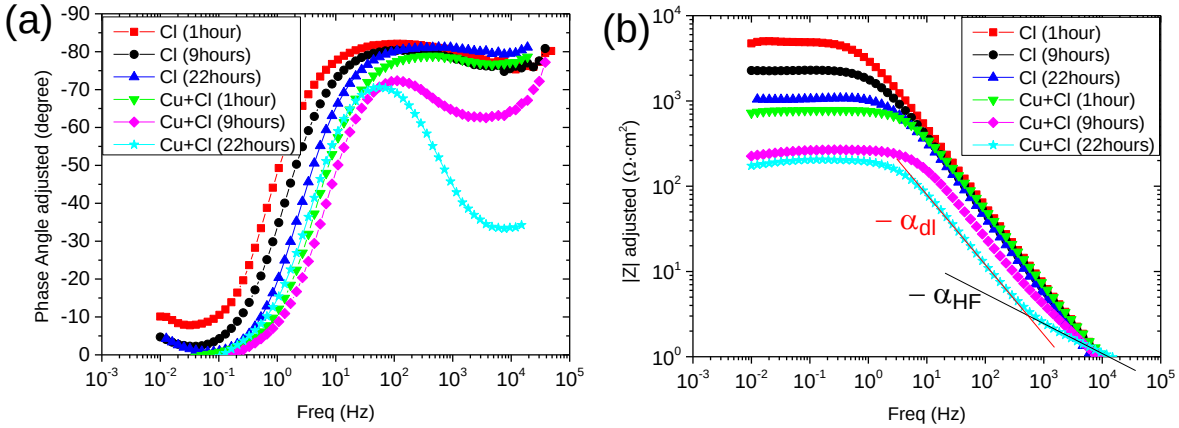

Figure 2. 8.- Corrected Bode plots recorded at OCP for the microporous nickel-chromium samples in both electrolytes after 22h of exposure: (a) Phase angle and (b) Impedance modulus.

A clear plateau is evident for all exposure times on the corrected phase shift for Cl electrolyte: it is located in the range from 70 to 280 Hz after 1 and 9h of exposure, and from 226 to 1.2 Hz after 22h. For a frequency larger than 200Hz a decrease of the phase shift is observed. This phenomenon could be attributed to the geometric effect corresponding to the non-uniform current and potential distribution [31,32].

On the other hand, although such plateau can be easily observed for Cu+Cl electrolyte after 1h of exposure, it is not evident after 9h, where two different and undefined shorter plateaus could be distinguished in the same frequency range. This behaviour confirms the finding in the uncorrected Bode plot (Figure 2. 7 (a)) where a new time constant (it becomes well defined after 22h) was appearing at HF. At this later time, if we assume that a plateau is present at HF, $\alpha_{HF} = 0.36$ is obtained using equation 2. In order to confirm this assumption, the α_{HF} parameter can also be obtained from the slope (-α) in the corrected Bode modulus plot (Figure 2. 8 (b)). It can be clearly observed the presence of two slopes for Cu+Cl electrolyte after 22h. The HF slope provides $\alpha_{HF} = 0.37$, value that matches with the one above confirming the presence of a new time constant. The calculation of the slope has been done at frequencies below 10 kHz in both corrected Bode plots just to avoid any sensitivity to artifacts, due to the low value of the imaginary part of the impedance [33].

Therefore, the presence of cupric cations in the electrolyte reveals the presence of a new time constant. It is well known that α typically adapts the values of 1, 0.5 and 0 if it corresponds to the behaviour of an ideal capacitor, a pure diffusion process or an ideal resistor, respectively [34]. According to the value obtained above, α_{HF} seems to be related to diffusion process, specifically related to copper species (e.g. migration) because their presence in Cu+Cl electrolyte are responsible of this time constant. The deviation from the ideal value of a diffusion phenomenon (i.e. from α = 0.5 to α = 0.36/0.37) could be related to the two-dimensional (e.g. slow adsorption reactions, non-uniform potential and current distribution) or three-dimensional (e.g. surface roughness and heterogeneities, electrode porosity) capacitance distribution [34]. Further studies will be done to find out a physical explanation, taking into account the complexity of this microporous system as well as the influence of oxidizing and aggressive ions in the electrolyte, where several reduction reactions can take place and could be detected by EIS [35].

Finally, related to the second slope, which has been assigned to the double layer capacitance, a value of α_{dl} = 0.84 was obtained (Figure 2. 8 (b)) which should be related to the C_{dl}. Such value is within the range (α_{dl} = 0.8-0.9) compared to the other measurements, indicating that the graphical calculation of this second slope can be done to obtain a reliable value.

2.3.2. Scanning technique. SKP tests

The SKP has been extensively used for measuring the potential at more localised scale over surfaces covered by a droplet. It allows to study in the proximity of the probe position the evolution of the corrosion phenomena: initiation of corrosion events, fixed anodic or cathodic spots, transitions from mixed potential of small local anodes and cathodes to dominantly larger cathodic or anodic sites, etc. [13].

The variation of the potential and the height for metal/drop systems was obtained simultaneously using the SKP droplet test (Figure 2. 9). From the beginning of the exposure to SKP chamber, electrolyte droplets started to concentrate due to the continuous water evaporation (thinner lines). It was similar independently of the electrolyte, reaching a height stabilization of the droplet approximately after 15 h. At that moment, an equilibrium was reached between the droplet and the environmental conditions of the SKP chamber (temperature and humidity). It is expected a similar concentration factor (i.e. the increase of the aggressiveness inside) for both type of droplets.

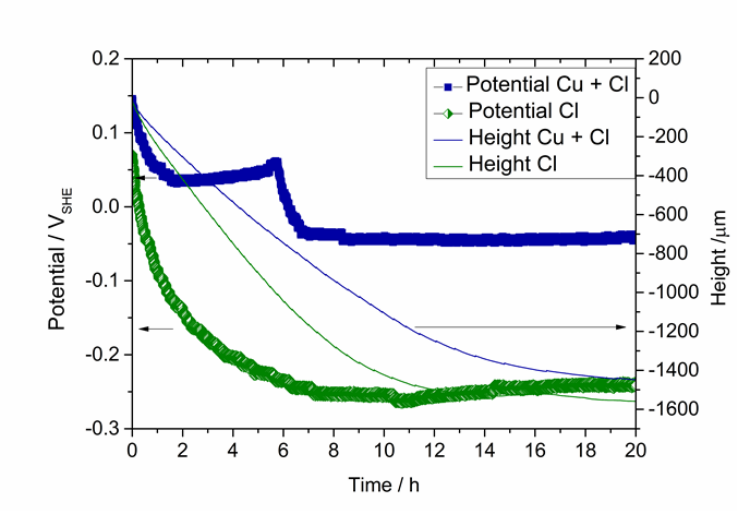

Figure 2. 9.- Potential and droplet height as a function of time under Cl electrolyte and Cu+Cl electrolyte droplets.

In contrast, the evolution of the potential as a function of time shows a different behaviour for both electrolytes (solid lines), indicating the impact of the electrolyte composition in the potential. In the case of Cl droplet, it is expected to have a different cathodic reaction (e.g. reduction of H^+ or O_2) than Cu+Cl one. If oxygen reduction reaction (ORR) was the main one, the oxygen diffusion has to be considered, which depends on the chloride concentration and the volume of the droplet. The potential curve for Cl shows a rapid potential decrease occurs until it was stabilized around 6-7h at ≈ -250 mV. At that time, the variation of the volume of the droplet and therefore the chloride concentration is reduced, until no evaporation is observed. The steady potential at the end of the test indicates that a stable corrosion process is taking place, where no significant changes occurs: a different anodic/cathodic distribution, bubble formation, building up of corrosion product in the proximities of the probe, etc. [10].

Related to the Cu+Cl curve, two potential plateaus can be seen. Firstly, a rapid potential drop lasting 1.5h is observed until it stabilizes around +40 mV. Unexpectedly, the potential value remains constant from 1.5 to 6h. Secondly, an abrupt potential decrease took place and immediately a steady state was reached. The potential difference between the first and the second potential plateau was found to be close to 100 mV. This value is quite similar to the OCP difference found between both electrolytes in the conventional electrochemical test (Figure 2. 3) and most probably is related to role of copper as will be discussed later (section 2.3.2.3.). Finally, at the end of the test, once both droplets have reached an steady state, they show a potential difference around 200mV. However, the main difference is that a white precipitate shows up inside Cu^{2+} containing droplets. The analysis of time-lapse images from the droplet is summarised

in Figure 2. 10, where precipitation was detected visually at 6h that corresponds with the drastic potential drop. In order to know if precipitation phenomenon was just an effect of Cu+Cl droplet evaporation, in parallel, an electrolyte droplet was placed on the top of a substrate covered by parafilm® to avoid the contact metal/electrolyte. At the end of the test a completely transparent droplet was obtained. This fact indicated that the precipitation inside the droplet was not just an evaporation issue and it is linked to the corrosion process going on.

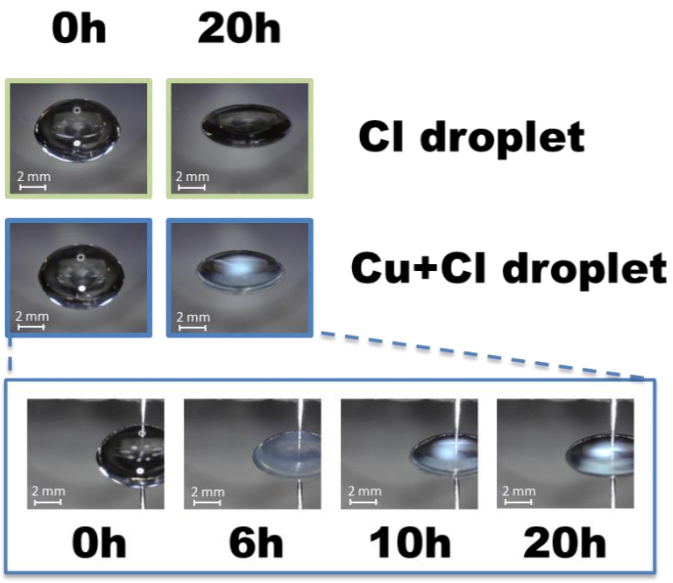

Figure 2. 10.- Cl and Cu+Cl electrolyte droplets pictures at the beginning (0h) and end (20h) of the test. Time-lapse images showing the precipitation process of Cu+Cl electrolyte

2.3.2.1. Electrolyte composition

Additional information is required to explain what is happening inside of the Cu+Cl droplet. Therefore, 1 mL droplets of both electrolytes were studied inside the SKP chamber with the aim of analysing remaining electrolyte. During the droplet test using Cu+Cl electrolyte, a similar curve (not shown) was obtained compared to the one using 50µl (Figure 2. 9), where two potential plateaus were found after 20h of exposure. The main difference is that larger time is needed for stabilisation of the droplet height, as a result of the larger droplet surface area/volume ratio [10], so the abrupt potential transition occurs also later.

A semi-quantitative study of the composition has been carried out by ICP-OES analysis using the remaining volume from the 1 mL droplet after 20h of exposure in the SKP

chamber. The pH was monitored and its value did not change with respect to the initial one (pH = 3.1). Due to the reduction of cupric ions and the formation of a white precipitate in the Cu+Cl electrolyte, copper content inside of the droplets was analyzed. Moreover, the concentration of nickel was also investigated as an indicator of the corrosion progress (anodic dissolution of the less noble nickel layer). In addition, the concentration was also obtained at the beginning of the test and after the first plateau for Cu+Cl electrolyte (Table 2. 2). Results have shown a higher content of Cu (123 ppm) than the initial one (96 ppm) just before the potential transition from the 1st plateau to the 2nd one. This fact can be explained due to the electrolyte concentration as result of water evaporation. No copper is released from the sample, as confirmed by the absence of copper in the Cl droplet analysis (corrosion is located in the less noble nickel layer). Interestingly, after white solid precipitation, no Cu was detectable in the droplet. This fact may indicate the presence of copper in the white precipitate and/or on the microporous system as a consequence of Cu^{2+} reduction during corrosion process. With respect to Ni, it must be said that it can be detected in the 1st plateau (98.7 ppm) before the potential transition occurs, indicating that corrosion had already started. A noticeable increase of the Ni content was found at the end of the test (870 ppm). The comparison of Ni concentration between droplets confirms that the presence of cupric cations in the electrolyte leads to a more severe corrosion attack, in agreement with the lower corrosion resistance found by EIS (Figure 2. 8 & Table 2. 1).

Table 2. 2.- ICP analysis results for Cu and Ni composition of Cu+Cl and Cl droplets.

Electrolyte	Sample	Cu (ppm)	Ni (ppm)
Cu+Cl	Initial	96	<0.1
	1st plateau	123	98.7
	2nd plateau (≈t:20h)	<0.1	870
Cl	20h	<0.1	439

2.3.2.2. Identification of the white precipitate

The absence of copper in the electrolyte at the end of the test indicates the formation of a copper salt that precipitates. Copper, when in a chloride electrolyte, forms complexes

coordinating with chloride anions. This fact, during copper reduction process, stabilizes Cu^{+} complexes so an stepwise reduction to Cu^{+} and later to Cu^{0} takes place in parallel with the chloride free route [36,37]. This reduction process could lead to metallic copper or Cu^{+} species, such as cuprous chloride complexes ($CuCl_{complex}$). Although several copper compounds can be formed, the most probable salt precipitating inside the droplet is solid cuprous chloride ($CuCl_s$), which is a very insoluble (0.047g/L [38]) white colored intermediate from Cu^{2+} reduction. Other copper precipitates such as cupric acetate (blue precipitate, 72g/L), $CuCl_2$ (brown precipitate, 757g/L [38]) and $CuCl_2{\cdot}2H_2O$ (blue precipitate, 757g/L [38]) are less probable due to their colour and higher solubility compared to CuCl. So, XPS has been used to determine the chemical composition of the white precipitate formed during the droplet test. Due to difficulties during surface preparation, the composition reveals that Na & Cl (both originating from residual electrolyte) are present together with adventitious carbon. Despite this issue, Cu and Ni were also detected in lower amount. The high-resolution XPS spectra of Cu 2p (Figure 2. 11) shows the shake-up satellite peaks (binding energy of 940.2 eV to 943 eV) along with a contribution at 934.5 eV are indicative of Cu^{2+} oxidation state, whereas the peak contribution at 932.5 eV is indicative of the presence of Cu^{+} and/or Cu^{0} [39,40]. The presence of Cu^{2+} along with Cu^{+} in XPS results is explained because $CuCl_s$ is very sensitive to oxidation by moist air and, probably, during sample preparation CuCl oxidized. In Figure 2. 12, pictures of the $CuCl_s$ precipitate inside the drop (a) and during XPS sample preparation (b, electrolyte removal step before air drying) allow the observation of the development of a greenish surface in accordance with $CuCl_s$ oxidation to Cu^{2+} species [41].

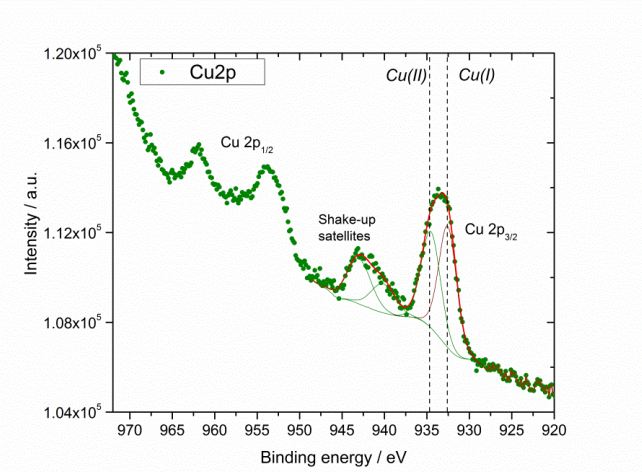

Figure 2. 11.- XPS spectra of the Cu2p region for the white solid precipitate.

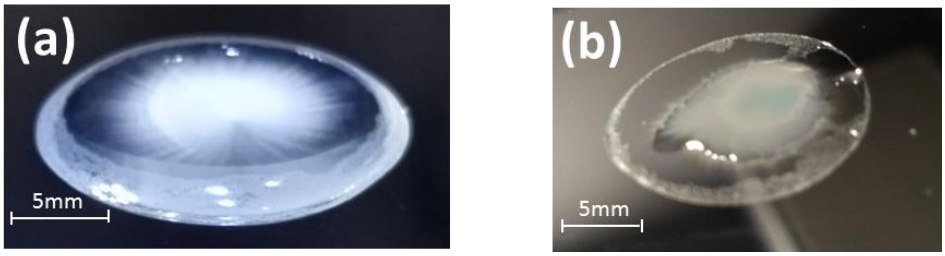

Figure 2. 12.- Image of (a) the CuCl precipitate in the droplet after the SKP test and (b) during sample preparation for XPS.

2.3.2.3. Phenomena inside the Cu+Cl droplet

Therefore, according to the information above, during corrosion process in the Cu+Cl droplet, Cu^{2+} is reducing to Cu^{+}, which probably will stabilize as $CuCl_{complex}$. It can either be partially re-oxidized to Cu^{2+} (by redox equilibrium and by oxygen), or to be reduced to metallic copper in a lower extent. As consequence of the evaporation process of the droplet, $CuCl_s$ precipitation takes place while, simultaneously, a sudden decrease in the potential values occurs. Two possible reasons for such abrupt potential change can be found in literature: i.) the beginning of corrosion as reported for SS304 under $MgCl_2$ droplets [12], and ii) the decrease in cathodic limiting current due to changes in the concentration of the oxidant [42]. Here, the later might be occurring but due to a change in the species responsible for the cathodic reaction. In fact, $CuCl_s$ precipitation is indicating that copper cations are changing from soluble Cu^{2+} towards an insoluble salt of Cu^{+} solid phase after suffering a reduction reaction (Table 2. 2). Therefore, taking into account that cupric cations are governing the cathodic reaction due to their oxidizing effect, a decrease in the cathodic limiting current would also be taking place. If so, this fact could explain why potential decrease at 6h (Figure 2. 9) happens at the same time as $CuCl_s$ precipitation (Figure 2. 10). It was previously observed that the presence of cupric ions in the electrolyte shifts the potential to more noble values (OCP results, Figure 2. 3). Consequently, the depletion of the soluble copper species inside the solution might have the opposite effect: a potential decrease. Therefore, the precipitation of $CuCl_s$ could explain the potential drop and furthermore, it could indicate the change of the cathodic reaction taking place in the 2nd plateau because the system changes from a Cu+Cl electrolyte (cupric ion reduction during the 1st plateau) to a Cl electrolyte (with the exception that a $CuCl_s$ precipate is present).

In order to confirm the assumption above, the OCP values obtained Vs. Ag/AgCl (electrochemical test, Figure 2. 3) have been translated to potential values Vs. SHE to

compare with the droplet test (SKP). The OCP for Cu+Cl electrolyte (10mV vs SHE, Figure 2. 3) and the SKP potential for 1st plateau in the droplet (40mV vs SHE, Figure 2. 9) are quite similar in both tests (OCP and SKP) when cupric ions reduction reaction occurs. On the other hand, the OCP for the electrochemical test under Cl electrolyte (-115mV vs SHE, Figure 2. 3) and the SKP potential in the droplet (-250 mV, Figure 2. 9) are different. Such discrepancy could be indicative that oxygen is playing a role in the cathodic reaction under Cl electrolyte. The increase of the chloride concentration due to the evaporation of the drop (concentration factor) will be negatively affecting O_2 diffusion and solubility, reducing the amount of oxygen available [11,43], and shifting the potential to lower values than expected in the droplet test of the SKP [43]. Probably, an additional comparison may be done but assuming that this is not fully correct, because it could be an effect of the $CuCl_s$ in the SKP potential: the SKP potential difference between the 1st and 2nd plateau ≈100mV in the Cu+Cl drop (Figure 2. 9), which is similar to the OCP difference obtained in the electrochemical test between both electrolytes (≈ 120 mV, Figure 2. 3). It is in agreement with the hypothesis of having two different cathodic reaction in the Cu+Cl droplet as a matter the precipitation process (before and after): cupric reduction reaction is governing in the 1st plateau, whilst a different cathodic reaction is governing in the 2nd plateau (Figure 2. 9).

Finally, it is important to be aware that certain deviation can be expected comparing potentials in the approaches above, considered that the Galvani potential difference between the Kelvin probe and the sample in a system metal-electrolyte is complex, which is given by [44]:

$$\Delta\Phi_{Ref}^{Me} = \Delta\Phi_{El}^{Me} + \chi_{El} + \Delta\Psi_{Ref}^{El} - \chi_{Ref} \qquad \text{Equation 3}$$

where $\Delta\Phi_{Ref}^{Me}$ is the Galvani potential difference between the metal and the probe, $\Delta\Phi_{El}^{Me}$ is the Galvani potential difference between the metal and the electrolyte, χ_{El} is the surface potential of the surface liquid water phase, $\Delta\Psi_{Ref}^{El}$ is the potential between the electrolyte and the probe and χ_{Ref} is the surface potential of the probe itself. Therefore, in the case of the Cu^{2+} droplets, the precipitation of $CuCl_s$ would probably have an extra impact in the potential value obtained with SKP (Equation 3) and additional terms related to the presence of $CuCl_s$ might contribute to the potential. Moreover, the concentration factor due to evaporation under the droplet test in the SKP can also affect to the solubility of O_2 in a chloride based electrolyte and the potential value.

2.3.2.4. Surface area scan

As a difference to the droplet test where the composition of the electrolyte plays an important role in the cathodic reaction (e.g. absence or presence of cupric ions), the potential maps obtained by SKP on surfaces exposed to the environmental conditions of the chamber (air, temperature, humidity in this study) are sensitive to ORR as a cathodic reaction due to the presence of a thin layer of water on the surface. Figure 2. 13 shows 3D potential maps and line scans of cleaned (rinsing $CuCl_s$ as well as the electrolyte) and dried surfaces that previously were exposed to Cl and Cu+Cl droplets. A homogeneous potential distribution between 0 and 60 mV is observed for Cl electrolyte after the exposure to the droplet similar to the initial values obtained before exposure (not shown). However, samples exposed to Cu^{2+} containing electrolyte showed a heterogeneous distribution of potential, where areas with more noble potentials appear (between 100 to 150 mV). It has been reported in literature that exposure to chloride along with Cu^{2+} cations has an impact in the potential: surface previously exposed to electrolyte showed SKP maps with higher values compared to the ones previously exposed just to chlorides [45]. The reasons for such a potential increase could be diverse: i) the formation of a thick oxide layer with different conductivity during the corrosion process of Al-Mg alloys was identified as the main responsible of the potential increase [45], ii) the presence of copper particles that catalyzes the ORR [45,46]. Here, nickel oxide is expected to be leached out for both electrolytes instead of building up an oxide layer during corrosion process, as has been observed by cross-section characterisation [5]. Therefore, the most probable cause is the presence of copper particles acting as localised cathodes and increasing the potential locally.

As a conclusion, copper species (either acting as a contaminant or from the reduction process) could remain in the microporous system promoting the potential differences. Finally, as a general conclusion of this section, the effect of oxidizing agents as well as the role of species with low solubility during evaporation process (both usually present in atmospheric corrosion events), can be monitored by SKP.

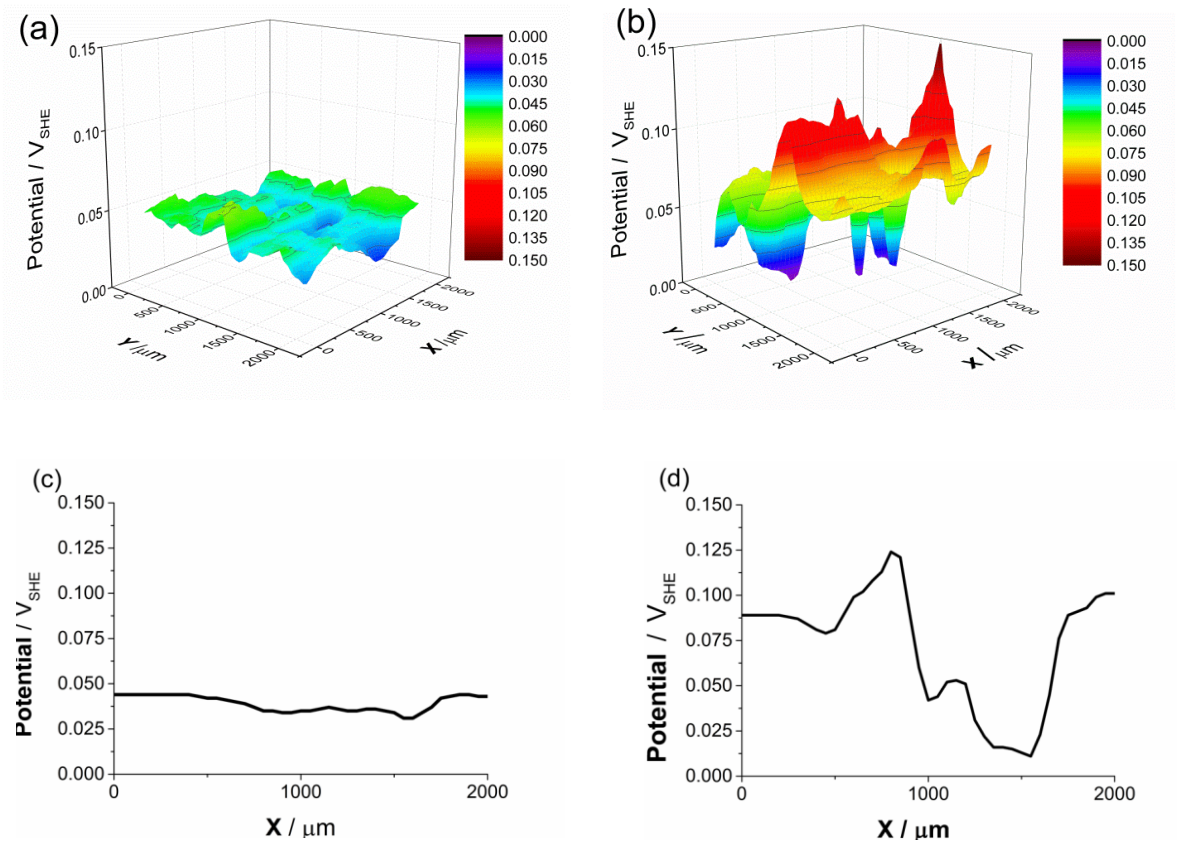

Figure 2. 13.- Potential distribution for microporous nickel-chromium sample exposed to Cl electrolyte: (a) 3D plot and (c) line scan ; and exposed to Cu+Cl electrolyte: (b) 3D plot and (d) line scan.

2.3.2.5. Morphological characterisation

Similar morphological characterisation study to the previous one in section 2.3.1.2 (samples exposed to electrochemical tests) has been done for samples tested in the SKP. Figure 2. 14 shows optical microscopy and FE-SEM images of dried surfaces that previously were exposed to Cl and Cu+Cl droplets (20h).

In contrast to the findings in Figure 2. 4, if both electrolytes are compared here, the main difference from these images is a slightly higher number of corrosion defects for samples exposed to Cl electrolyte (although the total damaged area is quite similar). One initial explanation could be related to the depletion of copper cations in dissolution within the drop (Cu+Cl electrolyte) after 6-7h of exposure due to the precipitation that might hinder their harmful effect as oxidizing agents, providing a similar visual attack under droplet test after 22h of exposure.

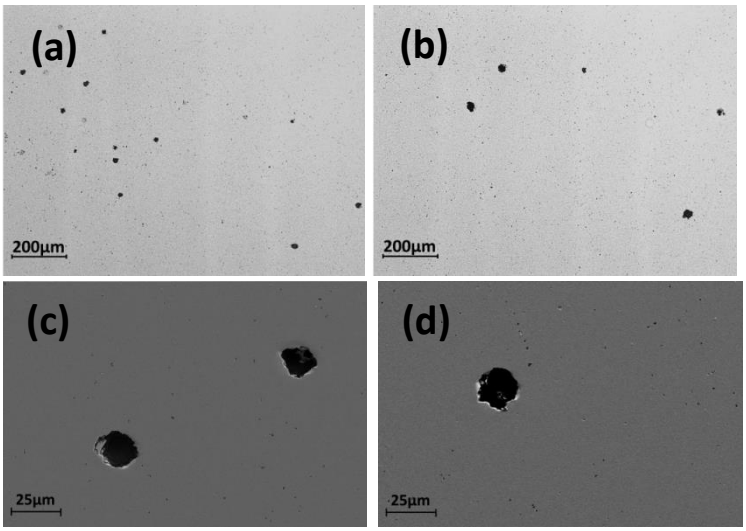

Figure 2. 14.- Images for microporous nickel-chromium sample by OM exposed to droplet test: (a) exposed to Cl electrolyte, (b) exposed to Cu+Cl electrolyte; and by FE-SEM: (c) exposed to Cl electrolyte, (d) exposed to Cu+Cl electrolyte.

If SKP droplet test and electrochemical test are compared for each electrolyte, a similar pore/defect size can be observed for Cl electrolyte but with a much higher number in the sample exposed to the bulk, whereas in the case of the Cu+Cl electrolyte, cupric ion can maintain the aggressiveness during the whole test in the bulk promoting higher attack, whilst in the drop test such aggressiveness is affected by the change in the cathodic reaction (from the 1st to 2nd plateau) and the diffusion due to the presence of a $CuCl_s$ precipitate. In fact, there are several differences between electrochemical test in a cell and the droplet test in the SKP chamber that could explain the morphological differences. Electrochemical tests were run at 49ºC (favored kinetic and diffusion of species) whereas droplet test were done at ambient temperature and under atmospheric conditions (relative humidity close to saturation). As a consequence of evaporation, the droplet concentration increased changing the diffusion and solubility of oxygen [11], which should have an impact if ORR is the cathodic reaction taking place. (e.g. in Cl electrolyte). Moreover, the length of oxygen diffusion paths can vary with the drop thickness/high ant it could cause the coalescence of large anodic and cathodic areas [13]. In contrast, the larger volume of electrolyte in the electrochemical test provides longer diffusion paths favoring the diffusion of corrosion products due to the large concentration gradient between the surface of the sample and the bulk electrolyte [47]. Additional and tailored tests are needed in order to elucidate the effect of each factor in the visual impact.

Finally, EDX analysis performed in the FE-SEM image (Figure 2. 14 (d)), did not show the presence of copper on the surface of chromium. So, if copper particles are the

responsible of the potential increase, they would be locating in micropores, defects, etc. rather than on chromium surface. Further studies are being done to find out whether copper is present or not and where it is located.

2.4. Conclusions

A thorough combination of conventional (OCP and EIS) and SKP techniques highlight a variety of findings difficult to be achieved if such tools/techniques are merely used alone. The following valuable information related to the corrosion process of micropores nickel-chromium systems has been obtained:

- Conventional electrochemical techniques clearly exhibited the aggressiveness of cupric cations: the typical shift toward positive OCP values of oxidizing agents together with the decrease of the R_{ct}.
- Interestingly, EIS diagrams showed an additional time constant at high frequency when cupric cations are present in the electrolyte. The graphical approach using corrected Bode plots not only confirms the new time constant, but also provides information about its physical meaning, most probably related with a diffusion phenomenon.
- SKP droplet test revealed the key role of Cu^{+} cations stabilized by the formation of chloride complexes. A massive Cu^{2+} reduction to Cu^{+} during the corrosion process occurred triggered by $CuCl_s$ precipitation. Additionally, surface maps showed the presence of regions with higher potential values previously exposed to Cu^{2+} containing electrolyte, indicating the effect of copper compounds in the potential of the surface.
- The morphological characterisation reveals different visual impact on the surface, increasing the size and decreasing the number of sites when Cu^{2+} is in the electrolyte. Despite FE-SEM images did not reveal the presence of copper compounds on the surface, it cannot be discarded its presence inside micropores, defects, etc.

The work presented in this chapter was previously published: Larraitz Ganborena, Jesús Manuel Vega, Berkem Özkaya, Hans-Jürgen Grande, Eva García-Lecina; Electrochimica Act., 2019, 318 (2019) 683-694

2.5. References

[1] R. Tremmel, Methods to Improve the corrosion performance of microporous nickel deposits, Plat. Surf. Finish. (1996) 24–28.

[2] Standard Test Method for Copper-Accelerated Acetic Acid-Salt Spray (Fog) Testing (CASS Test), Annu. B. ASTM Stand. B368 (2011) 1–5. doi:10.1520/B0368-09.2.

[3] D. Carl, Corrosion in the automobile industry, in: Man. Ind. Corros. Stand. Control, 1973: pp. 81–88.

[4] L. Pohlmann, G. Bauer, P. Hartmann, P. Wachter, C. Donner, Oscillatory passive active transition during the corrosion in nickel chromium layer systems, J. Solid State Electrochem. 17 (2013) 489–496. doi:10.1007/s10008-012-1949-3.

[5] R. Schmidt, K.O. Thiel, F. Von Horsten, C. Spickermann, G. Vazhenin, N. Baülke, P. Wachter, P. Hartmann, H.J. Schreier, Towards the mechanism of the accelerated corrosion of decorative nickel-chromium coatings in the presence of metals and their salts, Mater. Corros. 65 (2014) 959–967. doi:10.1002/maco.201307104.

[6] C. Langer, W. Wendland, K. Honold, L. Schmidt, J.S. Gutmann, M. Dornbusch, Corrosion analysis of decorative microporous chromium plating systems in concentrated aqueous electrolytes, Eng. Fail. Anal. 91 (2018) 255–274. doi:10.1016/j.engfailanal.2018.04.031.

[7] M. Stratmann, H. Streckel, On the atmospheric corrosion of metals which are covered with thin electrolyte layers-I. Verification of the experimental technique, Corros. Sci. 30 (1990) 681–696.

[8] M. Stratmann, H. Streckel, On the atmospheric corrosion of metals which are covered with thin electrolyte layers-II. Experimental results, Corros. Sci. 30 (1990) 697–714. doi:10.1016/0010-938X(90)90033-2.

[9] C. Chen, F. Mansfeld, Potential distribution in the Evans drop experiment, Corros. Sci. 39 (1997) 409–413. doi:10.1016/S0010-938X(97)83355-0.

[10] M.S. Thomson, G.S. Frankel, Atmospheric Pitting Corrosion Studies of AA7075-T6 under Electrolyte Droplets: Part I. Effects of Droplet Size, Concentration, Composition, and Sample Aging, J. Electrochem. Soc. 164 (2017) C653–C663. doi:10.1149/2.1051712jes.

[11] J.F. Li, B. Maier, G.S. Frankel, Corrosion of an Al-Mg-Si alloy under MgCl2 solution droplets, Corros. Sci. 53 (2011) 2142–2151.

doi:10.1016/j.corsci.2011.02.035.

[12] B. Maier, G.S. Frankel, Pitting Corrosion of Bare Stainless Steel 304 under Chloride Solution Droplets, J. Electrochem. Soc. 157 (2010) C302–C312. doi:10.1149/1.3467850.

[13] S.C. Morton, G.S. Frankel, Atmospheric pitting corrosion of AA7075-T6 under evaporating droplets with and without inhibitors, Mater. Corros. 65 (2014) 351–361. doi:10.1002/maco.201307363.

[14] A. Nazarov, T. Prosek, D. Thierry, Application of EIS and SKP methods for the study of the zinc/polymer interface, Electrochim. Acta. 53 (2008) 7531–7538. doi:10.1016/j.electacta.2007.11.053.

[15] G. Grundmeier, W. Schmidt, M. Stratmann, Corrosion protection by organic coatings: Electrochemical mechanism and novel methods of investigation, Electrochim. Acta. 45 (2000) 2515–2533. doi:10.1016/S0013-4686(00)00348-0.

[16] Z.H. Jin, H.H. Ge, W.W. Lin, Y.W. Zong, S.J. Liu, J.M. Shi, Corrosion behaviour of 316L stainless steel and anti-corrosion materials in a high acidified chloride solution, Appl. Surf. Sci. 322 (2014) 47–56. doi:10.1016/j.apsusc.2014.09.205.

[17] J. Stoulil, T. Prosek, A. Nazarov, J. Oswald, P. Kriz, D. Thierry, Electrochemical properties of corrosion products formed on Zn-Mg, Zn-Al and Zn-Al-Mg coatings in model atmospheric conditions, Mater. Corros. 66 (2015) 777–782. doi:10.1002/maco.201408058.

[18] G.A. Petrocelli, J. V., Hospadaruk, V, Dibari, “The Electrochemistry of Copper, Nickel and Chromium in the Corrodkote and CASS Test Electrolytes,” Plating. 50 (1962).

[19] G.S. Frankel, Pitting Corrosion of Metals, J. Electrochem. Soc. 145 (1998) 2186–2198. doi:10.1149/1.1838615.

[20] K.S.N. Murthy, R. Ambat, E.S. Dwarakadasa, The role of metal cations on the corrosion behaviour of 8090-T851 alooy in a pH 2.0 solution, 36 (1994) 1765–1775.

[21] H.J.W. Lenderink, M.V.D. Linden, J.H.W. De Wit, Corrosion of aluminium in acidic and neutral solutions, Electrochim. Acta. 38 (1993) 1989–1992. doi:10.1016/0013-4686(93)80329-X.

[22] M.A. Veloz, I. González, Electrochemical study of carbon steel corrosion in buffered acetic acid solutions with chlorides and H2S, Electrochim. Acta. 48 (2002) 135–144. doi:10.1016/S0013-4686(02)00549-2.

[23] M.A. Amin, S.S. Abd El-Rehim, E.E.F. El-Sherbini, R.S. Bayoumi, The inhibition of low carbon steel corrosion in hydrochloric acid solutions by succinic acid. Part I. Weight loss, polarization, EIS, PZC, EDX and SEM studies, Electrochim. Acta. 52 (2007) 3588–3600. doi:10.1016/j.electacta.2006.10.019.

[24] M. Keddam, O.R. Mattos, H. Takenouti, Reaction Model for Iron Dissolution Studied by Electrode Impedance, J. Electrochem. Soc. 128 (1981) 266–274. doi:10.1149/1.2127402.

[25] E.M. Sherif, S.-M. Park, Effects of 1,4-naphthoquinone on aluminum corrosion in 0.50M sodium chloride solutions, Electrochim. Acta. 51 (2006) 1313–1321. doi:10.1016/j.electacta.2005.06.018.

[26] H.H. Hassan, Inhibition of mild steel corrosion in hydrochloric acid solution by triazole derivatives: Part II: Time and temperature effects and thermodynamic treatments, Electrochim. Acta. 53 (2007) 1722–1730. doi:10.1016/J.ELECTACTA.2007.08.021.

[27] H. Nara, D. Mukoyama, T. Yokoshima, T. Momma, T. Osaka, Impedance Analysis with Transmission Line Model for Reaction Distribution in a Pouch Type Lithium-Ion Battery by Using Micro Reference Electrode, J. Electrochem. Soc. 163 (2016) A434–A441. doi:10.1149/2.0341603jes.

[28] R. de Levie, On porous electrodes in electrolyte solutions: I. Capacitance effects, Electrochim. Acta. 8 (1963) 751–780. doi:10.1016/0013-4686(63)80042-0.

[29] J. Baux, N. Caussé, J. Esvan, S. Delaunay, J. Tireau, M. Roy, D. You, N. Pébère, Impedance analysis of film-forming amines for the corrosion protection of a carbon steel, Electrochim. Acta. 283 (2018) 699–707. doi:10.1016/j.electacta.2018.06.189.

[30] M.E. Orazem, N. Pébère, B. Tribollet, Enhanced Graphical Representation of Electrochemical Impedance Data, J. Electrochem. Soc. 153 (2006) B129–B136. doi:10.1149/1.2168377.

[31] V.M.-W. Huang, V. Vivier, I. Frateur, M.E. Orazem, B. Tribollet, The Global and Local Impedance Response of a Blocking Disk Electrode with Local Constant-

Phase-Element Behavior, J. Electrochem. Soc. 154 (2007) C89–C98. doi:10.1149/1.2398889.

[32] V.M.-W. Huang, V. Vivier, M.E. Orazem, N. Pébère, B. Tribollet, The Apparent Constant-Phase-Element Behavior of a Disk Electrode with Faradaic Reactions, J. Electrochem. Soc. 154 (2007) C99–C107. doi:10.1149/1.2398894.

[33] Y.B. Amor, E.M.M. Sutter, H. Takenouti, M.E. Orazem, B. Tribollet, Interpretation of Electrochemical Impedance for Corrosion of a Coated Silver Film in Terms of a Pore-in-Pore Model, J. Electrochem. Soc. 161 (2014) C573–C579. doi:10.1149/2.1151412jes.

[34] J.-B. Jorcin, N. Pébère, B. Tribollet, CPE analysis by local electrochemical impedance spectroscopy, Electrochim. Acta. 51 (2006) 1473–1479. doi:10.1016/J.ELECTACTA.2005.02.128.

[35] J.D. Reid, A.P. David, Impedance behavior of a sulfuric acid-cupric sulfate/copper cathode interface, J. Electrochem. Soc. 134 (1987) 1389–1394. doi:10.1149/1.2100677.

[36] W. Shao, G. Pattanaik, G. Zangari, Influence of Chloride Anions on the Mechanism of Copper Electrodeposition from Acidic Sulfate Electrolytes, J. Electrochem. Soc. 154 (2007) D201–D207. doi:10.1149/1.2434682.

[37] H. Zhao, J. Chang, A. Boika, A.J. Bard, Electrochemistry of high concentration copper chloride complexes, Anal. Chem. 85 (2013) 7696–7703. doi:10.1021/ac4016769.

[38] D.R. Lide, S.R. Data, E.A. Board, G. Baysinger, S. Chemistry, C.E. Library, L.I. Berger, R.N. Goldberg, B. Division, H. V Kehiaian, K. Kuchitsu, G. Rosenblatt, D.L. Roth, D. Zwillinger, Handbook of Chemistry and Physics, CRC Press, n.d. doi:978-1466571143.

[39] I. Platzman, R. Brener, H. Haick, R. Tannenbaum, Oxidation of polycrystalline copper thin films at ambient conditions, J. Phys. Chem. C. 112 (2008) 1101–1108. doi:10.1021/jp076981k.

[40] M.C. Biesinger, Advanced analysis of copper X-ray photoelectron spectra, Surf. Interface Anal. 49 (2017) 1325–1334. doi:10.1002/sia.6239.

[41] L. O'Reilly, O.F. Lucas, P.J. McNally, A. Reader, G. Natarajan, S. Daniels, D.C.

Cameron, A. Mitra, M. Martinez-Rosas, A.L. Bradley, Room-temperature ultraviolet luminescence from γ-CuCl grown on near lattice-matched silicon, J. Appl. Phys. 98 (2005) 1–5. doi:10.1063/1.2138799.

[42] C.X. Li, X. Tan, J.F. Li, Z.Q. Zheng, Corrosion behavior of 1420 Al-Li alloy under MgCl2 drops in 33% relative humidity, Mater. Corros. 65 (2014) 476–484. doi:10.1002/maco.201206663.

[43] Q. Liu, M. Chen, Y. Yang, The effect of chloride ions on the electrochemical dissolution of chalcopyrite in sulfuric acid solutions, Electrochim. Acta. 253 (2017) 257–267. doi:10.1016/j.electacta.2017.09.063.

[44] G. Grundmeier, K.M. Jüttner, M. Stratmann, Novel Electrochemical Techniques in Corrosion Research, in: R.W. Cahn, P. Haasen, E.J. Kramer (Eds.), Mater. Sci. Technol. A Compr. Treat. Corros. Environ. Degrad., Wiley-VCH, 2000. doi:10.1002/9783527619306.

[45] E. Juzeliunas, K. Leinartas, W. Fürbeth, K. Jüttner, Study of initial stages of Al-Mg alloy corrosion in water, chloride and Cu(II) environment by a scanning Kelvin probe, Corros. Sci. 45 (2003) 1939–1950. doi:10.1016/S0010-938X(03)00026-X.

[46] A. Nazarov, D. Thierry, Rate-determining reactions of atmospheric corrosion, Electrochim. Acta. 49 (2004) 2717–2724. doi:10.1016/j.electacta.2004.01.066.

[47] S. Hastuty, A. Nishikata, T. Tsuru, Pitting corrosion of Type 430 stainless steel under chloride solution droplet, Corros. Sci. 52 (2010) 2035–2043. doi:10.1016/j.corsci.2010.02.031.

3

The impact of corrosion on microporous nickel-chromium coatings as a function of the electrolyte

3.1. Introduction

Decorative chromium coatings are known for their attractive appearance and good corrosion resistance. These coatings are usually made up of a top microporous chromium layer plated over a system of three distinct nickel layers (microporous, bright and semibright nickel, from top to bottom, respectively), having a plastic substrate (e.g. Acrylonitrile Butadiene Styrene (ABS)) with a copper layer above to ensure the proper adherence between the semibright nickel layer and the substrate (Figure 3. 1). This multilayer system has been designed to preserve the aesthetic appearance and to guide the corrosion front (through the micropores) to the bright nickel layer [1,2]. Therefore, a different potential (as a function of the microstructure and chemical composition [3,4]) for each nickel layer is required, which decreases as follows: semibright nickel > microporus nickel > bright nickel.

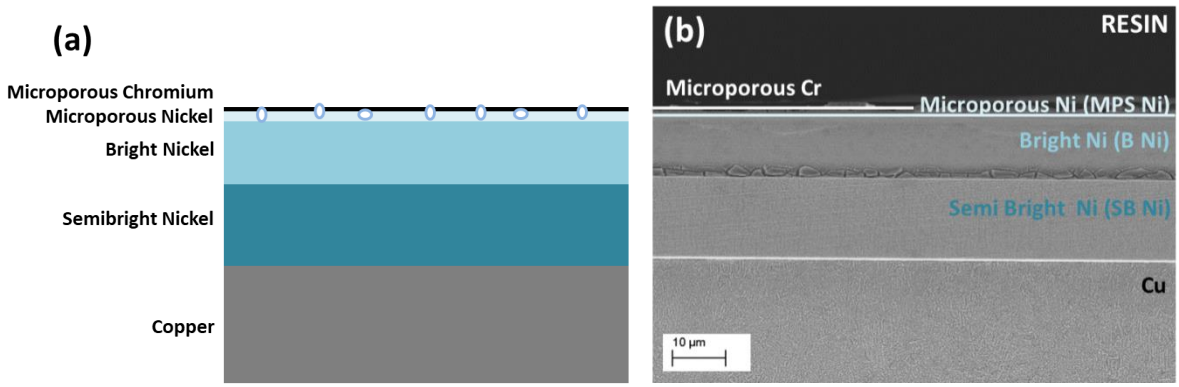

Figure 3. 1.- Microporous nickel-chromium multilayer coatings scheme (a) and FE-SEM cross section (b).

Due to the miscellaneous applications of these decorative coatings and the diversity of aggressive environments, its evaluation in terms of corrosion resistance has become an important issue. One of the most used methods for decorative chromium plating is the Copper-Accelerated Acetic Acid-Salt Spray test (CASS test, ASTM B368) [5], which is based on the nebulisation of the solution (acidic cupric chloride and sodium chloride mixture) at 49ºC inside of a chamber. It has been extensively used either for new development or quality control of these coatings thanks to the similar degradation observed under accelerated conditions and in-service life [6].

In addition to CASS test, electrochemical techniques have been successfully used to study the corrosion behaviour of decorative duplex nickel-chromium coatings. Polarisation curves revealed the beneficial effect of the presence of a microporous (high-pore-density distribution) chromium layer [7]. Potentiodynamic measurements were also in good agreement with the results of cross-section characterisation, showing the preferential corrosion attack of the nickel layer as a function of its (designed) potential value [8]. However, depending on the aggressive environment, semibright nickel switched its behaviour from cathodic (under exposure to acetic acid salt spray and corrodkote tests) to anodic (SO_2 test), most probable due to the presence of nickel sulphide ions on the surface to such an extent that were able to hinder the initial potential between nickel layers.

Nowadays, decorative systems including microporous nickel as a third nickel layer have revealed the change in corrosion mechanism from nickel dissolution by corrosion to chromium one caused by the absence of oxygen in the pores under saturated $CaCl_2$ electrolyte [9]. Moreover, the use of different deicing salts and the establishment of different galvanic couples, could lead to the development of heterogeneous corrosion attack over the same sample due to changes in corrosion parameters (aeration, pH, etc.) [10].

According to this, the aggressive environment (e.g. SO_2, cupric ions, etc.) seems to play a role, but most of the efforts in terms of research seem to be devoted to studying the harmful effect of chlorides. In fact, there are not too many published studies focused on the effect of cupric ions, which increases the corrosion rate for microporous nickel-chromium coatings [11,12]. Recently, Electrochemical Impedance Spectroscopy (EIS) and Scanning Kelvin Probe (SKP) results revealed that cuprous ions are involved in the corrosion process due to the reduction of cupric ions. Moreover, the different morphological impact/damage on the surface depends on the presence or absence of cupric ions in the electrolyte [13].

Nonetheless, taking into account that one of the most important application is the decorative one, it has not been explored in detail the reason why the visual impact is drastically different with and without cupric ions in the electrolyte [13]. In fact, it is crucial to know how the corrosion of nickel layers underneath chromium one affects to the latter.

The aim of this work is to understand how cupric ions combined to chloride ones affects to the corrosion mechanism of nickel layers for microporous nickel-chromium system, and therefore, its impact in the appearance of the surface. The study was made by

means of electrochemical measurements (OCP, EIS and potentiodynamic polarisation curves) and characterised by FE-SEM using different electrolytes: an electrolyte based on the composition of the CASS test and modified ones (varying cupric cations concentration). Results have drastically shown how corrosion affects to different nickel layers as a function of the type of electrolyte.

3.2. Experimental

3.2.1. Materials

Samples of 10 cm x 15 cm of microporous nickel-chromium multilayer coatings were obtained plated on ABS substrates from trivalent chromium baths. Three additional systems having the following nickel as a top layer were also obtained:

I. Microporous nickel (MPS Ni).
II. Bright nickel (B Ni).
III. Semibright nickel (SB Ni).

The thickness of each nickel layer and their relative potential difference between was determined by Simultaneous Thickness and Electrochemical Potential Test (STEP test) according to ASTMB764. Thickness was increasing from top to bottom: MPS Ni (1.40 ± 0.20µm) < B Ni (10.70 ± 1.40µm) < SB Ni (12.20 ± 1.70µm) and the potential difference was the following: 103 ± 11mV between MPS/B Ni layers and 189 ± 23mV between SB/B Ni layers.

Three electrolytes with different aggressiveness were used in the study: (1) 0.9M NaCl at pH 3.1 (Cl electrolyte), (2) 0.9M NaCl+1.5mM $CuCl_2$ at pH 3.1 (Cu+Cl electrolyte) and (3) 0.9M NaCl+3mM $CuCl_2$ at pH 3.1 (2xCu+Cl electrolyte) The electrolytes were prepared with analytical grade reagent and 18.5 MΩcm deionized water and adjusted to pH 3.1 with glacial acetic acid.

3.2.2. Electrochemical evaluation

Electrochemical tests were performed at 49ºC a minimum of three times in a flat and jacketed three electrode cell inside a Faraday´s cage and using a VSP-300 Biologic potentiostat. A three electrode configuration was used: a working electrode (1cm^2 of the sample) exposed to a volume of 250 mL of quiescent electrolyte, a platinum mesh as a counter electrode and a saturated calomel reference electrode (SCE, saturated KCl) as reference electrode. Open circuit potential (OCP) measurements were performed in

naturally aerated electrolytes during 22h whilst potentiodynamic tests were done using both naturally aerated (O_2) and deaerated (N_2 atmosphere) electrolytes. The polarisation experiments were divided in three steps: (1) 1.5h at OCP for naturally aerated and deaerated solutions, (2) a linear polarisation resistance (LPR) measurement in the potential range (E_{ocp}) ±10mV at 0.167mVs^{-1} scan rate, and (3) potentiodynamic scans at the same scan rate than step 2.

Anodic and cathodic branches were obtained, separately, in order to avoid any interference due to copper deposition as a consequence of potentiodynamic polarisation. Curves were starting from OCP to 300mV in the anodic direction and from OCP to -250mV in the cathodic one, respectively.

Corrosion current density (j_{corr}) calculations were made using Stern-Geary relation [14], given in the following equation:

$$j_{corr} = \frac{\beta_a \beta_c}{2.3 R_p (\beta_c - \beta_a)}$$

Where β_a and β_c are the anodic and cathodic Tafel slopes and R_p the polarisation resistance obtained from the LPR measurement.

3.2.3. Electrolyte transformation test

A particular test was designed to change the electrolyte composition during exposure of microporous nickel-chromium multilayer coatings to: (1) Cl electrolyte during 25 hours which was shifted to (2) Cu+Cl electrolyte by the addition of the copper salt during 22 more hours (47h in total). OCP was continuously measured, except for the range of time invested for the EIS measurement, within an interval of time of once per hour. EIS were done applying ± 10mV sinusoidal wave perturbation versus OCP, being the frequency range from 100kHz to 10mHz, with 10 points per decade. OCP and EIS tests were done using saturated calomel (SCE, saturated KCl) as reference electrode and a platinum mesh as counter electrode. Impedance data was graphically calculated by Zview© software. For comparison purposes, a reference test using the same electrolyte without any modification was done.

3.2.4. Characterisation

Field emission scanning electron microscope (FE-SEM) Zeiss Ultraplus was employed for cross-section characterisation of corrosion damage into the samples. A Leica DM4000M optical microscope was used for the superficial microstructure characterisation.

3.3. Results and Discussion

3.3.1. OCP under Cl and Cu+Cl electrolytes

In order to study the corrosion damage as a function of the presence of cupric ions in the electrolyte, microporous nickel-chromium multilayer samples were exposed to (1) Cl and (2) Cu + Cl electrolytes, respectively, at 49ºC. Figure 3. 2 shows the evolution of the potential with time during 22 hours.

A continuous decrease of OCP can be observed for Cl electrolyte showing two different slopes that tend to be stabilised. In the case of Cu+Cl electrolyte, a steady regime is reached at shorter time. The initial trend (i.e. potential decrease) is inverted around 2h of exposure showing a sudden and temporary increase of the potential, where the most important feature to be discussed is the different potential value reach at 22h. It can be explained due to their oxidising nature of Cu^{2+} ions [13,15,16].

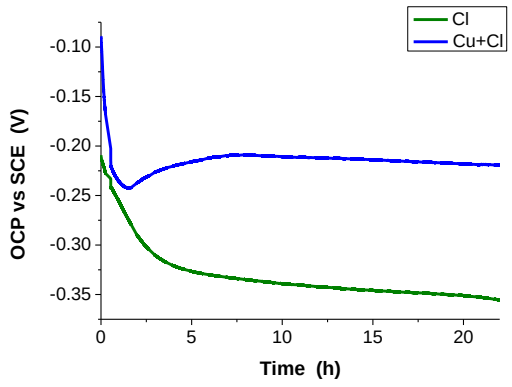

Figure 3. 2.- OCP versus time for decorative microporous nickel-chromium samples in (i) Cl and (ii) Cu+Cl electrolytes.

3.3.2. Surface modification

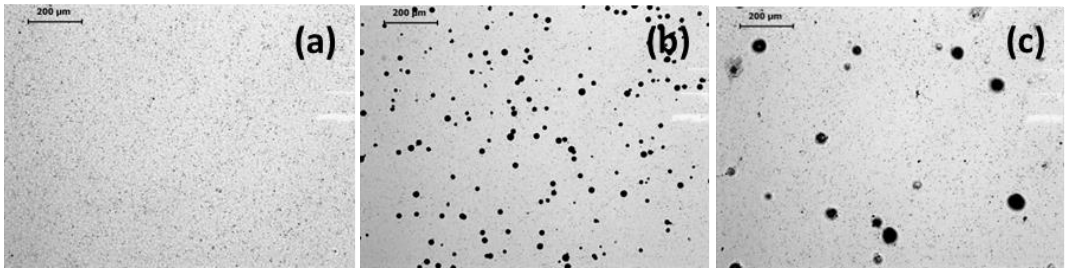

Figure 3. 3.- Images for microporous nickel-chromium sample by OM: (a) before exposure, (b) exposed 22 hours to Cl electrolyte, and (c) exposed 22 hours to Cu+Cl electrolyte.

Microporous nickel-chromium samples were characterised by optical microscopy after 22 hours of exposure to Cl and Cu+Cl electrolytes. Figure 3. 3 shows the images of the surface before (a) and after ((b) and (c)) exposure. Results have shown a different attack depending on the composition of the electrolyte: samples exposed to Cl electrolyte showed a homogeneous distribution of defects in number and size. In contrast, samples exposed to Cu+Cl electrolyte showed a lower amount of defects but bigger in size and randomly distributed. Such impact on the surface appearance comparing both electrolytes could be indicative of the corrosion process underneath chromium, independently of the increase of corrosion rate by the presence of cupric ions. It is going to be explored in the following section.

3.3.3. Cross-section characterisation by FE-SEM

In order to explore the damage on nickel layers underneath the chromium one, cross-section characterisation was made by FE-SEM after 22 hours of exposure to both electrolytes. Despite the corrosion defects were called pits in earlier decorative nickel-chromium systems without intended microdiscontinuities [7] [8], here will be called “active sites” to avoid misunderstanding with “pitting” terminology in passive metals and their alloys [15]. It will also allow to distinguishing from micropores that do not undergo corrosion.

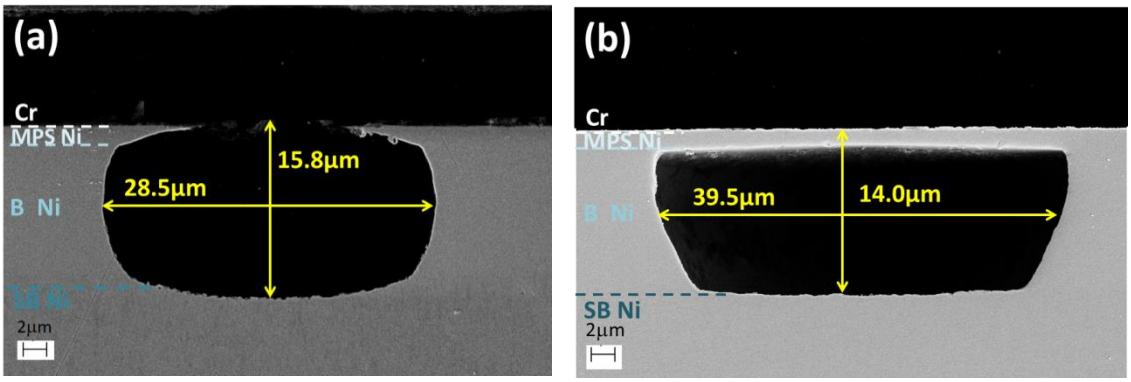

Figure 3. 4.- FE-SEM images of active sites developed in microporous nickel-chromium multilayer coatings exposed 22 hours to (a) Cl electrolyte and (b) Cu+Cl electrolyte. Legend showing the positon of each layer as a function of the thickness: Cr (chromium), MPS Ni (microporous nickel), B Ni (bright nickel) and SB Ni (semibright nickel), respectively.

Figure 3. 4 (a) is showing the preferential corrosion of B Ni layer in Cl electrolyte as well as the attack of MPS Ni layer. However, the later was designed to behave cathodically [1] as it was confirmed by the potential difference obtained by STEP test (103mV ± 11mV).

In contrast, specimens exposed to Cu+Cl electrolyte (Figure 3. 4 (b)) showed actives sites where the corrosion front was mainly located in the B Ni layer as it was expected. Indeed, the multilayer nickel system was design for having different electrochemical potential and once the galvanic coupling occurs, the noblest layers are cathodically polarised (i.e. SB or MPS Ni) and the lest noble nickel layer (i.e. B Ni) is anodically polarised [17]. Further characterisation will be done to explain it.

3.3.3.1. Shape of the active sites

A rectangular shape was observed by FE-SEM when copper is present in the electrolyte, preserving chromium/MPS Ni /SB nickel layers. However, the active sites in Cl electrolyte showed a rounded shape, which is favoured to undergo a lateral expansion through the B Ni layer once the SB Ni layer is reached in depth. Apparently, the thinning of the MPS Ni layer by corrosion has a premature impact in the undermining of the chromium layer, due to absence of the physical support that is providing the former. Indeed, the detachment of the corroded MPS Ni/chromium layers occurs as can be observed in

Figure 3. 5. Here, the both layers were broken when the thickness of the MPS Ni layer was below 300-400nm whilst the chromium layer maintain its 200nm along the entire micrography.

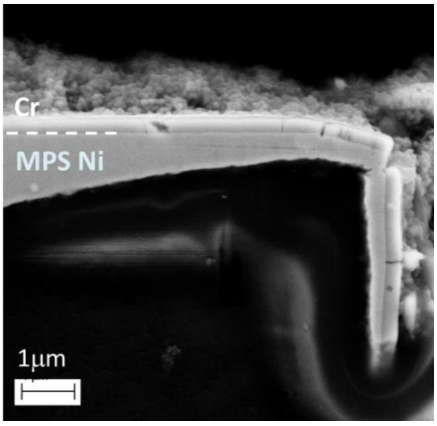

Figure 3. 5.- FE-SEM image showing the breakdown of the thinnest part of chromium + MPS Ni layers in an active site developed in microporous nickel-chromium multilayer coating exposed to Cl electrolyte and layers indications: Cr (chromium) and MPS Ni (microporous nickel).

3.3.3.2. Type and width of active sites

Additional information was obtained measuring parameters like height, width and the type of active sites, which have been classified in two different groups after 22h of exposure in both electrolytes: (A) closed ones (preserving the chromium layer on the top), and (B) opened ones (without top chromium layer). It has to be taken into account that actives sites were randomly distributed along the cross section after metallographic preparation of the sample, so these results have to be considered as representative values of the total population of active sites.

Table 3. 1 reveals that the electrolyte composition affects the morphology as well as the size of the damage. Cl electrolyte showed the narrowest actives sites (32.7 ± 9.4µm) and most of them were opened (70%) due to the corrosion attack of MPS Ni layer. In contrast, despite cupric ions are promoting the widest actives sites (88.0 ± 29.0µm) most of them were closed (72%). The enhanced lateral progress of corrosion front for Cu + Cl electrolyte is in agreement with the lower impedance and corrosion resistance previously reported [13].

Table 3. 1.- Features of active sites created in microporous nickel-chromium multilayer coatings after 22 hours of exposure to Cl and Cu+Cl electrolytes, respectively. Height and width are expressed as mean with its standard deviation.

Electrolyte	**Active sites features**					
	Height (µm)	Width (µm)	Opened		Closed	
			Minimum Width (µm)	%	Width range (µm)	%
Cl	16.8 ±1.5	32.7 ±9.4	28.5	70	20.0-40.6	30
Cu+Cl	13.8 ±0.9	88.0 ±29.0	87.6	28	39.5-165.5	72

However, a straightforward correlation between lower corrosion resistance and higher visual impact on the surface (Figure 3. 3) cannot be made. In fact, the breakdown of the thin chromium layer on the top was affected by different corrosion mechanisms depending on the electrolyte:

(i) Cl electrolyte. Despite of the lower width (28.5 µm), the dissolution of MPS Ni layer facilitates a premature undermining of the chromium one (increasing the number of open sites vs. closed ones) due to the absence of the mechanical support underneath (Figure 3. 5). This finding justifies the higher density of open active sites with lower diameter on the surface of microporous nickel-chromium multilayer samples exposed to Cl electrolyte compared to Cu+Cl one (Figure 3. 3).

(ii) Cu+Cl electrolyte. Thanks to the preservation of MPS Ni layer underneath the chromium one during corrosion, the top chromium layer has a better mechanical support compared to Cl electrolyte. Therefore, the active sites were able to reach a larger width (87.6µm was the minimum width observed for opened active sites), maintaining a higher number of closed active sites. Although the critical width/diameter ratio (taking into account their circular shape [17]) has been increased to promote the chromium layer undermining, the aggressiveness of Cu+Cl electrolyte provokes the presence of a lower amount of open active sites but with larger diameter on the surface compared to Cl electrolyte (Figure 3. 3).

3.3.3.3. Height of active sites

Regarding to the height of active sites, values were obtained measuring from the top of the chromium layer to the bottom. Theoretically, if SB Ni layer is not corroded (bearing in mind that it was designed to be the most noble nickel layer with a potential difference of 189mV ± 23mV vs. B Ni layer according to step test), the maximum height expected would be around 13-14 µm (the sum of plated chromium + MPS Ni + B Ni layers). However, active sites obtained after exposure to Cl electrolyte showed deeper values (around 16.8 ± 1.5µm), which were above the theoretical ones, indicating that SB Ni layer could had also been attacked during the progress of corrosion (Figure 3. 4(a)). Despite nickel layers were designed with a potential difference to guide the corrosion front only to the B Ni layer into a multilayer system, the three nickel layers were affected by corrosion in Cl electrolyte.

As a summary, it seems to be a correlation between the corrosion of the different nickel layers (Figure 3. 4) and the visual impact on the surface (Figure 3. 3), which is mainly determined by the aggressiveness of the electrolyte and the type of corrosion mechanism behind. The aesthetic of the chromium layer is favoured thanks to the physical support provided by MPS Ni layer (i.e. presence of closed active sites in Cu + Cl electrolyte versus open ones in Cl electrolyte). The corrosion of SB Ni layer in Cl electrolyte can be neglected in terms of impact on the surface.

3.3.4. Polarisation curves of microporous nickel-chromium multilayer samples

In order to find out an explanation to the different corrosion mechanism as a function of the electrolyte, a set of potentiontiodynamic polarisation tests were performed using different substrates and aeration conditions.

3.3.4.1. Complete samples

Polarisation curves were obtained for microporous nickel-chromium multilayer samples in naturally aerated Cl and Cu+Cl electrolytes, respectively (Figure 3. 6 (a)), and the different parameters are summarised in Table 3. 2. When comparing the results, there is an increase in the current density (fourfold higher) for Cu+Cl electrolyte (j_{corr} = 14.10 ± 3.10µAcm^{-2} vs. 3.7 ± 1.7µAcm^{-2} in Cl electrolyte), that can be explained by the oxidising effect of Cu^{2+} ions (also shown by a positive shift in the E_{corr}) [15,16]. The presence of Cu^{2+} ions also reduces the R_p to 1.5±0.3 kohm·cm^2 (6.7±1.2 kohm·cm^2 in Cl electrolyte),

indicating better corrosion behaviour in the absence of copper due to the lower aggressiveness of the electrolyte.

Table 3. 2.- Electrochemical parameters obtained for microporous nickel-chromium multilayer coatings in Cl and Cu+Cl electrolyte. Data are expressed as mean with standard deviation.

Electrolyte	E_{corr} (mV $_{vs\ SCE}$)	R_p (kohm·cm^2)	β_a (mV)	$-\beta_c$ (mV)	j_{corr} (μA·cm^{-2})
Cu + Cl (O_2)	-232 ±12	1.5 ±0.3	87 ±8	111 ±10	14.10 ±3.10
Cl (O_2)	-298 ±15	6.7 ±1.2	60 ±6	535 ±170	3.70 ±1.70

Regarding to the anodic branch of the polarisation curves, an active region with monotonic increase of current during the first 200mV of anodic overpotential was found independently of the electrolyte, suggesting a uniform corrosion related to nickel oxidation (anodic Tafel region (β_a) of ≈ 60-87mVdec^{-1}). At higher potentials, above 200mV of anodic overpotential, the slope of the polarisation curve changed abruptly and the current increased with a slower rate, probably due to the limited passage and access of species to the metal surface as consequence of the formation of a stable film of corrosion products.

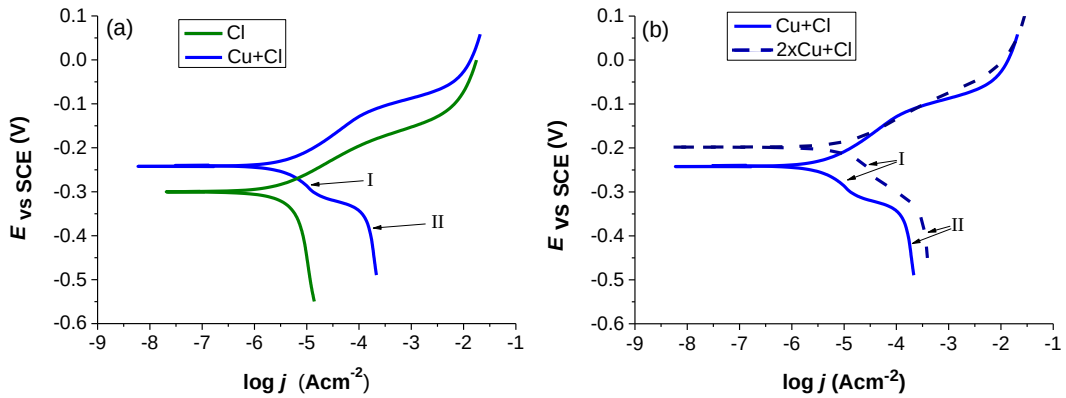

Figure 3. 6.- Polarisation curves corresponding to microporous nickel-chromium system in naturally aerated (a) Cl and Cu+Cl electrolyte, and (b) Cu+Cl electrolyte and 2xCu+Cl electrolyte.

On the other hand, cathodic branches showed a different trend. In the case of the Cl electrolyte, the possible reduction reactions were oxygen reduction reaction (ORR) or

proton reduction reaction. Despite the cathodic branch showed a limiting current density (j_L) as in mass transport controlled processes (e.g. oxygen diffusion), additional tests have been addressed below for better understanding the cathodic reactions. In contrast, a stepped shape was observed for Cu+Cl electrolyte, where the transition from step I to step II can be seen around -300mV (Figure 3. 6). The stepped shape of Cu+Cl electrolyte cathodic branch could be indicative of the stepwise Cu^{2+} ion reduction (i.e. from Cu^{2+} to Cu^{+}, and from Cu^{+} to Cu^{0}), as described in other systems [18]. Cupric ion, when in a chloride electrolyte, coordinates with chloride ions and forms complexes. This fact, during cupric ion reduction process, stabilises Cu^{+} in chloride complexes [13] so an stepwise reduction to Cu^{+} and later to Cu^{0} takes place [19,20]. The increase in the current at the beginning of the polarisation might correspond to Cu^{2+}/Cu^{+} reduction reaction, whereas the sudden current increase (before II) might correspond to Cu^{+}/Cu^{0} reduction, where a j_L value can also be obtained.

Finally, in order to confirm that cupric ion reduction was taking place in Cu+Cl electrolyte, polarisation tests were also performed using double Cu^{2+} concentration (2xCu+Cl electrolyte). Figure 3. 6 (b) exhibits the results that showed that cupric ion reduction was governing the cathodic reaction in Cu+Cl electrolyte instead ORR. Despite polarisation curves show similar trend for the anodic and cathodic branches, the increase of cupric ion concentration in the electrolyte led to an increase of the potential (shift to more positive values due to the oxidising effect of cupric ion), as well as an increase in the j_L in the cathodic branch.

It can be concluded that when cupric ions are added to the chloride solution a stepwise cupric ions reduction occurs as a cathodic reaction. Moreover, the oxidising effect [15,16] accelerates the corrosion of bright nickel [11–13] as can be observed by the lateral progress of corrosion front found for active sites developed in Cu+Cl electrolyte (Figure 3. 4).

3.3.4.2. Incomplete samples

Different nickel coatings were tested as a “top layer” in order to study their susceptibility to act as anode. The idea is to clarify the change in the corrosion mechanism studying the variation of the corrosion potential as a function of the electrolyte, and therefore, to explain the shape of the active sites [8]. Moreover, the motivation to study deaerated conditions in Cl electrolyte was to simulate the expected impact of the oxygen depletion within the active sites, especially when the active sites are closed [8,9].Therefore,

polarisation curves were obtained in Cl and Cu+Cl electrolytes under naturally aerated and deaerated conditions for each nickel layer (MPS, B and SB Ni, respectively).

3.3.4.2.1. Polarisation curves in Cl electrolyte

Figure 3. 7 shows a similar trend for all curves (different nickel layers in Cl electrolyte) obtained in naturally aerated and deaerated conditions, respectively. As it was described above for the complete system (with a chromium layer on the top), the six anodic branches exhibit a monotonic increase of current, indicating uniform nickel corrosion that later increases with a slower rate. However, cathodic branches are affected by the presence of oxygen: mass transport control (similar j_L is obtained for all samples at -470mV) related to the ORR is observed under aerated conditions, which is confirmed thanks to the absence of j_L under deaerated conditions in Figure 3. 7 (b).

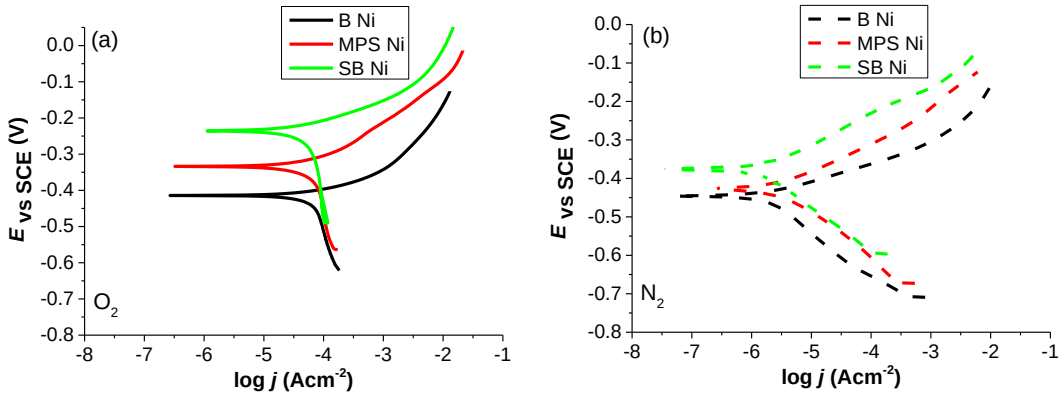

Figure 3. 7.- Polarisation curves corresponding to bright nickel (B Ni), microporous nickel (MPS Ni) and semibright nickel (SB Ni) layers in Cl electrolyte in (a) naturally aerated, and (b) deaerated conditions.

This finding confirms the role of oxygen during corrosion in Cl electrolyte. Indeed, if several parameters are compared (Table 3. 3), the main difference is found between aerated and deaerated conditions: R_p (O_2) < R_p (N_2) and j_L (O_2) >> j_{corr} (N_2) affecting to the corrosion kinetics. Although SB Ni seems to be the less prone to corrode among all nickels, it is difficult to find a difference between MPS Ni and B Ni in this electrolyte. Therefore, a detailed analysis focused on a thermodynamic parameter such as the corrosion potential has been done below.

As it was expected, the E_{corr} was increasing in the following order under aerated conditions: B Ni (-423mV) < MPS Ni (-333mV) < SB Ni (-235mV) that is due to the different chemical compositions of each nickel layer [3]. Despite E_{corr} values were shifted to more negative values under deaerated conditions, the same trend was observed (-461mV for B Ni < -429mV for MPS Ni < -383mV for SB Ni). However, the values are becoming closer in absence of oxygen, especially between B Ni and MPS Ni samples, indicating a similar susceptibility to be corroded from a thermodynamic point of view that could explain why the corrosion of MPS Ni layer occurs in the complete multilayer system.

Table 3. 3.- Electrochemical parameters obtained for different nickel layers in Cl electrolyte under aerated and deaerated conditions. Data are expressed as mean with standard deviation.

Sample/condition	E_{corr} ($mV_{vs\ SCE}$)	R_p ($kohm \cdot cm^2$)	b_a (mV)	$-b_c$ (mV)	j_{corr} ($\mu A \cdot cm^{-2}$)
B Ni O_2	-423±10	0.23±0.05	81±4	∞	-
MPS Ni O_2	-333±3	0.34±0.02	115±5	∞	-
SB Ni O_2	-235 ±15	0.40±0.02	70±6	∞	-
B Ni N_2	-461±12	2.96±0.27	59±7	120±6	5.8±0.7
MPS Ni N_2	-429±6	5.49±0.48	83±7	142±10	4.2±0.6
SB Ni N_2	-383±18	10.30±2.04	87±17	109±6	1.9±0.6

So, in order to do an analysis in depth of the variation of potential between layers under aerated and deaerated conditions, Table 3. 4 summaries the E_{corr} difference (ΔE_{corr}) by subtracting the value of the lest noble sample (B Ni) to MPS and SB Ni, respectively [21]. In general, the values obtained under aerated conditions are in agreement with the ones obtained by the STEP test , indicating that theoretically, the corrosion front should be focused on the lest noble layer (B Ni). However, under deaerated conditions ΔE_{corr} (MPS-B Ni) goes from 90mV (O_2) to 32 mV (N_2) and ΔE_{corr} (SB-B Ni) goes from 188mV (O_2) to 78mV (N_2). This finding might explain that the initial potential difference between nickel layers may be not maintained during the entire corrosion process due to oxygen depletion inside the active sites [8,9]. Therefore, it implies that the protection by galvanic

coupling with B Ni layer is hindered, and therefore, the corrosion attack of other Ni layers can be expected in Cl electrolyte (Figure 3. 4(a)).

Although MPS Ni layer underwent a large degree of corrosion (ΔE_{corr} (MPS-B Ni) = 32mV (N_2), Table 3. 4) SB Ni layer seems to be affected. Previous studies showed that at least a potential difference of 70-100mV is required for an effective corrosion protection of SB Ni layer by B Ni one [22]. Then, if ΔE_{corr} (SB-B Ni) reaches a value around 78mV (N_2) (Table 3. 4), the protection of SB Ni layer is reduced. It can explain the height values around 16.8 ± 1.5µm (Table 3. 1) after exposure to Cl electrolyte (Figure 3. 4(a), indicating that SB Ni layer has been partially corroded compared to active sites formed during exposure to Cu+Cl electrolyte (Figure 3. 4(b)), where the SB Ni layer is intact according its height value (13.8 ±0.9µm,Table 3. 1).

Table 3. 4.- Potential difference between nickel layers in Cl and Cu+Cl electrolytes

Ni layers	**ΔE_{corr}/ Cl (O_2)**	**ΔE_{corr}/ Cl (N_2)**	**ΔE_{corr}/ Cu+Cl (O_2)**	**ΔE_{corr}/ Cu+Cl (N_2)**
MPS - B Ni	90 ±11 mV	32 ±13 mV	46 ±4 mV	58 ±5 mV
SB - B Ni	188 ±18 mV	78 ±24 mV	116 ±3 mV	118 ±3 mV

As a summary for Cl electrolyte, the depletion of oxygen concentration inside the active sites led to changes that affect the susceptibility of corrosion for the different nickel layers, decreasing the potential differences between them and hindering the protection provided by the sacrificial B Ni layer.

3.3.4.2.2. Polarisation curves in Cu+Cl electrolyte

Polarisation curves of the different nickel layers in Cu+Cl electrolyte under naturally aerated (a) and deaerated (b) conditions are showed in Figure 3. 8. Once again, cupric ion reduction was proven to be the main cathodic reaction in Cu+Cl electrolyte. In fact, similar polarisation curves have been obtained independently of the presence/absence of O_2, where similar features are expected for the anodic and cathodic branches.

If potential values are obtained, the E_{corr} is increasing as expected: bright nickel (-227mV(O_2)/-229mV(N_2)) < microporous nickel (-181mV(O_2)/-171mV(N_2) < semibright

nickel (-111mV(O_2 and N_2)). Although this finding is in agreement with Cl electrolyte, here microporous and bright Ni layers did not undergo corrosion, which could be explained by the ΔE_{corr} values obtained under both aeration conditions (Table 3. 4). Apparently, the ΔE_{corr} are quite similar, indicating that the absence of oxygen inside the active site should not affect to the corrosion of the nickel layers. Indeed, ΔE_{corr} SB-B Ni is nearly the same (116 ±3 mV and 118 ±3 mV) and ΔE_{corr} MPS-B Ni has even slightly increased (from 46 ±4 mV to 58 ±5 mV). Therefore, in contrast to Cl electrolyte, the absence of oxygen does not affect the integrity of MPS and SB Ni layers when cupric ions are present in the electrolyte. Apparently, such a ΔE_{corr} seems to be enough to avoid the inversion to anode of SB Ni (which is in agreement with literature [22]) and MPS Ni layers, respectively, despite the fact that ΔE_{corr} for the latter is a bit lower (46-58 mV, Table 3. 4). Further research can be done in order to explain it, but the ΔE_{corr} MPS/B Ni threshold to avoid MPS Ni corrosion should be in between 30 and 50 mV.

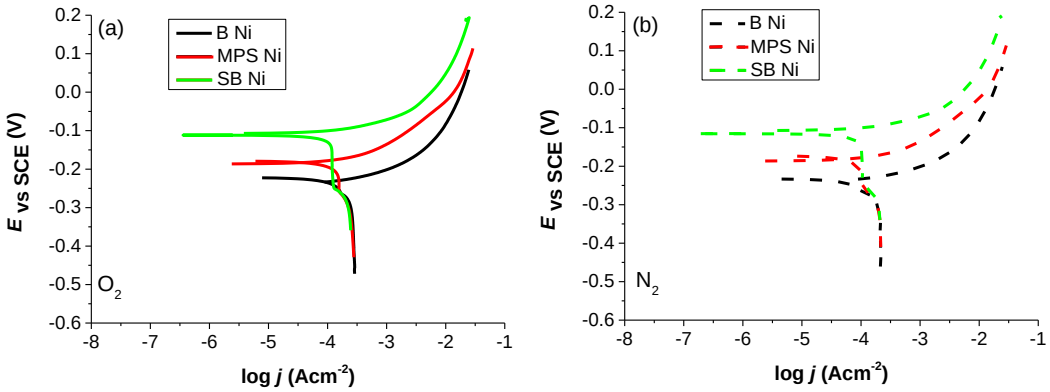

Figure 3. 8.- Polarisation curves corresponding to bright nickel (B Ni), microporous nickel (MPS Ni) and semibright nickel (SB Ni) layers in Cu+Cl electrolyte in naturally (a) aerated, and (b) deaerated conditions.

3.3.5. Electrolyte transformation test

This test was designed in order to confirm the impact of cupric ions in the corrosion mechanism of microporous nickel-chromium multilayer system varying the electrolyte composition and monitoring OCP and EIS values. Although the test was initially performed using Cl electrolyte, it was converted into Cu+Cl electrolyte after 25 hours of exposure within a total period of 47 hours. A second measurement was performed in parallel just using Cl electrolyte during 47h.

Figure 3. 9 (a) is showing the OCP evolution for such a test. As soon as $CuCl_2$ was added to the solution, there was a sudden shift of the OCP to more noble values [13,15,16], which is in agreement with the results in Figure 3. 2 comparing both electrolytes. Simultaneously, once $CuCl_2$ was added to the solution, the EIS results showed a drastic drop in charge transfer resistance (Figure 3. 9 (b)). Such new values are in agreement with the charge transfer resistance differences described previously in Cl and Cu+Cl electrolytes [13].

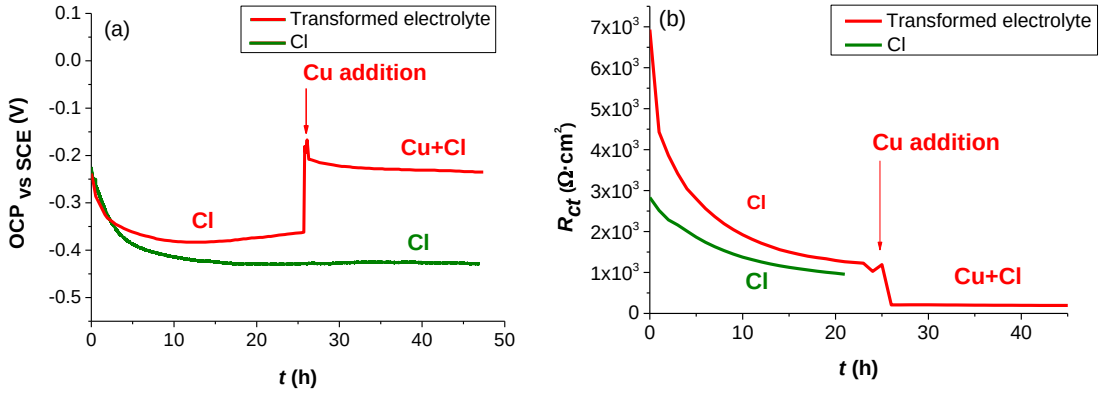

Figure 3. 9.- OCP versus time representation (a) in transformed electrolyte (red) and Cl electrolyte (green) and Rct versus time representation (b) in transformed electrolyte (red) and Cl electrolyte (green) for microporous nickel-chromium multilayer sample

On the other hand, cross-section characterisation by FE-SEM (Figure 3. 10) was made in order to corroborate the electrochemical findings. So far, the morphology of the active sites after 47 hours exposure to Cl electrolyte (Figure 3. 10 (a)) preserved a rounded shape similar to the one observed after 22h of exposure (Figure 3. 4 (a)). The main difference comparing them was the variety of sizes for active sites in Figure 3. 10 (a), most probably due to the larger time of exposure and the presence of more nucleation sites, respectively. In contrast, Figure 3. 10 (b) revealed the presence of two types of active sites:

i. A combination of mixed shapes (rounded and rectangular, Figure 3. 10(b)) are shown in detail in Figure 3. 11. Initially, the development of rounded active sites (typical after exposure to Cl electrolyte) was favoured (i.e. during the first 25 hours of the test). Later on, once the $CuCl_2$ was added, the lateral progress of the corrosion occurred favouring the rectangular shape (typical after exposure to Cu+Cl electrolyte). This morphological impact as a function of the electrolyte confirms that corrosion affects to microporous and bright

nickel attack in Cl electrolyte whilst only bright nickel is attack in Cu+Cl electrolyte. Such mixed actives sites are large compared to the ones obtained in Cl electrolyte (Figure 3. 10 (a)) due to the higher corrosion rate promoted by the presence of cupric ions. Interestingly, a mixed morphology facilitates to distinguish the boundary between bright and semibright nickel layers and confirms the attack of the later in Cl electrolyte (Table 3. 1).

ii. Rectangular active sites that were created just after the addition of $CuCl_2$, otherwise they should have mixed shape.

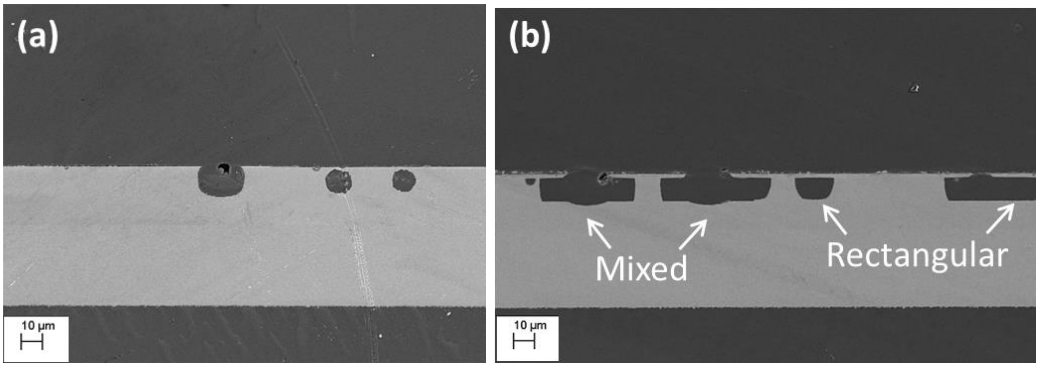

Figure 3. 10.- Cross section FE-SEM images of active sites developed in microporous nickel-chromium multilayer samples tested in Cl electrolyte (a) and transformed electrolyte (b) during 47 hours of test.

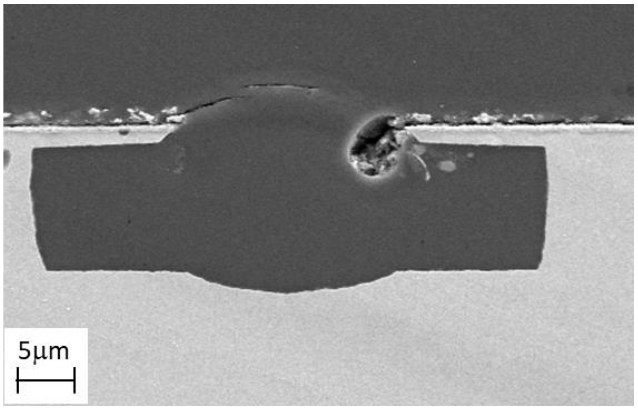

Figure 3. 11.- Cross section FE-SEM image of a mixed active site developed in microporous nickel-chromium multilayer samples tested in transformed electrolyte during 47 hours of test.

Once again, the impact of cupric ions in the corrosion has been proved. Its addition to a Cl electrolyte during a test (at 22h out of 47h) turned out the corrosion mechanism. Fresh

active sites preserving microporous nickel layer are developed in already existing active sites.

3.4. Conclusions

The corrosion mechanism of decorative microporous nickel-chromium multilayer coatings is highly affected by the type of electrolyte:

- Cu^{2+} cations reduction is governing the corrosion process in Cu + Cl electrolyte where bright nickel layer is acting as single anode. On the other hand, ORR is taking place in chloride electrolyte, where several anodes are found as a function of the O_2 concentration and depth of the active site.
- The aesthetic impact is mainly reveled by opened active sites, which depends on two key factors: the aggressiveness of the electrolyte (it mainly affects the width) and the type of corrosion mechanism (i.e. protection or not of MPS Ni layer). Whereas Cu^{2+} ions promote the development of wide active sites (which remain closed/unaffected below a certain threshold of width) due to its higher corrosion rate, the corrosion of MPS Ni layer in the electrolyte without cupric ions triggers the development of narrow and opened active sites (due to the earlier chromium layer undermining).
- Cu^{2+} cations not only increase the corrosion rate due to its oxidising effect, but also modify the corrosion mechanism itself. Bright nickel out of three nickel layers is the only one attacked as expected by electrochemical potential difference between them. However, in absence of Cu^{2+} cations in the electrolyte, the corrosion mechanism changes leading to MPS Ni layer corrosion along with B Ni one, although certain dissolution of SB Ni layer occurs. It can be explained because the ΔE_{corr} is not maintained between B Ni layer and MPS or SB Ni layers, respectively.

3.5. References

[1] R. Tremmel, Methods to Improve the corrosion performance of microporous nickel deposits, Plat. Surf. Finish. (1996) 24–28.

[2] M. Barnstead, J. Schweitzer, W. Schumacher, Investigations into the Performance of Multi-layer Nickel Coatings in Both CASS and Exhaust Gas Corrosion Testing, Plat. Surf. Finish. (2010) 30–36.

[3] M. Schlesinger, M. Paunovic, Modern electroplating, John Wiley & Sons, New

York, 2000.

[4] N. Imaz, E. García-Lecina, J.A. Díez, Corrosion properties of double layer nickel coatings obtained by pulse plating techniques, Trans. Inst. Met. Finish. 88 (2010) 256–261. https://doi.org/10.1179/002029610X12791981507767.

[5] Standard Test Method for Copper-Accelerated Acetic Acid-Salt Spray (Fog) Testing (CASS Test), Annu. B. ASTM Stand. B368 (2011) 1–5. https://doi.org/10.1520/B0368-09.2.

[6] D. Carl, Corrosion in the automobile industry, in: Man. Ind. Corros. Stand. Control, 1973: pp. 81–88.

[7] S.R. Maloof, The Electrochemical Behavior of Decorative Nickel-Chromium Coatings in 3 % NaCI under Potentiostatic Conditions, (n.d.) 1293–1298.

[8] G.N. Flint, S.H. Melbourne, The Corrosion of Decorative Nickel + Chromium Coatings: A Metallographic and Potential Study, Trans. IMF. 38 (1961) 35–44. https://doi.org/10.1080/00202967.1961.11869817.

[9] L. Pohlmann, G. Bauer, P. Hartmann, P. Wachter, C. Donner, Oscillatory passive active transition during the corrosion in nickel chromium layer systems, J. Solid State Electrochem. 17 (2013) 489–496. https://doi.org/10.1007/s10008-012-1949-3.

[10] C. Langer, W. Wendland, K. Honold, L. Schmidt, J.S. Gutmann, M. Dornbusch, Corrosion analysis of decorative microporous chromium plating systems in concentrated aqueous electrolytes, Eng. Fail. Anal. 91 (2018) 255–274. https://doi.org/10.1016/j.engfailanal.2018.04.031.

[11] R. Schmidt, K.O. Thiel, F. Von Horsten, C. Spickermann, G. Vazhenin, N. Bäulke, P. Wachter, P. Hartmann, H.J. Schreier, Towards the mechanism of the accelerated corrosion of decorative nickel-chromium coatings in the presence of metals and their salts, Mater. Corros. 65 (2014) 959–967. https://doi.org/10.1002/maco.201307104.

[12] G.A. Petrocelli, J. V., Hospadaruk, V, Dibari, “The Electrochemistry of Copper, Nickel and Chromium in the Corrodkote and CASS Test Electrolytes,” Plating. 50 (1962).

[13] L. Ganborena, J.M. Vega, B. Özkaya, H.-J. Grande, E. García-Lecina, An SKP and EIS study of microporous nickel-chromium coatings in copper containing electrolytes, Electrochim. Acta. 318 (2019) 683–694. https://doi.org/10.1016/j.electacta.2019.05.108.

[14] M. Stern, A.L. Geary, Electrochemical Polarization, J. Electrochem. Soc. 104 (1957) 559. https://doi.org/10.1149/1.2428653.

[15] G.S. Frankel, Pitting Corrosion of Metals, J. Electrochem. Soc. 145 (1998) 2186–2198. https://doi.org/10.1149/1.1838615.

[16] K.S.N. Murthy, R. Ambat, E.S. Dwarakadasa, The role of metal cations on the corrosion behaviour of 8090-T851 alooy in a pH 2.0 solution, 36 (1994) 1765–1775.

[17] G.A. Di Bari, Electrodeposition of nickel, in: Mod. Electroplat. Fifth Ed., 2010: pp. 79–114. https://doi.org/10.1002/9780470602638.ch3.

[18] Y. Liu, R.F. Schaller, E. Asselin, Effect of Fe(III) and Cu(II) on the passivation of Ti-2 in acidic chloride solutions, J. Electrochem. Soc. 166 (2019) C76–C82. https://doi.org/10.1149/2.1021902jes.

[19] W. Shao, G. Pattanaik, G. Zangari, Influence of Chloride Anions on the Mechanism of Copper Electrodeposition from Acidic Sulfate Electrolytes, J. Electrochem. Soc. 154 (2007) D201–D207. https://doi.org/10.1149/1.2434682.

[20] H. Zhao, J. Chang, A. Boika, A.J. Bard, Electrochemistry of high concentration copper chloride complexes, Anal. Chem. 85 (2013) 7696–7703. https://doi.org/10.1021/ac4016769.

[21] E.P. Harbulak, Simultaneous Thickness and Electrochemical Potential Determination of Individual Layers in Multilayer Nickel Deposits, Plat. Surf. Finish. 67 (2) (1980) 49–54.

[22] T. Dobrev, M. Monev, S. Nikolova, S. Rashkov, Compartive corrosion tests of multilayer Ni-Cr coatings, Surf. Coatings Technol. 31 (1987) 127–135.

4

SECM study of microporous nickel-chromium coatings: monitoring Cu^{2+} and oxygen reduction reactions

4.1. Introduction

Decorative nickel-chromium multilayer systems are usually composed by an outer microporous chromium layer on the top of three nickel layers. These nickel layers are adjusted to different potentials and the bottom one is plated over a plastic substrate previously coated by copper. The nickel deposits are plated in a way that the nickel layer with the lowest potential (Bright nickel one) is located in between microporous nickel (above) and semibright nickel (below) ones [1] (Figure 4. 1). Such a design was made to locate the anode in a single nickel, leading to the preferential corrosion of the nickel layer with the lowest potential (Figure 4. 1) in order to provide enhanced corrosion resistance and the minimum visual impact[2,3].

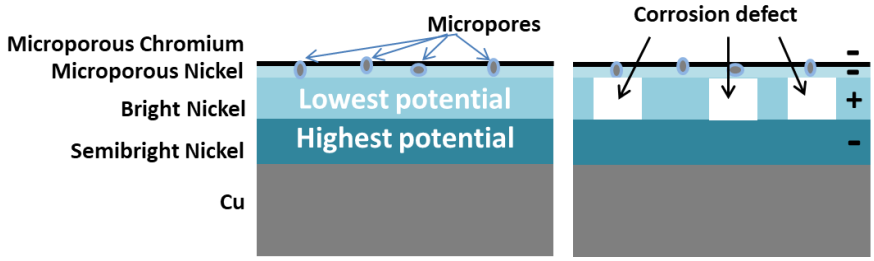

Figure 4. 1.- Microporous nickel-chromium multilayer coating scheme and corrosion mechanism of the system.

Despite the fact that Copper Accelerated Acetic Acid Salt Spray (CASS) test (ASTM B368 [4]) has been extensively used for the evaluation and development of decorative nickel-chromium coatings in the last decades, few studies have been focused on the role of cupric ions in the corrosion of these coatings [5,6]. It was observed that cupric ions increased the corrosion rate due to its oxidizing effect by means of electrochemical methods [5] and quantum chemical methods [6]. This finding has also been observed in 2024 aluminium alloy during exposure to chloride electrolytes. Apparently, Cu^{2+} was detected in the solution as well as its later reduction over Al-Cu-Mn-Fe containing particles (which were acting as cathodic sites) [11]. However, most of the studies on aluminium and aluminium alloys were mainly focused on the impact of copper rather than the presence or not of Cu^{2+} ions [7–10].

Recently, information about the degradation of microporous nickel-chromium systems due to the presence of cupric ions has been revealed. It was shown that cupric ions not only increase the corrosion rate of the nickel layers underneath chromium one, but also affect the corrosion mechanism and the appearance of the surface [12]. As it was

expected taking into account the design of these decorative systems, bright nickel layer was the only one attacked when Cu^{2+} ions are present in the electrolyte [Chapter 3]. In contrast, if Cu^{2+} ions are absent in the chloride based electrolyte, there is a change in the corrosion mechanism, leading also to the corrosion of microporous nickel layer and semibright nickel in a lower extent, along with bright nickel layer dissolution [Chapter 3]. Regarding to the reduction of Cu^{2+}, drop tests (using cupric ion containing chloride electrolyte) led to the observation of cupric ion reduction to cuprous ones by SKP. Interestingly, local potential maps of the surface showed the presence of areas with higher potentials values after exposure to such a drop test [12].

Nevertheless, it is still unclear why the reduction of cupric ions was causing a change in the corrosion mechanism and therefore, complementary studies are required. Scanning Electrochemical Microscopy (SECM) can be used for studying electrochemical reactions at localised scale. SECM is a versatile tool that includes different modes of operation [19], enabling the study of topography and electrochemical activity of samples in solution with a high spatial resolution. SECM allows the study of different features of corrosion processes such as, among others, kinetics [20], visualisation of anodic and cathodic sites [21] and repair of self-healing polymers coatings [22]. Generation/Collection (G/C) mode enables to monitor electroactive species generated during the course of the studied process by their collection. The generation of Cu^{+} due to Cu^{2+} reduction during Cu metal electrodeposition from $CuSO_4$ solution in the presence of chloride has been successfully studied by Surface Generation/Tip Collection (SG/TC) SECM [23]. Cu^{2+}/Cu^{+} has been employed as the internal redox couple in the electrolyte during the measurement of the local activity of coated membranes by tip collection [24].

The goal of this research was to understand the role of cupric ions and its impact in the corrosion mechanism. Samples were characterised by FE-SEM and GD-OES after exposure to an aggressive electrolyte containing cupric and chloride ions at pH 3.1. SECM was used for studying the corrosion process using two different scenarios: (i) the reduction of Cu^{2+} during the corrosion of fresh microporous nickel-chromium multilayer coatings, and (ii) the electrochemical activity of samples previously exposed to the electrolyte containing Cu^{2+}. Results have shown the presence of copper deposits on the surface of MPS nickel layer by FE-SEM and GD-OES. The activity of such copper particles was detected by monitoring the oxygen reduction reaction (ORR) in acidic chloride electrolyte by SECM, which also shown the stepwise reduction of Cu^{2+} to copper via Cu^{+}.

4.2. Experimental

4.2.1. Materials

Two different types of samples (absence or presence of porous on the surface) were obtained from trivalent chromium baths: microporous and non-porous nickel-chromium multilayer coatings. Although the former is the one of interest for this study, the later one was merely used for comparative purpose during the electrochemical measurements and further characterisation.

The electrolyte used was based on CASS test electrolyte which has the following composition: 0.9M NaCl + 1.5mM $CuCl_2$ (Cu+Cl electrolyte). Modified versions of the Cu+Cl electrolyte were used for SECM measurements: (i) 0.9M NaCl (Cl electrolyte) and (ii) 0.9M NaCl + 1.5mM $CuCl_2$ + 5mM $NiCl_2 \cdot 6H_2O$ (Cu+Cl+Ni^{2+}electrolyte). All solutions were prepared with analytical grade reagent and 18.5 MΩcm deionized water. The solution pH was adjusted to 3.1 by the addition of Glacial acetic acid.

4.2.2. Open Circuit Potential (OCP) measurements

Samples (1cm^2) were exposed to Cu+Cl electrolyte at 49ºC, mimicking the conditions of CASS accelerated test. Open circuit potential (OCP) measurements were performed in a flat corrosion cell with a volume of 250 mL of quiescent electrolyte using a VSP-300 Biologic potentiostat. Ag/AgCl (3M KCl) was used as reference electrode and a platinum mesh as counter electrode. Tests were run during 22 h and repeated at least three times.

4.2.3. Characterisation

A Gemini Ultraplus field emission scanning electron microscope (FE-SEM) from Zeiss was employed for the characterisation of the surface. Accelerating voltages of 8.0 and 10.0 kV were used to study samples with different top layer. Chromium layer was removed (i.e. chemically stripped) with the aim to characterise the underneath microporous nickel layer. Figure 4. 2 shows the three different scenarios for the top chromium layer: (a) as received, (b) partially stripped, and (c) completely removed.

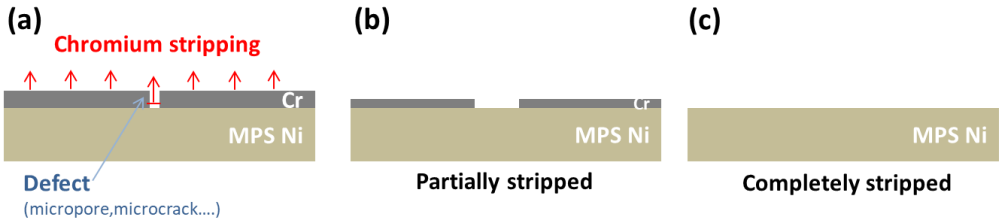

Figure 4. 2.- Cross section scheme of microporous nickel-chromium layers (a) exposed sample during the stripping process, (b) partial stripped, and (c) completely stripped.

Elemental depth profile characterisation was performed to microporous nickel-chromium samples after exposure to Cu+Cl electrolyte by Glow Discharge-Optical Emission Spectroscopy (GD-OES), using a Horiba Jobin-Yvon RF10000 instrument. Measurements were performed in argon at pressure of 650 Pa, 30W power and an area of 12.5 mm^2. Data was collected every 10ms during sputtering. For this particular test, blistering of the ABS substrate due to heating occurred during the measurement, which make difficult to determine the depth for each spot. Therefore, an additional measurement was performed after substitution of ABS by brass, where the thickness of nickel layers was lower on brass substrate than for ABS samples.

4.2.4. SECM

SECM experiments were done with a M470 electrochemical workstation from Bio-Logic. The probe used for the tests was a 15 µm diameter platinum ultramicroelectrode (UME) with RG-ratio (glass diameter to electrode diameter) of approximately 14.5. Standard calomel electrode (SCE, KCl saturated) and platinum foil were employed as reference and auxiliary electrodes, respectively. All tests were run at room temperature and repeated at least three times for reproducibility.

SECM experiments were carried out to microporus nickel-chromium multilayer samples under two different conditions: as-received and exposed ones (22h in Cu+Cl electrolyte at 49ºC), where an area of 0.2cm^2 was delimited by an adhesive tape (insulator) and exposed to the electrolyte.

4.2.4.1. Linear sweep voltammetry (LSV)

In order to identify the redox reaction of interest and determine the potential value to polarise the UME, LSVs were carried out in the bulk solution at a scan rate of 5mVs^{-1} for the different electrolytes.

4.2.4.2. Approaching curves

SECM studies were done without the use of an extra mediator to avoid any interaction with the electrolyte of interest. In Cu+Cl electrolyte, the Cu^{2+} present in the electrolyte was used as the redox mediator, whereas in Cl electrolyte O_2 was the redox mediator. The tip was placed at a distance close to 200µm above the surface (current value considered as limiting current (i_{lim})) and the approach curves were run after 1 hour of exposure to the electrolyte. Such curves were performed over the adhesive tape (insulating) and the microporous nickel-chromium coatings (active). The UME was moved towards the surface by 5µm steps at a rate of 10µm/s. Finally, experimental data of the approaching curves were normalized: current values were obtained dividing the tip current by the limiting current ($i_{norm} = i/i_{lim}$), and the position dividing the distance by the radius of the UME ($L_{norm}=d/a$).

4.2.4.3. Area scans

Surface area scans were carried out in an area of 500µmx500µm, using 25µm steps and the sample at OCP. A tip to sample distance of 20µm was used in Cu+Cl electrolyte, where SECM was operated in competition mode for Cu^{2+} (Figure 4. 3 (a)) and SG/TC mode for Cu^{+} under OCP (Figure 4. 3 (b)). Experiments done in Cl electrolyte were performed in competition mode (Figure 4. 3 (a)) and with a higher distance (30µm) in order to minimise the impact of the pH increase at localised scale by the oxygen reduction reaction (ORR) in the UME [31].

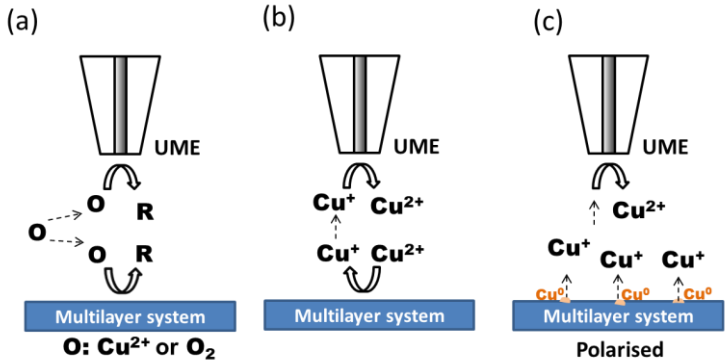

Figure 4. 3.- SECM operation modes: (a) competition, (b) SG/TC for Cu+ with the sample at OCP, and (c) SG/TC for Cu+ by sample transient polarization

4.2.4.4. Point measurements

Point measurements were performed over specific locations in SG/TC mode. UME was polarised for Cu^{+} collection while sample was transient polarised from OCP to the potential at which Cu^{0} oxidation occurs (Figure 4. 3(c)).

4.3. Result and Discussion

4.3.1. OCP measurement during Cu+Cl electrolyte exposure

Microporous and non-porous samples were exposed to Cu+Cl electrolyte at 49ºC for a period of 22h. The results of the OCP measurements are shown in Figure 4. 4**.**

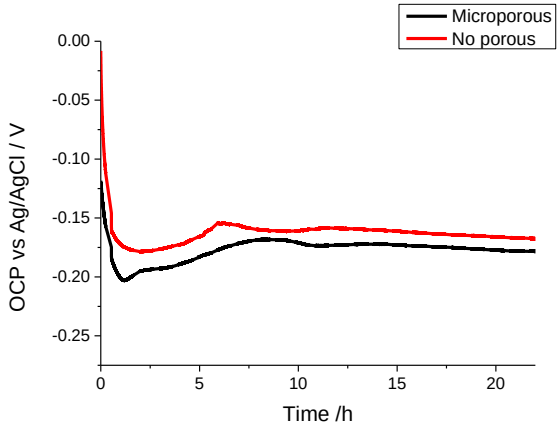

Figure 4. 4.- OCP data versus time for microporous and non-porous nickel-chromium samples in Cu+Cl electrolyte

Both samples showed a similar behavior during the exposure to Cu+Cl electrolyte despite the different porosity of the chromium layers, indicating a similar thermodynamic behaviour during the corrosion process. OCP values stabilised around a potential close to -0.170V after an initial sudden potential decrease that was inverted around the first 2 hours of exposure.

4.3.2. Surface characterisation

4.3.2.1. FE-SEM analysis

In order to detect the presence of copper after exposure to Cu+Cl electrolyte, samples previously exposed to the electrolyte were analysed by FE-SEM. Previous studies discarded the presence of copper on the top chromium layer under this electrolyte [12]. Therefore, the search of copper deposits was focused on the nickel underneath (i.e.

microporous and bright nickel layers). The surface of microporous nickel layer was studied removing the topmost chromium layer by stripping procedure.

Microporous nickel is exposed to the electrolyte mainly by two types of micro-discontinuities of the chromium coating: micropores and microcracks (both observable in Figure 4. 5 (a)). Micropores are intended for this system, they are achieved by the codeposition of nonconductive particles along with microporous nickel layer and create a galvanic coupling between chromium and the nickel underneath. In general, they improve the overall corrosion resistance of the multilayer system minimising the aesthetic impact [2,25]. On the other hand, microcracks are formed as a consequence of the chromium plating process, where hydrogen evolved from the reduction of protons promotes the formation of microcracks in the chromium layer [26]. Figure 4. 5 (b) shows the stripped surface of an unexposed sample after the removal of the chromium layer. The surface of the microporous nickel layer clearly indicates the presence of micropores and the absence of microcracks.

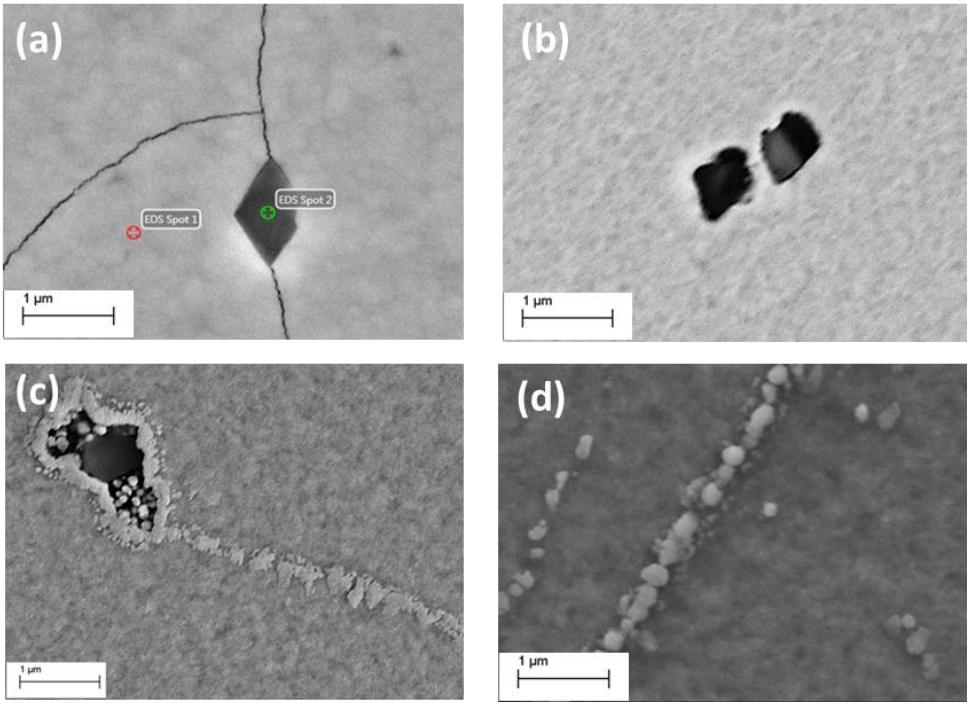

Figure 4. 5- FE-SEM micrographs of the surface of (a) microporous nickel-chromium sample without having been exposed to Cu+Cl electrolyte, (b) microporous nickel-chromium sample without having been exposed to Cu+Cl electrolyte after chromium layer stripping, (c) microporous nickel-chromium sample exposed 3.5 hours to Cu+Cl electrolyte and after chromium layer stripping, (d) microporous nickel-chromium samples exposed 22 hours to Cu+Cl electrolyte and after chromium layer stripping

Figure 4. 5 (c) and (d) are showing the images of stripped surfaces after 3.5 hours and 22 hours of exposure to Cu+Cl electrolyte, respectively. Micrograph in Figure 4. 5 (c) shows the presence of particles in the micropore and in the surrounding area. Moreover, a thread of particles departing from the end of the micropore was also slightly noticeable. The increase of exposure time, Figure 4. 5 (d), made these deposits more evident, where discrete particles ranging from 100 to 200 nm diameter arranged in rows were clearly observable over microporous nickel.

The chemical composition of the particles was determined by EDX point analysis of different particles (Figure 4. 5 (c) and (d)).The atomic percentage of copper varied from 64 to 74 at.% (where Ni was the remaining element) as a function of the particle thicknesses and the depth reached by the EDX beam [27]. It is interesting to point out that chloride was not detected in the compositional analysis of the particles. Cupric ion in a chloride electrolyte undergoes a stepwise reduction to Cu^{+} and later to Cu^{0} [28,29]. During cupric ion reduction, chloride ions stabilise cuprous anions by the formation of complexes. Therefore, the reduction process of Cu^{2+} could lead to Cu^{+} species as was already shown in a previous study with the formation of Cu^{+} (detected as CuCl precipitates) during the corrosion attack which, under evaporation conditions [12]. Then, according to the findings in Figure 4. 5 (c) and (d), a second reduction step (probably in a lower extent than the former) could explain the formation of these copper deposits.

The noticeable arrangement of Cu particles in threads observed in Figure 4. 5 (d), which is not linked to the proximity of any micropore or corrosion defect, indicated that chromium microcraks could be one of the main pathways for the cupric ions in the electrolyte to reach microporous nickel underneath. In order to explore this hypothesis, non-porous samples were used. Figure 4. 6 (a) shows the absence of micropores in as-received specimens, where only microcracks are clearly visible. On the other hand, Figure 4. 6 (b) shows how the partial stripping on samples previously exposed to Cu+Cl electrolyte (22 hours) increased the width of the microcracks but did not completely erase them. It is possible to establish that the initial position of the microcrack was somewhere close to the centre of the furrows, where copper deposits (confirmed by EDX) are found in agreement with Figure 4. 5 (d).

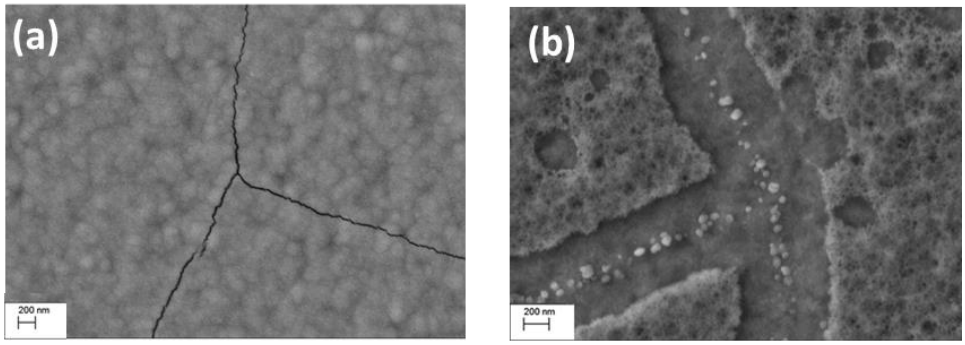

Figure 4. 6.- FE-SEM micrographs of the surface of (a) no porous microporous nickel-chromium sample without having been exposed to Cu+Cl electrolyte and (b) non-porous nickel-chromium sample exposed 22 hours to Cu+Cl electrolyte and after partial chromium layer stripping

These results proved the contribution of microcracks in the exposure of microporous nickel to the electrolyte. Taking into account that the main cathodic reaction is Cu^{2+} reduction (Chapter 3), and that such could lead to copper precipitation, it seemed that the reduction reaction to copper was taking place over microporous nickel layer.

As a summary, it seems reasonable to consider microcracks, along with the well-known role of micropores, as key features in the overall corrosion behaviour of the decorative nickel-chromium multilayer coatings. The finding of copper deposits over microporous nickel could be indicative of the behaviour of microporous nickel layer as a cathodic site, triggering its protection compared to bright nickel while exposure to Cu+Cl electrolyte [30].

4.3.2.2. GD-OES Analysis

In addition to FE-SEM characterisation, and with the aim of determining where were located the copper deposits, samples previously exposed to Cu+Cl electrolyte (22 hours) were also analysed by GD-OES. Figure 4. 7 shows the compositional depth profile of the samples for Cr, Ni, Cu and S (Cu and S data were multiplied by a factor of 100 to fit them in this scale). The beginning and end of the bright nickel layer is revealed thanks to the presence sulphur in its composition compared to the other nickel layers. Results showed an increase in copper content mainly in the depth corresponding to the position of microporous nickel, indicating that copper was preferentially present in such a layer. It confirmed that the copper deposition (and therefore the reduction reactions) were mainly

taking place on microporous nickel layer, which acted as a cathode and could explain its protection from corrosion.

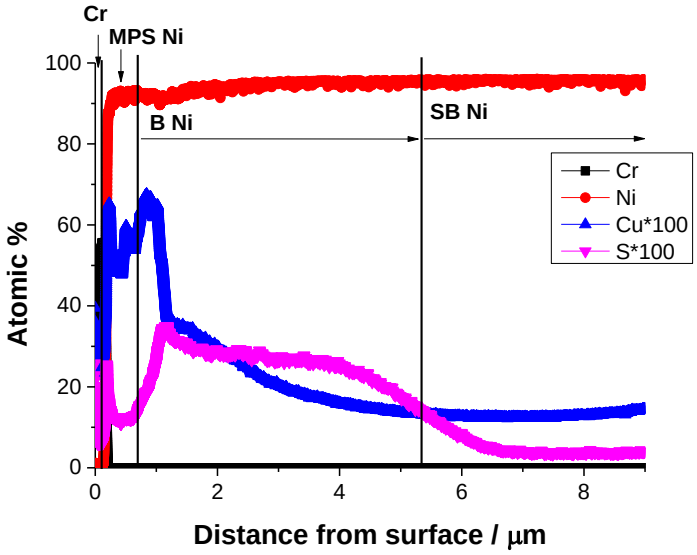

Figure 4. 7.- GD-OES elemental depth profile for microporous nickel-chromium multilayer coatings after 22 hours exposure to Cu+Cl electrolyte. Layers indications: Cr (chromium), MPS Ni (microporous nickel), B Ni (Bright nickel) and SB Ni (Semibright nickel)

4.3.3. SECM monitoring of as received

4.3.3.1. Determination of UME´s potentials in Cu+Cl electrolyte

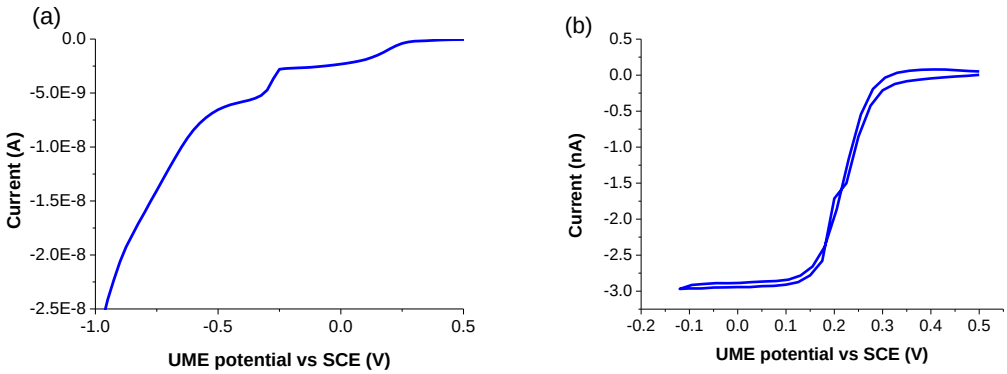

Figure 4. 8.- Linear sweep voltammetry of Cu+Cl electrolyte. Initial potential 0.5V; sweep rate 10mV/s, final potential -1.0 V (a) and Cyclic voltammogram in Cu+Cl electrolyte recorded at 10mV/s at the UME over a potential range from 0.5V to -0.12V (b).

Cu^{2+} reduction was identified as the main cathodic reaction in the corrosion process of this multilayer systems under exposure to Cu+Cl electrolyte [Chapter 3]. SECM was used to explore at localised scale the reduction reactions where ions of copper are involved during the corrosion process. In order to determine the potential at which the reduction reactions took place, LSV experiments were carried out in Cu+Cl bulk electrolyte. Figure 4. 8 (a) shows the LSV of the UME in Cu+Cl electrolyte scanned in the negative direction from 0.5V. The onset potential for Cu^{2+} reduction to Cu^{+} was observed at potential of 0.3V (see zoom in Figure 4. 8 (b)) by the detection of a reduction current [28,29]. A limiting current was reached from 0.1V to -0.25V, indicating that the Cu^{2+} reduction reaction to Cu^{+} was under diffusion control. The next inflexion point (-0.25V) corresponds to the onset of the reduction of Cu^{+} to Cu^{0}, where a limiting current was not well defined. If potential goes below -0.475V, once again an abrupt reduction of the current was observed. This new onset corresponds to hydrogen evolution from protons reduction [28]. These results clearly show the well-resolved stepwise reduction from Cu^{2+} to Cu^{+}, and from Cu^{+} to Cu metal, respectively, taking place in Cl^{-} solution following reactions (1) and (2) [23,28]:

$$Cu^{2+} + 2Cl^{-} + e \leftrightarrow CuCl_2^{-} \qquad (1)$$

$$CuCl_2^{-} + e \leftrightarrow Cu^{0} + 2Cl^{-} \qquad (2)$$

Therefore, the reduction of cupric ions to cuprous ones could be studied by two modes of the SECM: (i) competition at 0.02V and (ii) surface generation/tip collection (SG/TC) mode at 0.40V. In the first approach (i), sample and the UME are competing for Cu^{2+}. The UME had to be polarised to a potential where Cu^{2+} reduction had reached the limiting current, such as 0.020V (See Figure 4. 8 (b)), allowing the identification of the sites of the sample where Cu^{2+} was consumed. On the other hand, at the SG/TC mode (ii), the UME had to be polarised at a potential to provoke the Cu^{+} oxidation to Cu^{2+}. Therefore, the reduction of Cu^{2+} by the sample would be indirectly monitored by the UME.

4.3.3.2. Approaching curves

As it was previously indicated, specimens were mounted exposing a sample area of 0.2cm^2 to the electrolyte delimited by an adhesive tape (insulator). Approaching curves were performed over the sample (conductive) and the insulator tape surrounding it. The goal was: (i) to determine the separation between the UME and the sample for to running

area scans, and (ii) to confirm if the corrosion process has already started by the time that approaching curve were run.

Figure 4. 9 is showing normalised approaching curves on the surface of the sample and insulator, where the UME was polarised at 0.020V in order to ensure a diffusion limited reduction of Cu^{2+} to Cu^{+}. The curve over the insulator is showing a strong negative feeedback response typical of a passive substrate. Such a behaviour is characterised by a sharp current decrease once the UME was close to the surface, at distances lower to L_{norm}=*7.5*, due to Cu^{2+} diffusion towards the tip was hindered by geometrical factors.

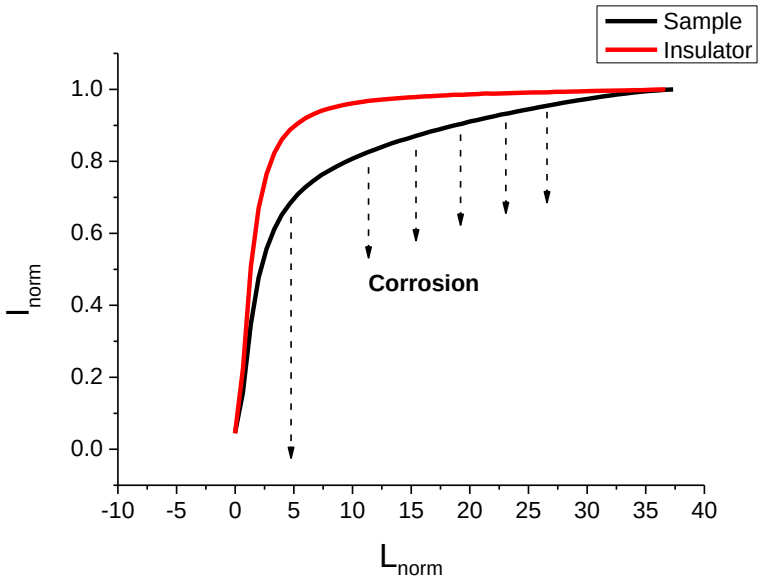

Figure 4. 9.- Comparison of approach curves towards microporous nickel-chromium sample (black line) and the insulating substrate (red line) with Cu2+ redox mediator

However, in the case of the curve over the sample, a current decrease was observed by the UME at distances larger than L_{norm}=*7.5.* This is due to the competition for Cu^{2+} between the sample and the tip, which is justified by a lower concentration of cupric ions in the bulk. Therefore, the noticeable decrease in the current was a clear indication that corrosion was taking place. On the other hand, at distances smaller than L_{norm}=*7.5*, the diffusion of cupric ion was hindered by the blocking effect of the surface, where a sharp decrease of the current was obtained. At the proximity of the surface, the geometrical factor became more apparent [31].

Finally, according to the resultas, a distance of 20µm between tip and sample was determined as a suitable for the measurements.

4.3.3.3. Area scans of as-received samples

Mappings of the surface at OCP were conducted over samples under Cu+Cl electrolyte to study the corrosion process by in-situ monitoring the Cu^{2+} ion reduction. As it was previously explained, the Cu^{2+} reduction reaction can be monitored either directly or indirectly, using two types of operation modes of the SECM: (i) directly by detecting Cu^{2+} using competition mode, and (ii) indirectly by detecting the presence of Cu^{+} using SG/TC mode.

Figure 4. 10 (a) and (b) show the area scans after 2h of exposure to the electrolyte using the competition and SG/TC mode, respectively. In Figure 4. 10 (a) the current values corresponded to Cu^{2+} reduction (negative sign) and the coloured area in red indicated the presence of a lower amount of Cu^{2+} ions to be reduced by the UME. Therefore, indicating higher cathodic activity of the sample, that was already consuming Cu^{2+} in that spots. On the other hand, Figure 4. 10 (b) is showing a similar map where the current values corresponded to the Cu^{+} oxidation (positive sign). In this case, coloured area in red indicated a higher concentration of Cu^{+} detected by the UME, and once again, it indirectly confirmed that Cu^{2+} ions were being consumed due to the cathodic activity of the sample in that location.

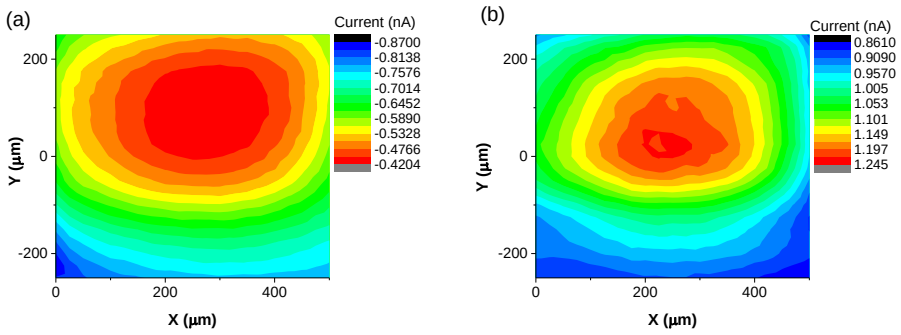

Figure 4. 10.- SECM images of microporous nickel-chromium in competition (a) and SG/TC (b) modes measuring Cu2+ reduction and Cu+ generation, respectively. The UME potential of 0.020V in (a) and 0.400V in (b) after 2h immersion in Cu+Cl electrolyte.

Therefore, although both graphs are monitoring opposite reactions (i.e. consumption and formation of Cu^{2+}, respectively), the colour code in both representations reveals higher cathodic activity in reddish areas than in bluish ones. In fact, both areas with a higher cathodic activity nearly overlapped: the lowest reduction current (below 0.5nA) measured

at 0.02V (Cu^{2+} competion mode, Figure 4. 10 (a)), and the highest oxidation values (between 1.1-1.24nA) obtained at 0.4V (SG/TC mode, Figure 4. 10 (b)).

In order to monitor the cathodic reaction with time (from 2h to 48h), SG/TC mode for Cu^{+} was chosen instead competition mode for Cu^{2+}. The aim was to avoid any problem with the CuCl precipitation in the tip that could hinder its sensing capacity during competition mode [29]. Therefore, the evolution with time of the cathodic activity of microporous nickel-chromium samples exposed to Cu+Cl electrolyte is shown in Figure 4. 11. If Figure 4. 10 (b) and Figure 4. 11 (a) are compared, the highest current (close to 1.5nA) remains in the same area. However, at longer exposure time (48h in Figure 4. 11 (b)), new cathodic sites appear. Additionally, in the initial cathodic area a discrete spot with an enhanced cathodic activity remained, which reached much higher values (1.7nA) compared to lower exposure time.

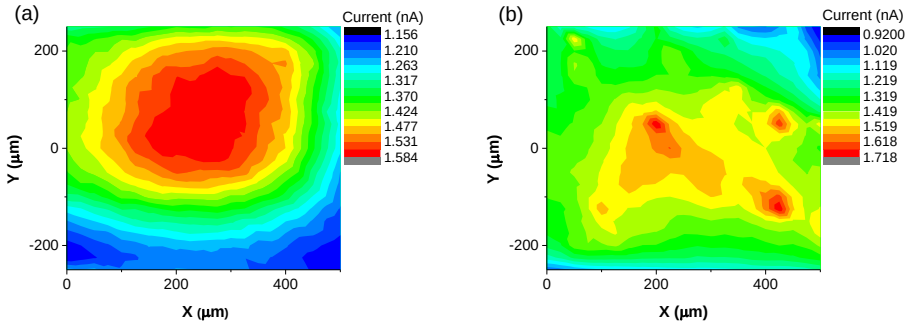

Figure 4. 11.- SECM images of microporous nickel-chromium in Cu+ SG/TC mode after 24h (a) and 48h (b) exposure to Cu+Cl electrolyte

As a summary, it was possible to detect the corrosion process since early exposure to the Cu+Cl electrolyte. It was possible to detect the formation of stable cathodes where Cu^{2+} reduction was taking place. The evolution with time (beyond 24h) led to the increase of the cathodes activity and to the establishment of new cathodic sites over the surface of the sample was observed at longer exposures (48h).

4.3.4. SECM monitoring of exposed samples

SECM was also used to detect the presence of copper deposits in samples previously exposed to Cu+Cl during 22h at 49ºC (similar to the sample characterised in Figure 4.

5). The idea was to explore their catalytic activity and locate them by monitoring the ORR in a Cl electrolyte (absence of cupric ions). Therefore, SECM competition mode was used to monitor the ORR (Figure 4. 3 (a)) in order to determine the location of cathodes. Moreover, in order to confirm the presence of copper in that locations, further oxidation and simultaneous monitoring with the SECM was performed. Subsequently, the UME was placed over those areas of interest in a second step, using the experimental approach shown in Figure 4. 3 (c): to simultaneously polarise the sample (for oxidising the copper deposits) as well as the UME to monitor the Cu^{+} ions released by the sample using SG/TC mode.

4.3.4.1. Determination of UME´s potential in Cl electrolyte

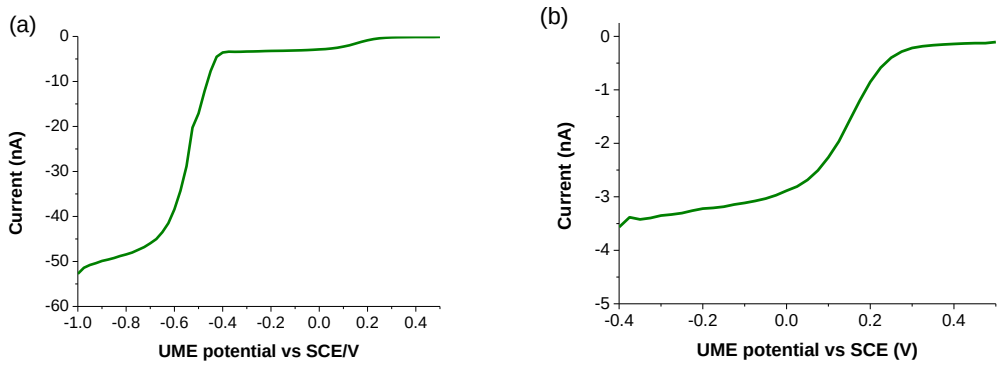

Figure 4. 12.- Linear sweep voltammetry of Cl electrolyte. Initial potential 0.5V; sweep rate 10mV/s, final potential -1.0 V (a) and -0.4V (b).

Figure 4. 12 shows the results for the LSV of the UME in Cl electrolyte from 0.5V to -1.0V in Figure 4. 12 (a) and to -0.4V in Figure 4. 12 (b). Cathodic current values due to ORR can be detected from 0.29V, reaching a limiting current in the potential range from -0.05 to -0.4V. Moreover, a second onset corresponding to hydrogen evolution can be observed at more negative potentials. Therefore, -0.25V was chosen for polarising the UME in order to compete with sample for oxygen consumption.

4.3.4.2. Determination of sample´s polarisation potential in Cl electrolyte

The idea of this section was to promote the oxidation of previously deposited copper particles by dissolving them in Cl electrolyte and further detection of Cu^{+} ions. Figure 4. 13 (a) shows the cyclic voltammogram of a copper plate in Cl electrolyte. A large anodic peak was observed from -0.12V to 0V as consequence of Cu^{0} dissolution to Cu^{+} ions, whereas in the reverse scan at potentials close -0.17V the reduction of Cu^{+} to Cu^{0} is

identified [28]. Therefore, -0.08 V was found as a suitable potential for polarising the sample for Cu^0 oxidation.

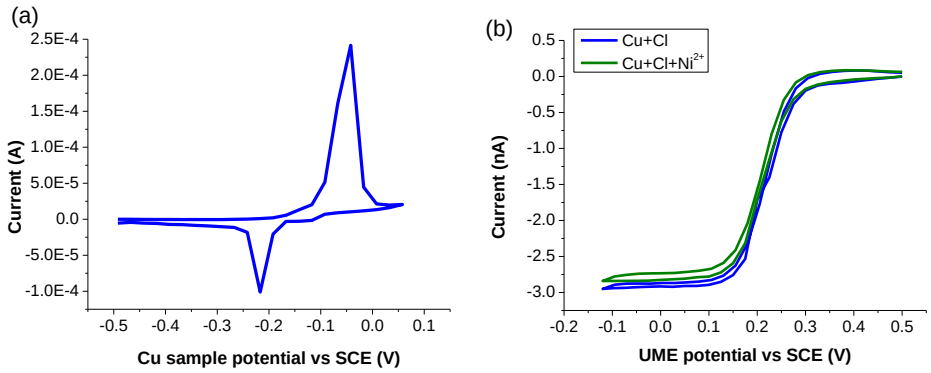

Figure 4. 13.- (a) Cyclic voltammograms in Cl electrolyte at Cu sample over a potential range from -0.5V to 0.1V, and (b) Cu+Cl and Cu+Cl+Ni2+ electrolyte CV at the UME over a potential range from 0.5V to -0.12V

In order to discard the side effects of Ni^{2+} ions (present in the electrolyte due to polarisation of the sample) during the detection Cu^+ by the UME, Figure 4. 13 (b) shows the voltammograms of Cu+Cl and Cu+Cl+Ni^{2+} electrolytes. It can be observed that the presence of Ni^{2+} did not interfere Cu^+ oxidation/Cu^{2+} reduction reactions.

4.3.4.3. Area scans

First of all, area scan were conducted with the sample under OCP and polarising the UME to -0.250V under SECM competition mode to detect ORR. The main downside is that the UME promoted the local increase of the pH which could affect the corrosion process under study [31]. Therefore, in order to minimise that effect, the distance from probe to sample was increased up to 30µm (higher than in the case of cupric ion reduction). Figure 4. 14 (a) shows the area scan after 1 hour of exposure to Cl electrolyte. ORR (negative sign) was measured in the UME, where the red colour indicated the lowest current values as a consequence of the presence of a localised cathode consuming oxygen.

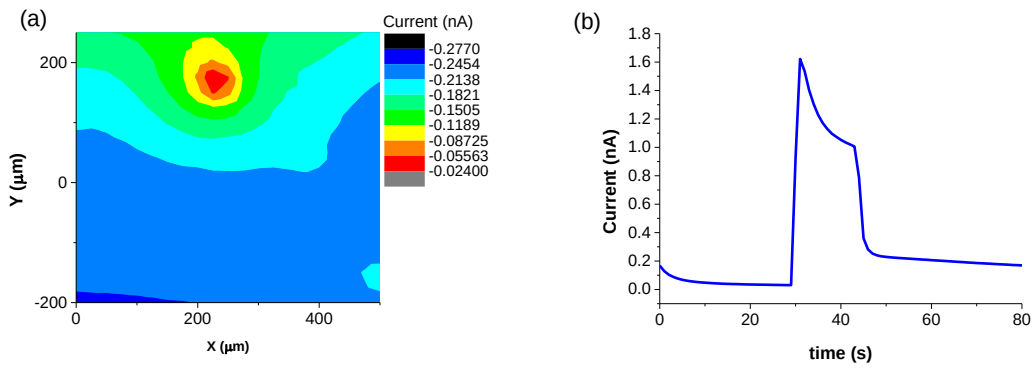

Figure 4. 14.- SECM images of microporous nickel-chromium previously exposed to Cu+Cl in competition for O_2 consumption in Cl electrolyte (a) and UME point measurement over the higher oxygen consuming spot in (a) polarised to 0.400V for Cu+ detection while polarising the sample to -0.080V pulses for Cu particles oxidation.

Once this cathode was located (approximately at X:225µm,Y:175µm coordinates), the experimental conditions for SECM measurements were changed: the sample was polarised by pulse (in order to oxide the copper particles) and the UME (polarised to 0.400V for Cu^+ detection by SG/TC mode). The point measurement shown in Figure 4. 14 (b) shows the result of the oxidation current measured by the UME during the transient polarisation of the sample. When the sample was at OCP, the UME in Cu^+ SG/TC mode measured a baseline current lower than $1.0 \cdot 10^{-10}$ A. However, when polarising the sample, Cu^+ oxidation current increased up to $1.6 \cdot 10^{-9}$ A and gradually decreased during the pulse until stabilisation around $1.0 \cdot 10^{-9}$ A. Once the pulse was stopped, the current measured by the UME diminished nearly reaching initial current baseline. After few pulses, no Cu^+ oxidation current was measured by the UME, pointing out that the complete dissolution of the Cu particles had already taken place.

As a conclusion, results in Figure 4. 14 confirmed that Cu^0 particles were deposited during the exposure to Cu+Cl electrolyte (Figure 4. 5). Interestingly, the localised cathodes (higher ORR activity) were identified as sites where Cu^0 had been deposited. This ORR catalytic activity could be locally increasing the pH and, if exceeding pH 4 [18], could be having an extra effect in the microporous nickel layer protection, favouring microporous nickel passivation.

4.3.5. Effects of copper deposition in the corrosion mechanism

It was observed that the corrosion mechanism of microporous nickel-chromium samples is different as a function of the electrolyte. The exposure to Cl electrolyte led to the

corrosion of three layers: mainly bright nickel along with microporous nickel layer (and even semibright nickel layer in a lower extent). It was shown that changes in oxygen concentration during the corrosion process drastically affect the corrosion potentials of the nickel layers, diminishing the potential difference between bright and microporous nickel layers, favouring the corrosion of the later [Chapter 3].

In contrast, the simple addition of Cu^{2+} ions to the Cl electrolyte was found to have a drastic impact in the corrosion mechanism. Interestingly, the corrosion front was only focused on the bright nickel layer, despite the fact that the potential difference with microporous nickel layer was similar in both electrolytes. How can be explained the protection of microporous nickel layer during exposure to Cu+Cl electrolyte?

The answer should be found in the type of cathodic reduction governing the process when cupric ions are present in the electrolyte. Due to the presence of chloride ions in the electrolyte, reduction from cupric ions to Cu^0 takes place via two single-electron steps. The first step leads to the reduction from Cu^{2+} to Cu^+, which was visualised/identified under different experiments: the SKP droplet tests [12], by the cathodic loops in the polarisation curves of microporous and semibright nickel layer [Chapter 6], and the SECM tests in SG/TC for Cu^+. Finally, the complete reduction process leads to the preferential deposition of copper particles over microporous nickel layer (Figure 4. 5). Therefore, microporous nickel layer behaves as a cathodic site whilst bright nickel layer behaves as the anodic one. Additionally, the protection of microporous nickel layer could be explained by several hypotheses:

(i) The formation of a protective layer of cuprous-chloride complexes ($CuCl$, $CuCl_2^-$) due to the reduction reactions of cupric ions on the surface, that could protect the nickel surface as has been previously observed in other materials [14,15].

(ii) The presence of copper particles, that have been deposited on the surface of microporous nickel layer, which could act as local microcathodes: e.g. ORR catalyst [10,16,17]. According to the low pH (3.1) in the electrolyte, none of the bare nickel layers exposed as consequence of the evolution of the corrosion process is supposed to be passivated. However, such copper particles could be acting as local microcathodes and increasing the pH locally above a critical value able to protect the nickel (pH>4 [18]).

As a summary, Figure 4. 15 shows an scheme of the corrosion mechanism in microporous nickel-chromium coatings in Cu+Cl electrolyte, where the different reduction reactions of the copper ions and oxygen are depicted along with the corrosion progress as consequence of the corrosion of the bright nickel layer.

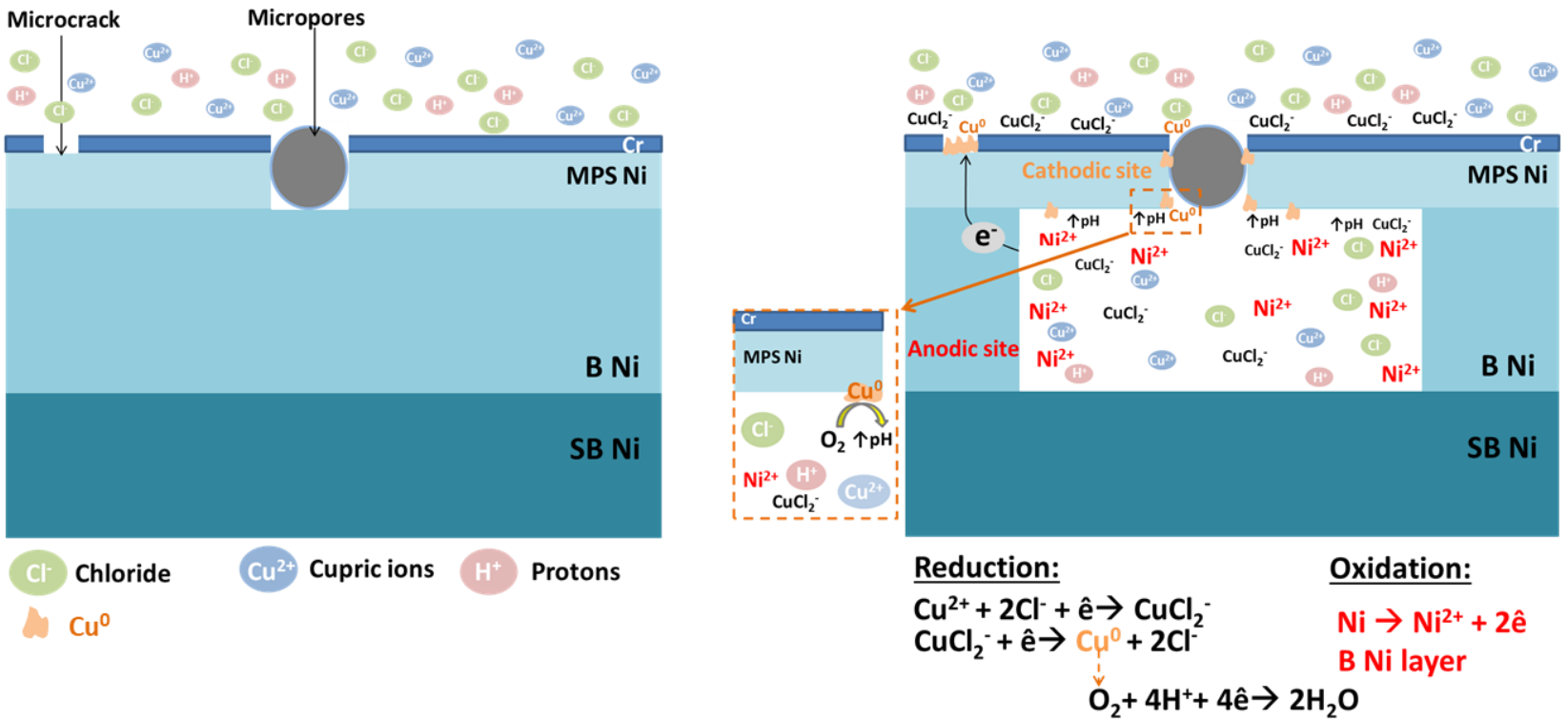

Figure 4. 15.- Corrosion mechanism of microporous nickel-chromium coating in Cu+Cl electrolyte.

4.4. Conclusions

Results showed that the combination of SECM experiments with different characterisation techniques facilitates the understanding of the reduction of cupric ions in acidic chloride electrolyte and the providing of an explanation in order to justify why microporous nickel layer remains under protection during the corrosion process. The following conclusions were found:

- Microcracks, along with micropores, were revealed to be the preferential pathways of the electrolyte to reach microporous nickel surface.
- The Cu^{2+} stepwise reduction to Cu^0 during decorative nickel-chromium corrosion was demonstrated by SECM: in-situ measurement of Cu^{2+} reduction to Cu^+ (competition and SG/TC modes) and indirect evidence of Cu^+ reduction to Cu^0 probed by oxidation of ex-situ deposited Cu^0 to Cu^+ by transient pulses (SG/TC mode).
- The deposition of Cu^0 takes place preferentially over the microporous nickel exposed to the electrolyte through micropores or microcracks. The presence of copper particles is able to protect the microporous nickel layer which behaves cathodically, having bright nickel layer as an anode.
- Cu^0 particles deposited in the sample showed ORR catalytic activity. This catalytic activity indicated the presence of localised cathodes on the top of microporous nickel layer and therefore, favoured a local increase of the pH at the proximity of the Cu^0 particles that could be favouring the passivation of microporous nickel and its corrosion protection.

4.5. Bibliography

[1] G.A. Di Bari, Electrodeposition of nickel, in: Mod. Electroplat. Fifth Ed., 2010: pp. 79–114. https://doi.org/10.1002/9780470602638.ch3.

[2] R. Tremmel, Methods to Improve the corrosion performance of microporous nickel deposits, Plat. Surf. Finish. (1996) 24–28.

[3] D.L. Snyder, Decorative chromium plating basics, Met. Finish. 110 (2012) 14–21. https://doi.org/10.1016/S0026-0576(13)70110-7.

[4] C. Test, Standard Test Method for Copper-Accelerated Acetic Acid-Salt Spray (Fog) Testing, 02 (2003) 6–9.

[5] G.A. Petrocelli, J. V., Hospadaruk, V, Dibari, “The Electrochemistry of Copper, Nickel and Chromium in the Corrodkote and CASS Test Electrolytes,” Plating. 50 (1962).

[6] R. Schmidt, K.O. Thiel, F. Von Horsten, C. Spickermann, G. Vazhenin, N. Baülke, P. Wachter, P. Hartmann, H.J. Schreier, Towards the mechanism of the accelerated corrosion of decorative nickel-chromium coatings in the presence of metals and their salts, Mater. Corros. (2014). https://doi.org/10.1002/maco.201307104.

[7] M.G.A. Khedr, A.M.S. Lashien, The role of metal cations in the corrosion and corrosion inhibition of aluminium in aqueous solutions, 33 (1992) 137–151.

[8] K.S.N. Murthy, R. Ambat, E.S. Dwarakadasa, The role of metal cations on the corrosion behaviour of 8090-T851 alooy in a pH 2.0 solution, 36 (1994) 1765–1775.

[9] V. Uksiene, K. Leinartas, R. Juškenas, A. Sudavičius, E. Juzeliūnas, Magnetron-sputtered Al-Mg coatings - Structural, microgravimetric and voltammetric characterisation in water, chloride and Cu(II) environment, Electrochem. Commun. 4 (2002) 747–752. https://doi.org/10.1016/S1388-2481(02)00450-2.

[10] M. Chiba, Y. Nakayama, T. Hiraga, H. Takahashi, Y. Shibata, Synergistic effects of Cl- and Cu2+ ions on corrosion of pure Al and Al alloys in aqueous solutions at 363 K, Surf. Interface Anal. 45 (2013) 1626–1630. https://doi.org/10.1002/sia.5265.

[11] H.M. Obispo, L.E. Murr, R.M. Arrowood, E.A. Trillo, Copper deposition during the corrosion of aluminum alloy 2024 in sodium chloride solutions, J. Mater. Sci. 5 (2000) 3479–3495.

[12] L. Ganborena, J.M. Vega, B. Özkaya, H.-J. Grande, E. García-Lecina, An SKP and EIS study of microporous nickel-chromium coatings in copper containing electrolytes, Electrochim. Acta. 318 (2019) 683–694. https://doi.org/10.1016/j.electacta.2019.05.108.

[13] E. Juzeliunas, K. Leinartas, W. Fürbeth, K. Jüttner, Study of initial stages of Al-Mg alloy corrosion in water, chloride and Cu(II) environment by a scanning Kelvin probe, Corros. Sci. 45 (2003) 154–158. https://doi.org/10.1016/S0010-938X(03)00026-X.

[14] Q. Liu, M. Chen, Y. Yang, The effect of chloride ions on the electrochemical dissolution of chalcopyrite in sulfuric acid solutions, Electrochim. Acta. 253 (2017) 257–267. https://doi.org/10.1016/j.electacta.2017.09.063.

[15] A.A. Hermas, K. Ogura, T. Adachi, Accumulation of copper layer on a surface in the anodic polarization of stainless steel containing Cu at different temperatures, Electrochim. Acta. 40 (1995) 837–844. https://doi.org/10.1016/0013-4686(94)00365-8.

[16] M. Kendig, S. Jeanjaquet, Cr (VI) and Ce (III) Inhibition of Oxygen Reduction on Copper, J. Electrochem. Soc. 149 (2002) B47–B51. https://doi.org/10.1149/1.1430717.

[17] M.B. Vukmirovic, N. Vasiljevic, N. Dimitrov, K. Sieradzki, Diffusion-Limited Current Density of Oxygen Reduction on Copper, J. Electrochem. Soc. 150 (2003) B10–B15. https://doi.org/10.1149/1.1526554.

[18] N. Hernández, R. Moreno, A.J. Sánchez-Herencia, J.L.G. Fierro, Surface behavior of nickel powders in aqueous suspensions, J. Phys. Chem. B. 109 (2005) 4470–4474. https://doi.org/10.1021/jp0448954.

[19] J. Kwak, A.J. Bard, Scanning Electrochemical Microscopy. Apparatus and Two-Dimensional Scans of Conductive and Insulating Substrates, Anal. Chem. 61 (1989) 1794–1799. https://doi.org/10.1021/ac00192a003.

[20] C. Nowierski, J.J. Noël, D.W. Shoesmith, Z. Ding, Correlating surface microstructures with reactivity on commercially pure zirconium using scanning electrochemical microscopy and scanning electron microscopy, Electrochem. Commun. 11 (2009) 1234–1236. https://doi.org/10.1016/j.elecom.2009.04.008.

[21] A.C. Bastos, A.M. Simões, S. González, Y. González-García, R.M. Souto, Imaging concentration profiles of redox-active species in open-circuit corrosion processes with the scanning electrochemical microscope, Electrochem. Commun. 6 (2004) 1212–1215. https://doi.org/10.1016/j.elecom.2004.09.022.

[22] Y. González-García, J.M.C. Mol, T. Muselle, I. De Graeve, G. Van Assche, G. Scheltjens, B. Van Mele, H. Terryn, SECM study of defect repair in self-healing polymer coatings on metals, Electrochem. Commun. 13 (2011) 169–173. https://doi.org/10.1016/j.elecom.2010.12.005.

[23] A.P. O'Mullane, A.K. Neufeld, A.M. Bond, Monitoring cuprous ion transport by scanning electrochemical microscopy during the course of copper electrodeposition, J. Electrochem. Soc. 155 (2008) 538–541. https://doi.org/10.1149/1.2936177.

[24] M. Nebel, S. Neugebauer, H. Kiesele, W. Schuhmann, Local reactivity of diamond-like carbon modified PTFE membranes used in SO2 sensors, Electrochim. Acta. 55 (2010) 7923–7928. https://doi.org/10.1016/j.electacta.2010.02.031.

[25] M. Barnstead, J. Schweitzer, W. Schumacher, Investigations into the Performance of Multi-layer Nickel Coatings in Both CASS and Exhaust Gas Corrosion Testing, Plat. Surf. Finish. (2010) 30–36.

[26] D.B. Lee, Oxidation of Cr-C electroplating between 400 and 900°C in air, Mater. Corros. 59 (2008) 598–601. https://doi.org/10.1002/maco.200804143.

[27] A.A. El Warraky, A.M. El Aziz, K.A. Soliman, A.A. El Warraky, K.A. Soliman, Copper redeposition and surface enrichment during the dissolution of Al-Cu alloys in different concentrations of NaCl solution . Part 2 – spectroscopic analysis measurements, Anticorros. Methods Mater. 54 (2007) 163–172. https://doi.org/10.1108/00035590710748632.

[28] C.P. De Leon, F.C. Walsh, Research and Development Techniques 1: Potentiodynamic Studies of Copper Metal Deposition, Trans. Inst. Met. Finish. 81 (2003) 95–100. https://doi.org/10.1080/00202967.2003.11871523.

[29] H. Zhao, J. Chang, A. Boika, A.J. Bard, Electrochemistry of high concentration copper chloride complexes, Anal. Chem. 85 (2013) 7696–7703. https://doi.org/10.1021/ac4016769.

[30] G.S. Chen, M. Gao, R.P. Wei, Microconstituent-Induced Pitting Corrosion in Aluminum Alloy 2024-T3No Title, Corrosion. 52 (1996) 8–15. https://doi.org/10.5006/1.3292099.

[31] L.C. Abodi, Y. Gonzalez-Garcia, O. Dolgikh, C. Dan, D. Deconinck, J.M.C. Mol, H. Terryn, J. Deconinck, Simulated and measured response of oxygen SECM-measurements in presence of a corrosion process, Electrochim. Acta. 146 (2014) 556–563. https://doi.org/10.1016/j.electacta.2014.09.010.

5

Towards a correlation between Copper Acetic Acid-Salt Spray test and electrochemical results for decorative multilayer nickel-chromium coatings

Capítulo sujeto a confidencialidad por parte de la autora

6

Annex I-Chapter 3

6.1. Corrosion mechanism as a function of the electrolyte

In order to explain the corrosion mechanism for microporous nickel-chromium multilayer coatings, certain similarities can be found compared to pitting corrosion [1]. In the present study, there is a galvanic coupling between the different metallic layers and theoretically, their potential values are increasing from bright nickel < microporous nickel < semibright nickel < passive chromium. If there is only electric contact between the uppermost chromium and the microporous nickel layer below (e.g. the discontinuity or pore provoked by the non-conductive particle does not reach the bright nickel layer), it can be partially dissolved until the corrosion front reaches the most anodic layer: bright nickel one. Therefore, pores are acting as weak points/defects where nickel oxide film breakdown occurs (probably passive) favoured by the adsorption of chloride ions [2], consequently, promoting nickel dissolution [3].

Up to here, the explanation above about the corrosion mechanism is common for both electrolytes. So, the main difference seems to occur at the beginning of corrosion of the bright nickel.

6.1.1. Cl electrolyte

Although an isotropic growth in height and width of the active sites throughout bright nickel layer can be seen until semibright nickel layer is reached, microporus nickel layer behaves differently depending on the presence/absence of cupric ions in the electrolyte. Its passivation could be hindered due to:

(1) The adsorption of chloride to the bare microporous nickel surface [4].
(2) The fast oxygen depletion that could happen inside the active site [5], that is able to decrease the potential difference (ΔE_{corr}) between the different nickel layers observed [Chapter 3, section 3.3.4.2.1.]. This also may be happening to semibright nickel layer in a lower extent, once the corrosion front reaches newly exposed bare surface.

Finally, in a later stage of corrosion progress, chromium top layer undermines due to the lack of the mechanical support as a consequence of the dissolution of the microporous nickel layer. The opening of active sites raises oxygen concentration and could favour both, the passivation of the remaining microporous nickel and the preferential bright nickel layer corrosion according to the potential differences.

6.1.1.1. Deaerated polarisation curves

In order to obtain more information about the cathodic reactions, polarisation curves were also obtained in the absence of oxygen (deaerated conditions). Figure 6. 1 shows the comparison of the polarisation curves obtained in naturally aerated and deaerated conditions for Cl electrolyte.

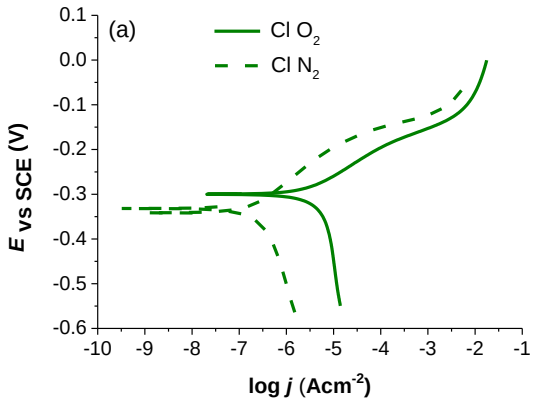

Figure 6. 1.- Polarisation curves corresponding to microporous nickel-chromium system in naturally aerated and deaerated Cl.

As observed in Chapter 3 with the incomplete samples (section 3.3.4.2.1.) aeration also affected the corrosion process of microporous nickel-chromium coatings in Cl electrolyte (Figure 6. 1), where a negative shift in corrosion potential was observed. With respect to the different electrochemical parameters (Table 6. 1), the main variations were found in βc, jcorr and Rp. The decrease in the cathodic slope ($-\beta c$) in the absence of oxygen indicates its impact on the cathodic reaction. In fact, it can be confirmed by the decrease of jcorr in one order of magnitude and the considerable increase in Rp.

Therefore, it can be concluded that in naturally aerated electrolytes ORR is taking part in the cathodic process [6]. Accordingly, previous results (using the same substrate and electrolyte in the droplet test with the Scanning Kelvin Probe chamber) had already indicated the role of oxygen in the cathodic reaction [7]. Indeed, the increase of the chloride concentration due to the evaporation of the drop shifted the potential to lower potentials as consequence of the lower O_2 diffusion and solubility [7].

Table 6. 1.- Electrochemical parameters obtained for microporous nickel-chromium multilayer coatings in Cl electrolyte. Data are expressed as mean with standard deviation.

Condition	E_{corr} (mV $_{vs\ SCE}$)	R_p (kohm·cm^2)	β_a (mV)	$-\beta_c$ (mV)	j_{corr} (µA·cm^{-2})
NaCl aerated	-298 ±15	6.7±1.2	60±6	535±170	3.70±1.70
NaCl dearated	-351±15	116.4±32.1	76±4	217±25	0.40±0.01

6.1.1.2. Confirmation of the effect of nickel layers potential difference decrease in corrosion. Study of pH effect in chloride electrolyte

In order to confirm whether the trend of potential differences established between nickel layers in Cl electrolyte (as consequence of O_2 depletion) could be the reason for the attack of microporous and superficial damage in semibright nickel, test were done under neutral 5% chloride solution (N-Cl) investigating the potential differences between nickel layers and the layers affected by corrosion.

6.1.1.2.1. Incomplete samples in N-Cl electrolyte

ORR is the cathodic reaction in the corrosion process in N-Cl electrolyte and takes place at the outer chromium layer [5], therefore, the anodic reaction would be preferentially taking place in the less noble nickel layer.

The electrochemical behaviour of each nickel layer, shown in Figure 6. 2, was studied in aerated and deaerated N-Cl electrolyte. Under aerated conditions, Figure 6. 2 (a), semibright nickel layer (E_{corr}:-144mV), showed the noblest potential value, followed by microporous (E_{corr}:-228mV) and bright nickel layer (E_{corr}:-235mV), which showed very similar potential values between them.

The three nickel layers showed different anodic branches in the polarisation curves. All of them showed a region in which the current density was low and nearly independent of the potential, which could be related to a pseudo-passive region. However, the potential range was different, lasting approximately 100mV of anodic overpotential for bright nickel, 200mV for microporous nickel and 300mV (the whole anodic polarisation) for semibright nickel. Probably, the formation of a $Ni(OH)_2$ film on the nickel surface, that

due to a series of electrochemical reactions evolved to the passive NiO, was the responsible of such a pseudo-passive response. In the case of microporous nickel and bright nickel, the increase of potential during polarisation promoted the interaction between chloride ions and the nickel surface and led to the breakdown of the pseudo-passive layer [8], causing an increase of current with the potential.

With respect to the cathodic branches, the current increased at a slower rate than in Cl electrolyte indicating a slower corrosion rate.

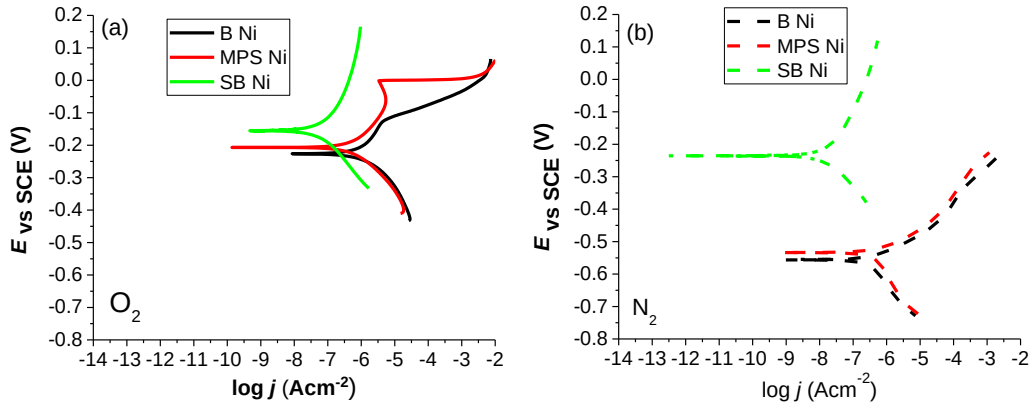

Figure 6. 2.- Polarisation curves corresponding to bright nickel, microporous nickel and semibright nickel layers in N-Cl electrolyte in naturally (a) aerated, and (b) deaerated conditions.

The absence of oxygen in N-Cl electrolyte changed completely the electrochemical response of the nickel layers. With respect to the results under aerated conditions, a decrease in the potential, especially pronounced in the case of bright and microporous nickel, was observed along with a decrease in the measured current. Moreover, changes in the anodic branches of bright and microporous nickel were also noticeable and their polarisation curves nearly overlapped. The pseudo-passive region identified in aerated conditions has disappeared and a monotonic increase of current with potential was observed, pointing out to a uniform corrosion. Whereas to the cathodic branches, Tafel slope did not change significantly with respect to aerated conditions

Semibright nickel layer (E_{corr}:-240mV) exhibited once again the noblest potential values, followed by microporous nickel (E_{corr}:-530mV) and bright nickel (E_{corr}:-554mV), the less noble nickel layer. Special attention will be paid to the trend of the potential differences established in deaerated N-Cl electrolyte that simulate the probable low oxygen concentration expected inside the active sites. For the microporous/bright nickel pair a

value of 22mV ± 13mV was measured, very close to the values observed under the same aeration conditions for Cl electrolyte. On the other hand, semibright/bright nickel couple potential difference value was higher than 300mV. According to the observed trend in potential differences between layers, a priori, microporous nickel layer corrosion could be expected along with bright nickel degradation, as it happened under Cl electrolyte exposure, whereas semibright nickel layer corrosion would not be expected due to the large potential difference with bright nickel layer.

6.1.1.2.2. FE-SEM metallographic characterisation of microporous nickel-chromium multilayer samples exposed to N-Cl electrolyte

In order to verify the damaged nickel layers due to the exposure to N-Cl electrolyte, nickel-chromium multilayer samples previously exposed to the electrolyte were characterised by FE-SEM.

As a consequence of the lower aggressiveness of N-Cl electrolyte with respect to Cl electrolyte, larger exposure times were studied in order to reach to a corrosion stage where the different nickel layers were exposed to the electrolyte and therefore, to correctly evaluate the preferential damaged layer during corrosion. However, this study revealed that the size and amount of active sites developed were not very reproducible. Probably, the lower aggressiveness of the electrolyte promoted the corrosion on the defects that are prone to be attacked than in the rest of the microporous surface.

Figure 6. 3 is showing cross section of actives sites after exposures of 36 (a) and 48 hours (b) to N-Cl electrolyte. The corrosion impact on the different nickel layers can be observed in Figure 6. 3 (a), where microporous nickel and chromium layers are still present. However, the shape of the active site reveals that the exposure to N-Cl electrolyte had partially corroded (more thinner) microporous nickel layer along with bright nickel one. With regards to semibright nickel layer, in both cases (Figure 6. 3 (a) and (b)), corrosion led to the formation of flat based active sites with a height close to 11.8µm, indicating that semibright nickel was not attacked in N-Cl electrolyte, independently of the corrosion progress. The sample exposed 48 hours to the electrolyte (Figure 6. 3 b) showed large active sites without microporous nickel and chromium layers above. It might be due to the chromium undermining provoked by the corrosion of microporous nickel. Such active site is showing a different shape than the ones found in Cl electrolyte (rounded one with higher height values and a more damaged semibright nickel layer).

Therefore, metallographic observations were in agreement with the electrochemical behaviour of the nickel layers, the low potential difference close to 20mV between microporous and bright nickel seemed to be indicative of a decreasing potential difference trend that favoured microporous nickel corrosion along with bright nickel, whereas the high potential difference of more than 300mV between semibright and bright nickel was more than enough for the preservation of semibright nickel layer.

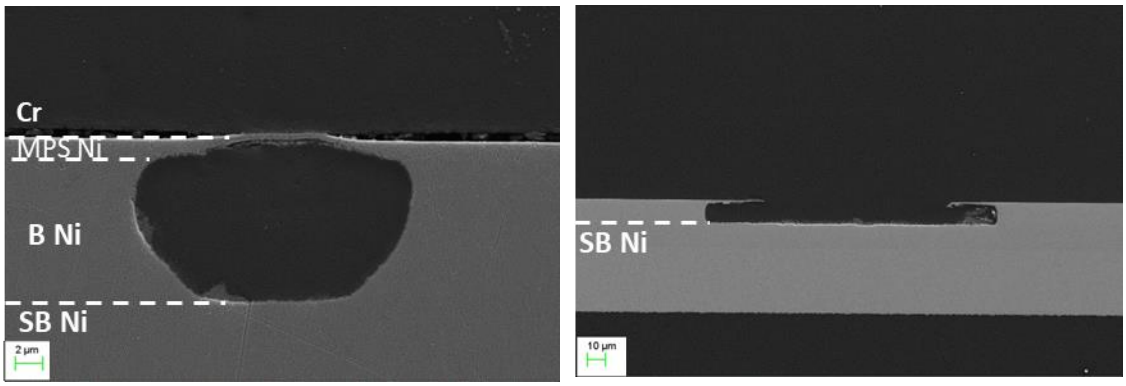

Figure 6. 3.- FE-SEM images of actives sites developed in microporous nickel-chromium multilayer coatings after 36 hours (a) and 48 hours (b) of exposure to N-Cl electrolyte

As a conclusion, the study in N-Cl electrolyte confirmed that the decrease in the potential difference between nickel layers suffered in deaerated Cl electrolyte could be the reason for the unexpected microporous layer attack and rounded shape of the active sites, indicative of a slight semibright nickel layer attack, along with the preferential bright nickel layer corrosion.

6.1.2. Cu+Cl electrolyte. Anodic polarisation curves in Cu+Cl electrolyte of the incomplete samples

In order to explore how the copper-chloride complexes are involved in the corrosion process in Cu+Cl electrolyte, cathodic and anodic branches were obtained in one round for each nickel as top layer. Same experimental as followed in section 3.2.2 but anodically polarising from -250mV to 300mV vs OCP.

An electrolyte containing Cu^{2+} but without Cl^- was used for semibright nickel samples polarisation., with a composition of 1.5mM $CuSO_4$ + 0.5M Na_2SO_4. The pH was adjusted to 3.1 with glacial acetic acid.

Figure 6. 4 shows the results obtained in naturally aerated (a) and deaerated (b) conditions. As previously discussed in section 3.3.4.2.2., similar polarisation curves were obtained under both conditions as consequence of cupric ion reduction as the main cathodic reaction in Cu+Cl electrolyte.

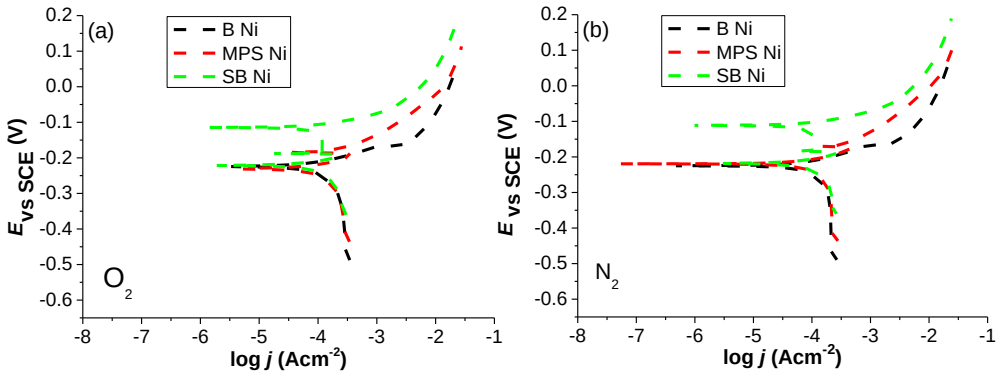

Figure 6. 4.- Polarisation curves corresponding to bright nickel (B Ni), microporous nickel (MPS Ni) and semibright nickel (SB Ni) layers in Cu+Cl electrolyte in naturally (a) aerated, and (b) deaerated conditions.

Two different regions were identified in the anodic branches of the polarisation curves of both aeration conditions and similar E_{corr} were obtained to the ones previously described (Section 3.3.4.2.2.). However, a different and interesting feature was observed for microporous and semibright nickel in the cathodic branch: negative currents were found in Cu+Cl electrolyte between -180 and -235mV. These negative currents observed in anodic polarisations are called 'cathodic loops' and have been previously noticed in the studies of certain materials exposed to different solutions. Literature has assigned them to oxygen reduction [11], hydrogen evolution [12] and copper chloride complexes redox [9] among other reactions. In this case, ORR and hydrogen evolution reaction may not be the reason for the cathodic loops in that they were not observed in Cl electrolyte. Hence, copper chloride complexes redox (Cl^- and Cu^{2+} form a series of chloro-complexes such $CuCl^0$, $CuCl_2^-$ or $CuCl_3^{2-}$ [9]) could be the most reasonable cause for the cathodic loops observed. Indeed, a particular anodic polarisation test using an electrolyte without chlorides (Cu^{2+} and SO_4^{2-} ions) of semibright nickel layer did not show any cathodic loop (Figure 6. 5).

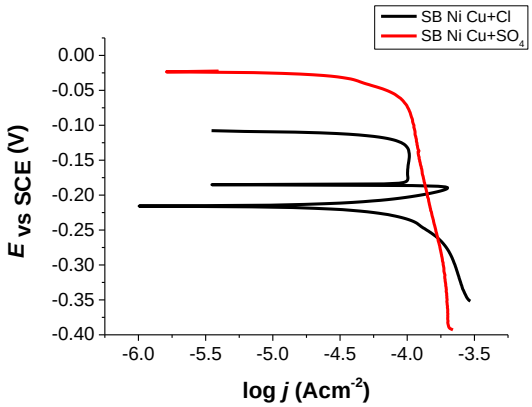

Figure 6. 5.- Detail of the cathodic branches of SB Ni samples exposed to Cu+Cl electrolyte (black line) and Cu electrolyte without chlorides (red line).

The presence of cathodic loops in the polarisation curves of microporous and semibright nickel samples revealed an enhanced redox activity of copper-chloride complexes in those nickel layers compared to bright nickel layer. It pointed out to a tendency for cupric ions to be reduced over microporous or semibright nickel layers rather than on the top of bright Ni layer. These results could be indicative of a cathodic behaviour of microporous and semibright nickel layers compared to bright nickel layer in the complete system in Cu+Cl electrolyte, as observed in chapter 4. Therefore, the role of cupric ions in the reduction reactions could explain why, despite ΔE_{corr} MPS/B nickel is only around 50 mV in Cu+Cl electrolyte, no damage is observed over microporous nickel layer when microporous nickel-chromium samples were exposed to the electrolyte (Figure 3.4 (b)).

6.2. References

[1] G.S. Frankel, Pitting Corrosion of Metals, J. Electrochem. Soc. 145 (1998) 2186–2198. https://doi.org/10.1149/1.1838615.

[2] B. Macdougall, D.F. Mitchell, G.I. Sproule, M.J. Graham, Incorporation of Chloride Ion in Passive Oxide Films on Nickel, (n.d.).

[3] S.G. Real, M.R. Barbosa, A.J. Arvia, Influence of Chloride Concentration on the Active Dissolution and Passivation of Nickel Electrodes in Acid Sulfate Solutions, J. Electrochem. Soc. 137 (1990) 1696–1702.

[4] R. Schmidt, K.O. Thiel, F. Von Horsten, C. Spickermann, G. Vazhenin, N. Bäulke, P. Wachter, P. Hartmann, H.J. Schreier, Towards the mechanism of the accelerated corrosion of decorative nickel-chromium coatings in the presence of

metals and their salts, Mater. Corros. 65 (2014) 959–967. https://doi.org/10.1002/maco.201307104.

[5] L. Pohlmann, G. Bauer, P. Hartmann, P. Wachter, C. Donner, Oscillatory passive active transition during the corrosion in nickel chromium layer systems, J. Solid State Electrochem. 17 (2013) 489–496. https://doi.org/10.1007/s10008-012-1949-3.

[6] K.S.N. Murthy, R. Ambat, E.S. Dwarakadasa, The role of metal cations on the corrosion behaviour of 8090-T851 alooy in a pH 2.0 solution, 36 (1994) 1765–1775.

[7] L. Ganborena, J.M. Vega, B. Özkaya, H.-J. Grande, E. García-Lecina, An SKP and EIS study of microporous nickel-chromium coatings in copper containing electrolytes, Electrochim. Acta. 318 (2019) 683–694. https://doi.org/10.1016/j.electacta.2019.05.108.

[8] D. V. Vasquez Moll, R.C. Salvarezza, H.A. Videla, A.J. Arvia, The Pitting Corrosion of Nickel in Different Electrolyte Solutions Containing Chloride Ions, J. Electrochem. Soc. 132 (1985) 754–760. https://doi.org/10.1149/1.2113953.

[9] Q. Liu, M. Chen, Y. Yang, The effect of chloride ions on the electrochemical dissolution of chalcopyrite in sulfuric acid solutions, Electrochim. Acta. 253 (2017) 257–267. https://doi.org/10.1016/j.electacta.2017.09.063.

[10] E. Juzeliunas, K. Leinartas, W. Fürbeth, K. Jüttner, Study of initial stages of Al-Mg alloy corrosion in water, chloride and Cu(II) environment by a scanning Kelvin probe, Corros. Sci. 45 (2003) 1939–1950. https://doi.org/10.1016/S0010-938X(03)00026-X.

[11] J.W. Lee, K. Osseo-Asare, H.W. Pickering, Anodic Dissolution of Iron in Ammoniacal Ammonium Carbonate Solution, J. Electrochem. Soc. 132 (1985) 550–555. https://doi.org/10.1149/1.2113885.

[12] R.P. Frankenthal, On the Passivity of Iron-Chromium Alloys I . Reversible Primary Passivation and Secondary Film Formation, J. Electrochem. Soc. 114 (1967) 542–547. https://doi.org/10.1149/1.2426646.

Conclusions

The corrosion mechanism of microporous nickel-chromium coatings, mainly used for decorative applications, has been widely explored under CASS conditions (tests under accelerated chambers, conventional electrochemical techniques and localised ones, respectively). The key findings of this PhD can be summarised as follows:

1. The main cathodic reaction in CASS electrolyte is the reduction of Cu^{2+} ions to Cu^{+}. Cu^{+} ions are strongly stabilised by chloride anions thanks to the formation of Cu^{+}/chloride complexes and Cu^{+} reduces to Cu^{0} in a lower extent.

2. Oxygen reduction reaction (ORR) is the main cathodic reaction when cupric ions are not present in the electrolyte. It implies that changes in oxygen concentration modify the potential difference between nickel layers, favouring the corrosion of microporous nickel attack along with bright nickel layer corrosion.

3. Cu^{2+} cations not only increase the corrosion rate due to its oxidising effect, but also modify the corrosion mechanism itself. Bright nickel out of three nickel layers is the only one attacked as expected by electrochemical potential difference between them. However, in absence of Cu^{2+} cations (where ORR is taking place) in the electrolyte, the corrosion mechanism changes leading to microporous nickel layer corrosion along with bright nickel one, although certain dissolution of semibright nickel layer occurs. It can be explained due to ΔE_{corr} is not maintained between bright Ni layer and microporous or semibright nickel layers, respectively. Therefore, a different corrosion mechanism occurs as a function of the cathodic reactions governing the corrosion process.

4. Microcracks together with micropores are a preferential pathway for the electrolyte to reach nickel layers and are playing an important role in the protection of microporous nickel layer when cupric ions are present in the electrolyte.

5. The deposition of Cu^{0} takes place preferentially over the microporous nickel exposed to the electrolyte through micropores or microcracks. The presence of copper particles is able to protect the microporous nickel layer which behaves cathodically, having bright nickel layer as an anode. Additionally, Cu^{0} particles could act as

microcathodes where ORR reaction is catalysed. This implies a local increase of the pH, favouring microporous nickel layer passivation.

6. A short-list of electrochemical parameters were explored to predict the behaviour of nickel-chromium coatings in CASS test. Chemometric tools seem to be very promising to predict the corrosion behaviour. In fact, a prediction model based on PLS-DA was built and validated (75% of the samples were correctly classified) as a proof of concept. Numerical variables were obtained from the following experimental data after exposure to CASS electrolyte: the first 7h of OCP and R_p and EIS at 1h. Further development and improvement of the model to increase its performance can be achieved by increasing the number of samples.

As a final remark, electrochemical techniques have provided complementary and valuable information of the corrosion mechanism of multilayer nickel-chromium systems in combination with a detailed characterisation. In addition, all the experimental parameters such as OCP, Rp, EIS among others have been used to build a prediction model about the corrosion performance in CASS test. The presence of a correlation using electrochemical results is able to decrease the testing time as a quality control tool as well as minimise the error due to a subjective visual evaluation of the corrosion performance of the coatings.

List of contributions

Congresses

Why copper-accelerated acetic-acid salt spray test (CASS)? The corrosivity of copper salts

Eva García Lecina, Larraitz Ganborena, Jesús Manuel Vega, Hans Jürgen Grande, Constanze Donner, Philip Wachter, Werner Richtering

2nd International Conference Automotive Corrosion Protection
April 2017, 25-26. Berlin

Oral

The effect of cupric ions in the corrosion mechanism of Nickel-chromium multilayer systems

Eva García Lecina, Larraitz Ganborena, Hans Jürgen Grande, Jesús Manuel Vega

Eurocorr 2017,
September 2017, 03-06. Prague

Poster

The role of cupric ions in the corrosion mechanism of nickel-chromium multilayer system under CASS electrolyte

Larraitz Ganborena, Hans Jürgen Grande, Eva García Lecina, Jesús Manuel Vega

Automotive Surface Conference
November, 30-December, 01, 2017, Berlin

Oral

Cupric chloride ions effect on decorative nickel-chromium multilayer coatings

Larraitz Ganborena, Eva García Lecina, Jesús Manuel Vega, Hans-Jürgen Grande

SMT32-32nd International Conference on Surface Modification Technologies
June, 27-29, 2018, Donostia-San Sebastián

Oral

Combination of scanning and conventional electrochemical techniques to study the corrosion of microporous metallic coatings

Larraitz Ganborena, Hans Jürgen Grande, Eva García Lecina, Jesús Manuel Vega

Electrochemical Methods in Corrosion Research Conference
July, 22-27, 2018, Cambridge

Oral

Study of cupric ion effect in Nickel-Chromium multilayer systems corrosion by localised techniques

Larraitz Ganborena, Hans Jürgen Grande, Eva García Lecina, Jesús Manuel Vega

Eurocorr 2018,
September 2018, 09-13, Krakov

Poster

Understanding the different corrosion mechanism of microporous nickel-chromium coatings due to the presence of cupric ions in a chloride based electrolyte

Larraitz Ganborena, Hans Jürgen Grande, Eva García Lecina, Jesús Manuel Vega

Eurocorr 2019,
September 2019, 09-13, Sevilla

Poster

In situ cupric ion reduction and reduced copper particles catalytic activity characterisation by scanning electrochemical microscopy (SECM) upon decorative nickel-chromium corrosion in cupric ion containing chloride electrolyte

Larraitz Ganborena, Yaiza Gonzalez-Garcia, Hans-Jürgen Grande, Eva García-Lecina, Jesús Manuel Vega

Eurocorr 2020,
September 2020, 06-10, Virtual

Poster

Publications

An SKP and EIS study of microporous nickel-chromium coatings in copper containing electrolytes

Larraitz Ganborena, Jesús Manuel Vega, Berkem Özkaya, Hans-Jürgen Grande, Eva García-Lecina

Electrochimica Acta, 2019, 318, 683-694
DOI: 10.1016/j.electacta.2019.05.108